

2023-02-07

TRANSIENT STABILITY ENHANCEMENT IN A TRANSMISSION LINE USING ADAPTIVE NEURO-FUZZY-BASED UNIFIED POWER FLOW CONTROLLER [CASE STUDY: NORTH-WEST REGION ETHIOPIAN 400kV TRANSMISSION POWER SYSTEM]

YECHALE, AMOGNE ALEMU

<http://ir.bdu.edu.et/handle/123456789/15541>

Downloaded from DSpace Repository, DSpace Institution's institutional repository



BAHIR DAR UNIVERSITY

BAHIR DAR INSTITUTE OF TECHNOLOGY

SCHOOL OF RESEARCH AND POSTGRADUATE STUDIES

FACULTY OF ELECTRICAL AND COMPUTER ENGINEERING

MASTER OF SCIENCE IN POWER SYSTEM ENGINEERING

TRANSIENT STABILITY ENHANCEMENT IN A TRANSMISSION

LINE USING ADAPTIVE NEURO-FUZZY-BASED UNIFIED

POWER FLOW CONTROLLER

[CASE STUDY: NORTH-WEST REGION ETHIOPIAN 400kV

TRANSMISSION POWER SYSTEM]

BY

YECHALE AMOGNE ALEMU

February 07, 2023

Bahir Dar, Ethiopia

Transient Stability Enhancement in a Transmission Line Using Adaptive Neuro-Fuzzy-Based Unified Power Flow Controller

By:

Yechale Amogne

A thesis submitted to the School of Research and Postgraduate Studies of Bahir Dar Institute of Technology, Bahir Dar University, in partial fulfillment of the requirements for the award of the degree of Master of Science in Power System Engineering in Electrical and Computer Engineering Faculty.

Advisor: Dr.-Ing. Belachew Bantyriga

**February 07, 2023
Bahir Dar, Ethiopia**

DECLARATION

Transient stability enhancement of transmission line using ANFIS-based-UPFC | 2023

DECLARATION

This is to certify that the thesis entitled "Transient Stability Enhancement in a Transmission Line Using Adaptive Neuro-Fuzzy-Based Unified Power Flow Controller", submitted in partial fulfillment of the requirements for the degree of master of science in power system engineering under electrical and computer engineering faculty, Bahir Dar institute of technology is a record of original work carried out by me and has never been submitted to this or any other institution to get any other degree or certificates. I also state that, as required by these rules and regulations, I have properly cited and referenced all non-original material and results. The assistance and help I received during the course of this thesis have been duly acknowledged.

Yechale Amogne

Name of the candidate


Signature

Feb-07-2023

Date

This thesis has been submitted for examination with my approval as a university advisor. I recommend the thesis be submitted for oral defense.

Dr.-Ing. Belachew Bantvirga

Name of Advisor


Signature

06.02.2023

Date

©2023


Yechale Amogne Alemu

All Rights Reserved

**BAHIR DAR UNIVERSITY
BAHIR DAR INSTITUTE OF TECHNOLOGY
SCHOOL OF RESEARCH AND GRADUATE STUDIES
FACULTY OF ELECTRICAL AND COMPUTER ENGINEERING**


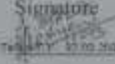

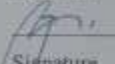
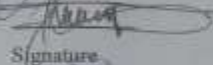

Thesis Approval Sheet

I hereby confirm that the changes required by the examiners have been carried out and incorporated into the final thesis.

Name of Student: Yechale Amogne Signature:  Date: Feb 07-2023

As members of the board of examiners, we examined this thesis entitled "Transient Stability Enhancement in a Transmission Line Using Adaptive Neuro-Fuzzy-Based Unified Power Flow Controller" by Yechale Amogne. We hereby certify that the thesis is accepted for fulfilling the requirements for the award of the degree of Masters of Science in "Power System Engineering".

Approved by:

Name of Advisor	Signature	Date
<u>Dr.-Ing. Belachew Bantvirga</u>		<u>06.02.2023</u>
Name of External Examiner	Signature	Date
<u>Dr. Tefera Terefe</u>		<u>27-02-2023</u>
Name of Internal Examiner	Signature	Date
<u>Dr. Teketay Mulu</u>		<u>16/02/2023</u>
Name of Chairperson	Signature	Date
<u>Dr. Girmaw Teshager</u>		<u>17/02/2023</u>
Name of Chair Holder	Signature	Date
<u>Mr. Yosef Berhan</u>		<u>14/3/2023</u>
Name of Faculty Dean	Signature	Date
<u>Dr. Teketay Mulu</u>		<u>17/02/2023</u>



ACKNOWLEDGEMENT

First and foremost, I thank Jesus Lord for his blessings throughout my research work, which enabled me to successfully complete the research. He has given me the strength and perseverance to complete this thesis.

I would like to express my deep and sincere gratitude to my advisor, Dr.-Ing. Belachew Bantyriga, for giving me the opportunity to do the research and providing valuable guidance throughout this research. I have been greatly inspired by his dynamism, vision, integrity, and motivation. He has taught me how to conduct research and present the findings in the most understandable way. Being able to work and study under his supervision was a tremendous honor and privilege. I am extremely grateful for what he has offered me.

I extend my sincere thanks to Woldia University for sponsoring me to pursue my MSc in the field of Electrical Power Systems Engineering at Bahir Dar University. Also, I would like to thank EEP staff members at the Bahir Dar substation. They generously gave their time to offer me valuable data and information to accomplish my work. Every result described in this thesis could not be accomplished without their kind cooperation in providing the necessary technical information.

I am incredibly appreciative of my parents' love, support, sacrifices, and efforts in raising and educating me. I am grateful to my mother, Genet A., and my sister Mulugojjam A., for their support throughout this thesis work and for their love, compassion, and prayers.

Finally, my thanks go to all the people who supported me to finish this thesis work, either directly or indirectly.

Yechale Amogne Alemu

ABSTRACT

A power system is a complex, nonlinear, and dynamic system, with its operating parameters continuously changing with time. High-voltage transmission power systems are frequently subject to transient instability problems due to the complexity of large load lines and faults, which results in power losses and higher voltage deviation. This problem can lead to catastrophic events such as cascading failure and/or widespread blackouts. Based on the collected data in 2021 G.C from the EEP office, Ethiopia's high-voltage transmission power system in the North-West region is a victim of this problem. Due to the growth in demand for electrical energy, the maximum capacity of the transmission lines should be increased to ensure a secure and uninterrupted power supply to consumers. This can be achieved by means of the installation of flexible AC transmission system (FACTS) devices. To address the problem, this thesis uses ANFIS-based UPFC for high-voltage transmission lines. Preference was given to this device for its fast-acting reactive power compensation on high-voltage transmission networks. The PSO algorithm was used to locate the optimal placement of the UPFC. Voltage error and rate of change of voltage error, which are extracted from PI-based UPFCs, are the inputs to the ANFIS controller. Of the extracted data, 70% is used for ANFIS training, and 30% is used for ANFIS testing. Different disturbances, such as three-phase with ground fault and single-phase with ground fault, are used to demonstrate the performance of the suggested controller. For instance, when a three-phase with ground fault occurs at the midpoint of the Beles to Bahir Dar transmission line, the settling time of rotor angle deviation, rotor speed, rotor speed deviation, and output active power of synchronous generators using ANFIS-based UPFC is reduced by 70.58 %, 37.75 %, 37.75 %, and 43.75 %, respectively, compared to a system without UPFC. The active power loss reduced by PI-based UPFC and ANFIS-based UPFC on the Beles to Bahir Dar transmission line at peak load is 51.25 % and 71.50 %, respectively, compared to a system without UPFC. On the other hand, the active power loss reduced by PI-based UPFC and ANFIS-based UPFC on the Bahir Dar to D/Markos transmission line at peak load is 20 % and 47.9 %, respectively, compared to a system without UPFC. ANFIS-based UPFC provides a better result than PI-based UPFC for transient stability enhancement in terms of percentage overshoot and settling time.

Keywords: *FACTS, UPFC, PI Controller, ANFIS, power system, PSO*

TABLE OF CONTENTS

ACKNOWLEDGEMENT	iv
ABSTRACT.....	v
TABLE OF CONTENTS.....	vi
LIST OF FIGURES.....	x
LIST OF TABLES	xiv
LIST OF ABBREVIATIONS	xvi
CHAPTER ONE	1
1. INTRODUCTION	1
1.1 Background of The Study	1
1.2 Classification of Power System Stability.....	3
1.2.1 Rotor Angle Stability	3
1.2.2 Voltage Stability	4
1.2.3 Frequency Stability	4
1.3 Motivation	5
1.4 Statement of the Problem	6
1.5 Objectives.....	7
1.5.1 General Objective	7
1.5.2 Specific Objectives	7
1.6 Significance of The Thesis.....	7
1.7 Scope of The Study	8
1.8 Methodology	8
1.9 Organization of The Thesis	9
CHAPTER TWO	11
2. LITERATURE REVIEW AND THEORETICAL BACKGROUND	11

2.1	Background of The Case Study Area.....	11
2.2	Literature Review.....	14
CHAPTER THREE		19
3.	MODELLING AND DESIGN OF UNIFIED POWER FLOW CONTROLLER....	19
3.1	Overview of FACTs Device.....	19
3.2	Overview of the UPFC and its Operation Principle.....	20
3.2.1	Introduction.....	20
3.2.2	Operation Principle of Unified Power Flow Controller.....	22
3.3	Mathematical Modeling of Unified Power Flow Controller.....	26
3.3.1	Mathematical Modeling of Shunt Converter	26
3.3.2	Shunt Converter Control Variable Reference.....	29
3.3.3	Mathematical Modeling of Series Converter.....	31
3.3.4	Series Converter Control Variable Reference.....	33
3.3.5	Mathematical Modelling of DC Link Capacitor.....	34
3.4	Controller Design of Unified Power Flow Controller.....	36
3.4.1	Controller Design of Shunt Converter	37
3.4.2	Simulink Model of Shunt Converter Controller	38
3.4.3	Controller Design of Series Converter.....	42
3.4.4	Simulink Model of Series Converter Controller.....	43
CHAPTER FOUR.....		47
4.	DESIGN OF ADAPTIVE NEURO-FUZZY-BASED UNIFIED POWER FLOW CONTROLLER AND ITS OPTIMAL LOCATION	47
4.1	Optimal Location of Unified Power Flow Controller Using Modified PSO Integrated With Newton Raphson Algorithm.....	47
4.1.1	Power Flow Study using Newton Raphson Algorithm.....	47
4.1.2	Power Flow Problem.....	47

4.1.3	Modified Particle Swarm Optimization	50
4.1.4	Problem formulation for Particle Swarm Optimization.....	52
4.2	UPFC Converter Sizing.....	56
4.3	Design of Adaptive Neuro-Fuzzy Inference System for Unified Power Flow Controller	61
4.3.1	Background of Neuro Fuzzy Inference System	61
4.3.2	Significance of Adaptive Neuro Fuzzy Inference System	61
4.3.3	Types of Membership Function	62
4.3.4	Architecture of Adaptive Neuro-Fuzzy Inference System.....	64
4.3.5	Design of Neuro Fuzzy Based Unified Power Flow Controller	65
4.3.6	Accuracy of ANFIS Training Data	68
4.3.7	ANFIS Rule Base.....	69
4.3.8	ANFIS Inference System and its Architecture.....	70
4.4	Cost Analysis of Unified Power Flow Controller	71
4.4.1	Annual Energy Loss (MWh) for Each Line in Three Different Scenarios .	74
4.4.2	Payback Period for UPFC Investment Cost.....	80
CHAPTER FIVE		81
5.	SIMULATION RESULT AND DISCUSSION	81
5.1	Introduction	81
5.2	Fault types and its percentage of occurrence in the North-West Region High Voltage Transmission Line	82
5.3	System Performance at Base Case for an Average Load	83
5.4	The Waveforms of NWR 400kV Transmission Line Before and After UPFC Series Voltage Injection	86
5.5	System Response for a Disturbance with and without UPFC	87

5.5.1	System Response when a Fault Occurred at the Midpoint of the Tana Beles to Bahir Dar Transmission Line.....	87
5.5.2	System Response when a Fault Occurred at the Midpoint of the Bahir Dar to D/Markos Transmission Line	94
5.5.3	Sending end and receiving end active power for the NWR transmission line at peak load	100
5.5.4	Voltage magnitude at all buses after incorporating UPFC to the system .	106
CHAPTER SIX.....		107
6.	CONCLUSION AND RECOMMENDATION.....	107
6.1	Conclusion.....	107
6.2	Recommendation and Suggestion for future work.....	108
REFERENCE.....		109
APPENDICES		117

LIST OF FIGURES

Figure 1. 1:Classification of power system stability.....	3
Figure 1. 2:Methodology of the overall system	9
Figure 2. 1:North-West region 400kV and 230kV transmission line route.....	12
Figure 2. 2:Single line diagram of North West region power system above 66kV	13
Figure 3. 1:Classification of FACTs device	20
Figure 3. 2:Basic UPFC schematic diagram	21
Figure 3. 3:A power system with two machines connected by a transmission line with voltage sources v_{sh} and v_{se} representing the UPFC	22
Figure 3. 4:Phasor relationship between the voltage source V_{se} and the line current I_{se} for series compensation	24
Figure 3. 5:Phasor relationship between the midpoint voltage V_m and the series voltage source V_{se} , for phase shifter operation.....	25
Figure 3. 6:Single phase circuit representation of a power flow in UPFC [38].....	26
Figure 3. 7:Shunt device model of UPFC.....	27
Figure 3. 8:Shunt current reference computation	31
Figure 3. 9:Series device model of UPFC	31
Figure 3. 10:Series current reference computation	34
Figure 3. 11:DC link capacitor voltage control model	34
Figure 3. 12:D-Q frame shunt converter control of UPFC	38
Figure 3. 13:SIMULINK model of shunt converter controller.....	39
Figure 3. 14:PI based AC voltage regulator for i_{q-ref}	40
Figure 3. 15:Control variable computation for v_{shd}^* and v_{shq}^*	40
Figure 3. 16:PI based DC voltage regulator for i_{d-ref}	41
Figure 3. 17:Shunt voltage source converter (switches).....	41
Figure 3. 18:D-Q frame of series converter control of UPFC	43
Figure 3. 19:SIMULINK models of series converter controller.....	44
Figure 3. 20:Simulink model of d-axis and q-axis reference current computation of series controller of UPFC.....	45
Figure 3. 21:D-axis and Q-axis reference voltage of series converter.....	45
Figure 3. 22:Series voltage source converter (switches)	46

Figure 4. 1:A typical bus of power system	47
Figure 4. 2:Flow chart of the modified PSO for UPFC placement.....	55
Figure 4. 3:Convergence characteristics at peak load for 50 iteration.....	56
Figure 4. 4:Fundamental frequency model of UPFC.....	58
Figure 4. 5:Architecture of adaptive neuro fuzzy inference system	64
Figure 4. 6:Block diagram of adaptive neuro fuzzy inference system for iq-reference ...	66
Figure 4. 7:Block diagram of adaptive neuro fuzzy inference system for id-reference ...	66
Figure 4. 8:ANFIS based iq-reference computation.....	67
Figure 4. 9:ANFIS based id-reference computation.....	67
Figure 4. 10:Accuracy of ANFIS training data for UPFC model.....	69
Figure 4. 11:Fuzzy inference rules of ANFIS.....	69
Figure 4. 12:ANFIS Sugeno inference system	70
Figure 4. 13:Anfis model structure	71
Figure 5. 1:Percentage of fault occurring in NWR recorded in 2021 G.C	83
Figure 5. 2:Base case rotor speed deviation response without disturbance dw(pu)	84
Figure 5. 3: Base case rotor angle deviation response (rad) without disturbance.....	84
Figure 5. 4:Base case rotor speed response(pu) without disturbance	85
Figure 5. 5:Base case output active power P_{eo} (pu) response without disturbance	85
Figure 5. 6:The voltage waveforms of NWR 400kV transmission line before and after series injected voltage by UPFC	87
Figure 5. 7:Rotor angle deviation response for 3ph-G fault occurred at the midpoint of the Tana Beles to Bahir Dar transmission line with and without UPFC	88
Figure 5. 8:Rotor speed response for 3ph-G fault occurred at the midpoint of the Tana Beles to Bahir Dar transmission line with and without UPFC	88
Figure 5. 9:Rotor speed deviation response for 3ph-G fault occurred at the midpoint of the Tana Beles to Bahir Dar transmission line with and without UPFC	89
Figure 5. 10:Output active power response for 3ph-G fault occurred at the midpoint of the Tana Beles to Bahir Dar transmission line with and without UPFC	89
Figure 5. 11:Rotor angle deviation response for 1ph-G fault occurred at the midpoint of the Tana Beles to Bahir Dar transmission line with and without UPFC	91

Figure 5. 12:Rotor speed response for 1ph-G fault occurred at the midpoint of the Tana Beles to Bahir Dar transmission line with and without UPFC 91

Figure 5. 13:Rotor speed deviation response for 1ph-G fault occurred at the midpoint of the Tana Beles to Bahir Dar transmission line with and without UPFC 92

Figure 5. 14:Output active power response for 1ph-G fault occurred at the midpoint of the Tana Beles to Bahir Dar transmission line with and without UPFC 92

Figure 5. 15:Rotor angle deviation response for 3ph-G fault occurred at the midpoint of the Bahir Dar to D/Markos transmission line with and without UPFC 94

Figure 5. 16:Rotor speed response for 3ph-G fault occurred at the midpoint of the Bahir Dar to D/Markos transmission line with and without UPFC 95

Figure 5. 17:Rotor speed deviation response for 3ph-G fault occurred at the midpoint of the Bahir Dar to D/Markos transmission line with and without UPFC 95

Figure 5. 18:Output active power response for 3ph-G fault occurred at the midpoint of the Bahir Dar to D/Markos transmission line with and without UPFC 96

Figure 5. 19:Rotor angle deviation response for 1ph-G fault occurred at the midpoint of the Bahir Dar to D/Markos transmission line with and without UPFC 97

Figure 5. 20:Rotor speed response for 1ph-G fault occurred at the midpoint of the Bahir Dar to D/Markos transmission line with and without UPFC 98

Figure 5. 21:Rotor speed deviation response for 1ph-G fault occurred at the midpoint of the Bahir Dar to D/Markos transmission line with and without UPFC 98

Figure 5. 22:Output active power response for 1ph-G fault occurred at the midpoint of the Bahir Dar to D/Markos transmission line with and without UPFC 99

Figure 5. 23:Sending end active power from Tana beles to Bahir Dar transmission line 100

Figure 5. 24:Receiving end active power from Tana beles to Bahir Dar transmission line without UPFC 101

Figure 5. 25:Receiving end active power from Tana beles to Bahir Dar transmission line with PI-based UPFC 101

Figure 5. 26:Receiving end active power from Tana beles to Bahir Dar transmission line with ANFIS-based UPFC 102

Figure 5. 27:Sending end active power from Bahir Dar to D/Markos transmission line 103

Figure 5. 28:Receiving end active power from Bahir Dar to D/Markos transmission line without UPFC	104
Figure 5. 29:Receiving end active power from Bahir Dar to D/Markos transmission line with PI-based UPFC	104
Figure 5. 30:Receiving end active power from Bahir Dar to D/Markos transmission line with ANFIS-based UPFC	105

LIST OF TABLES

Table 4. 1:Bus voltage magnitude using PSO at three loading scenarios.....	55
Table 4. 2:Block parameters of shunt and series transformer.....	60
Table 4. 3:Characterstics of PID controller	67
Table 4. 4:Power loss from Beles to Bahir Dar line under various load	72
Table 4. 5:Power loss from Bahir Dar to D/Markos line under various load	72
Table 4. 6:Power loss from Bahir Dar to Mota line under various load.....	72
Table 4. 7:Power loss from Bahir Dar to Alamata line under various load.....	73
Table 4. 8:Power loss from Bahir Dar to Gonder I line under various load.....	73
Table 4. 9:Power loss from Bahir Dar to Gonder II line under various load.....	73
Table 4. 10:Power loss from D/Markos to Mota line under various load.....	73
Table 4. 11:Power loss from Bahir Dar to Dangila line under various load.....	74
Table 4. 12:The Annual energy loss from Bahir Dar to D/Markos line without UPFC...	75
Table 4. 13:The Annual energy loss from Bahir Dar to D/Markos line with ANFIS-based-UPFC.....	75
Table 4. 14:The Annual energy loss from Bahir Dar to Mota line without UPFC.....	75
Table 4. 15:The Annual energy loss from Bahir Dar to Mota line with ANFIS-based-UPFC	76
Table 4. 16:The Annual energy loss from Bahir Dar to Alamata line without UPFC.....	76
Table 4. 17:The Annual energy loss from Bahir Dar to Alamata line with ANFIS-based-UPFC.....	76
Table 4. 18:The Annual energy loss from Bahir Dar to Gonder I line without UPFC.....	77
Table 4. 19:The Annual energy loss from Bahir Dar to Gonder I line with ANFIS-based-UPFC.....	77
Table 4. 20:The Annual energy loss from Bahir Dar to Gonder II line without UPFC....	77
Table 4. 21:The Annual energy loss from Bahir Dar to Gonder II line with ANFIS-based-UPFC.....	77
Table 4. 22:The Annual energy loss from D/Markos to Mota line without UPFC	78
Table 4. 23:The Annual energy loss from D/Markos to Mota line with ANFIS-based-UPFC	78
Table 4. 24:The Annual energy loss from Bahir Dar to Dangila line without UPFC.....	78

Table 4. 25:The Annual energy loss from Bahir Dar to Dangila line with ANFIS-based-UPFC.....	78
Table 4. 26:Typical investment cost for different FACTs controller [54].....	79
Table 4. 27:Ethiopias energy tariff for all consumer levels.....	80
Table 4. 28:Total energy saved annually for all transmission lines.....	80
Table 5. 1: Fault type occurring in NWR and its duration of interruption	82
Table 5. 2:Comparison of the system response for different variables with and without UPFC when 3ph-G fault occurred at the midpoint of the Tana Beles to Bahir Dar transmission line	90
Table 5. 3:Comparison of the system response for different variables with and without UPFC when 1ph-G fault occurred at the midpoint of the Tana Beles to Bahir Dar transmission line	93
Table 5. 4:Comparison of the system response for different variables with and without UPFC when 3ph-G fault occurred at the midpoint of the Bahir Dar to D/Markos transmission line	96
Table 5. 5:Comparison of the system response for different variables with and without UPFC when 1ph-G fault occurred at the midpoint of the Bahir Dar to D/Markos transmission line	99
Table 5. 6:Loss minimized after incorporating UPFC to the transmission line.....	102
Table 5. 7:Loss minimized after incorporating UPFC to the transmission line.....	105
Table 5. 8:Voltage magnitude at all buses after incorporating UPFC to the system	106

LIST OF ABBREVIATIONS

ANFIS	Adaptive Neuro Fuzzy Controller
ANN	Artificial neural network
ANNs	Artificial Neural Networks
EELPA	Ethiopian Electric Light and Power Authority
FACTS	Flexible AC Transmission System
FIS	Fuzzy Inference System
FPSS	Fuzzy Power System Stabilizer
GD	Gradient Descent
GTO	Gate Turn-off Thyristor
GUI	Graphical User Interface
IEEE	Institute of Electrical and Electronics Engineers
IGBT	Insulated Gate Bipolar Transistor
IPFC	Interline Power Flow Controller
KCL	Kirchhoff's Current law
KVAR	kilovolt Amps Reactive
KVL	Kirchhoff's voltage law
LFO	Load Frequency Control
LSE	Least Square Estimation
MF	Membership Function
NR	Newton Raphson

NWR	North West region
PI	Proportional Integral
PID	Proportional Integral Derivative
PLL	Phase Lock Loop
PSO	Particle Swarm Optimization
PWM	Pulse Width Modulation
SMIB	Single machine infinite bus
SSSC	Static Synchronous Series Compensator
STATCOM	Static Synchronous Compensator
STATCON	Static Synchronous Condenser
SVC	Static Var Compensator
TCR	Thyristor Controlled Reactor
TCSC	Thyristor Controlled Series Capacitor
THD	Total harmonic distortion
UPFC	Unified Power Flow Controller
VSC	Voltage Source Convertor

CHAPTER ONE

1. INTRODUCTION

1.1 Background of The Study

Power system is a complex nonlinear and dynamic system, with its operating parameters continuously changing with time. The dynamic nature of the power system causes frequent disturbances in the system which can drive the system to an unstable state. This continuous disturbances will lower the power system reliability and power quality index of the system [1]. Different types of power system instability have emerged as a result of the continued increase of interconnections, the application of new controls and technology, and improved performance under severely stressful conditions in power systems. Due to the environment of power system interconnection and commercialization, today's modern power system confront severe challenges [2].

Power system stability is the ability of power system, for a given initial operating condition, to regain a state of operating equilibrium after being subjected to some form of physical disturbance, with most system variables bounded so that system integrity is preserved. In general, the integrity of the system is maintained when practically the entire power system remains intact with no tripping of generators or loads, except for those disconnected by isolation of the faulted elements or intentionally tripped to preserve the continuity of operation of the rest of the system. Instability arises when a disturbance causes a persistent imbalance between supply and demand. Stability is a situation of equilibrium between supply and demand [3].

Transient stability is the ability of the power system to sustain the synchronism following a sudden large disturbance. These alterations could be brought on by a quick application of load, a loss of generation, a loss of a large size load, or a system breakdown [4]. In power plants, several synchronous generators are connected to the bus having the same frequency and phase sequence as the generators. Therefore, for a stable operation, we have to synchronize the bus with the generators over the entire duration of generation and transmission [5] [6].

The power system, which is frequently mechanically controlled, connects generating units to load centers via high voltage transmission lines. To fully utilize the existing generating units and to load existing transmission lines close to their thermal limits, stability has to be maintained at all times. Replacing mechanical controllers by reliable and high speed power electronic devices can solve the problem. This can be achieved with the proper control strategy of FACTS devices which could greatly increase the transient stability margin. FACTS devices are increasingly used as cost effective measures to improve transmission capacity, oscillation damping and stability improvement. This allows increased utilization of existing network closer to its thermal loading capacity, and thus avoiding the need to construct new transmission lines [7].

Amongst the available FACTS devices, the Unified Power Flow Controller (UPFC) is the most versatile one that can be used to enhance system stability. The UPFC is capable of both supplying and absorbing real and reactive power, which consists of two AC-to-DC converters. One of the two converters is connected in series with the transmission line through a series transformer and the other in parallel with the line through a shunt transformer. The DC side of the two converters is connected through a common capacitor, which provides DC voltage for the converter operation [8].

As the UPFC's series branch injects a voltage with variable magnitude and phase angle, it can exchange real power with the transmission line, improving both the line's capability for power flow and its transient stability limit. The shunt converter exchanges a current of controllable magnitude and power factor angle with the power system. It is normally controlled to balance the real power absorbed from or injected to the power system by the series converter plus the losses by regulating the dc bus voltage at a desired value. Different advanced control techniques are used and simulated to control UPFC input parameters. The combination of fuzzy logic and neural network are used for the purpose of providing robust control and transient stability over a wide range of power system operating conditions [9].

1.2 Classification of Power System Stability

Based on the physical mechanism responsible for the instability, power system stability is classified into three major groups as depicted in the figure below.

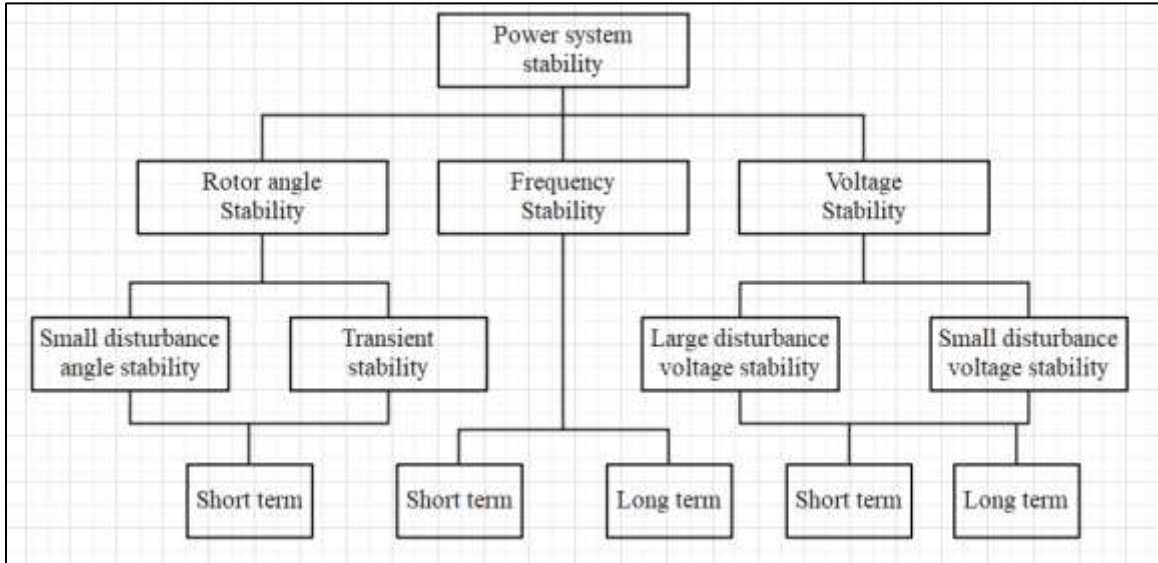


Figure 1. 1:Classification of power system stability

1.2.1 Rotor Angle Stability

The ability of the interconnected synchronous machines functioning in the power system to maintain the state of synchronism is referred as rotor angle stability (i.e torque balance of synchronous machine). The impact of the generator's rotor angle on two synchronous generators operating in parallel and supplying active power to the load [10].

Rotor angle stability can be classified into two categories.

- ❖ **Small disturbance (small signal) stability:** ability to maintain synchronism in the presence of small disruptions. Due to small disturbance nonlinear differential equations can be linearized . it is easy to solve such problem.
- ❖ **Large disturbance (transient) stability:** Ability to maintain synchronism under large disturbances. Since disturbances are large, nonlinear differential equations cannot be linearized. It has to be solved numerically. It is difficult to solve. However, we can use a graphical approach called equal area criterion for analyzing the stability of a single machine connected to an infinite bus using the classical model.

1.2.2 Voltage Stability

The ability of a power system to maintain steady, acceptable voltages at all of its buses during normal operation and following a disturbance is known as voltage stability (or reactive power balance). A power system's voltage is stable under normal operating conditions, but when a malfunction or other disturbance occurs, the voltage becomes unstable, leading to a steady and uncontrollable drop in voltage [11].

If the post-disturbance equilibrium voltage near loads is below acceptable bounds, a power system may undergo voltage collapse as a result of the voltage instability. Another definition of voltage collapse is the process through which voltage instability benefits from a very low voltage profile in the critical area of the system. Total or partial blackouts may result from voltage collapse. Voltage collapse and voltage instability are frequently used interchangeably. Voltage stability can be classified into two categories [12].

- ❖ **Large disturbance (transient) voltage stability:** It is concerned with maintaining system stability in order to control voltages after a significant disturbance such as faults, loss of load, or loss of generation.. Non-linear time domain simulations with appropriate modelling can be used to study large disturbance voltage studies. The study period may extend from a few seconds to tens of minutes. It is a long-term study.
- ❖ **Small disturbance (small signal) voltage stability:** A power system's operational state is described as having small disturbances voltage stability When there are small disturbances in the system, the voltage near the loads does not fluctuate or remains close to the pre-disturbance values. In order to examine the idea of small disturbance stability, a small-signal model of the system is necessary . If V-Q sensitivity is positive for every bus, a system is voltage stable and unstable if V – Q sensitivity is negative for at least one bus.

1.2.3 Frequency Stability

The ability of a power system to retain steady frequency after a significant disturbance between the generation and load is known as frequency stability. The frequency of the entire system will be affected if the total power supplied to the system by the prime movers is less than what is consumed by the loads, including losses. The imbalance is global rather than local. Frequency stability may be short-term or long-term [13].

1.3 Motivation

Historically, Ethiopia has been plagued by frequent voltage fluctuations and power outages. A 2020 World Bank report estimated that 80 % of Ethiopian manufacturing and retail firms experienced on average 8.2 electrical outages in a typical month, with an average outage duration of 6 hours [14].

Citizens, businesses and government institutions alike continually complain about these power disruptions and the effect it has on their ability to get on with day to day life. The poor quality due to transient stability problem are often cited as major limiting factors in sustaining the nation's impressive economic growth. In industry and business, without the availability and assurity of a stable and constant grid power supply, the use of expensive off-grid generators is commonplace. The World Bank, in their 2020 report, estimated that almost half (48.9%) of the total electricity demand from manufacturing and retail firms was satisfied by the use of off-grid generators [14].

The economy in Ethiopia is one of the fastest growing in the world, with an average growth rate of 10.8% since 2005. Due to the rapid GDP growth, demand for electricity has been steadily increasing. With a national peak demand of 2,500 megawatts dropping to 700 megawatts off-peak, until recently generating capacity was a mere 2,400 megawatts, but in the last few years, because of new resources coming online, capacity has risen to 4,500 megawatts, but availability has been let down due to weaknesses in the transmission line maximum power transfer capacity. This problem is particularly severe in the north-west region high voltage transmission power system. The reduction of power outages and maximising the capacity of power transfer for high-voltage transmission lines through full utilisation of the existing transmission facilities with improved power system stability form the foundation of this thesis study [14].

1.4 Statement of the Problem

The current energy markets, economy, and population growth, combined with the power demand, increase the complexity of power systems that operate close to their maximum capacity limits. This results in high operational costs, and in the worst case, it is exposed to a partial power system collapse or total blackout of the power system. From a cost perspective, taking immediate corrective action on the existing system network as soon as the disturbance occurs must be prioritised over installing new power plants. Transient instability brings extensive problems to the power system networks, such as breakdowns of machinery, an increase in maintenance costs, a loss of product time for the manufacturing industry, etc. A transmission line fault is a major disturbance that causes power system instability.

The Ethiopian power system in the North West Region (NWR) frequently suffers from this problem due to different disturbances and power interruptions that occur at different events. In 2021, the total power interruption in the North West region of Ethiopia's interconnected power system recorded for 10 months was 210.92 hours. This power interruption affects both the normal operation of power system components as well as the economy of the country. Therefore, considering this problem, it is better to minimise the impact of interruption by means of transient stability enhancement using an adaptive neuro-fuzzy-based flexible AC transmission system (FACTS) device.

This thesis is primarily concerned with enhancing the transient stability of the NWR Ethiopian power system through the use of an adaptive neuro-fuzzy-based unified power flow controller (UPFC), which is one of the fast and versatile FACT devices. For the study area's transient stability to be efficient and effective, the UPFC must be properly sized and placed.

1.5 Objectives

1.5.1 General Objective

The main objective of this thesis work is to investigate the enhancement of transient stability and loss minimization in a transmission line in the North-West region using an adaptive neuro-fuzzy-based unified power flow controller.

1.5.2 Specific Objectives

- To observe the existing network structure and operating condition of North-West region high voltage transmission power system.
- To develop mathematical model for shunt, series and DC component of UPFC.
- To design and model the size of ANFIS-based-UPFC and determine its placement using Particle Swarm Optimization.
- To compare the system with ANFIS-based UPFC and without UPFC, with a conventional controller.
- To calculate the total loss reduced after incorporating ANFIS-based-UPFC.
- To analyse the cost before and after using the Unified Power Flow Controller.

1.6 Significance of The Thesis

Transient stability analysis and enhancement of power systems help to ensure the security and reliability of electrical energy following severe disturbances. When the entire power system remains intact with no tripping, except for those that are tripped to protect the power system due to the faulted elements, the system's integrity can be preserved. The purpose of this thesis is to design a unified power flow controller using artificial intelligence. This is essential:

- To ensure the security and reliability of the NWR interconnected power system.
- To reduce cascaded line outages and system blackouts of the power system.
- To increase the life span of the electrical and mechanical equipment.
- To decrease the bankruptcy which occurs during power interruption (especially in the manufacturing industry) and to decrease the cost of maintenance.
- To increase the power transfer capacity of transmission line.

1.7 Scope of The Study

The main focus of this thesis is to develop an ANFIS-based UPFC that is capable of enhancing the transient stability of NWR's 400 kV interconnected power system. This covers the design and sizing of UPFC controllers. The designed controller is optimally placed using PSO. This thesis compares ANFIS-based UPFC with PI-based UPFC under different disturbance scenarios with various transient stability performance indices such as percentage overshoot and settling time. Active power transfer in transmission lines is also studied before and after incorporating UPFC. Simulation have been performed in a MATLAB/SIMULINK environment.

1.8 Methodology

To complete this thesis, a sequence of tasks is conducted based on the following steps:

- ❖ **Literature Review:** Review different papers such as journal articles, books, book sections, articles in a periodical, conference proceedings, reports, and other papers related to transient stability improvement using a different controller.
- ❖ **Data Collection:** The following data have been collected from NWR office and literatures:
 - Transmission line data and bus data
 - Generator data
 - Transformer data
 - Average load, peak load, and minimum load of the system
 - SCADA single line digram of the network
 - Interruption duration time of each load
 - Type of fault occurred during each interruption
- ❖ **Data Analysis:** The raw data that has been collected from the NWR office is analysed to model the system in MATLAB/Simulink. The transmission line data, bus data, generation data, and load data are used to optimally place UPFC using particle swarm optimization.
- ❖ **System Modeling and Simulation:** The proposed study network was modelled and analysed in MATLAB according to the existing network of the NWR Ethiopian Power Network. Once the system is designed, PI-based UPFC and ANFIS-based UPFC are

applied, and the comparative analysis of their performance to improve power system stability is carried out. Next, the simulation of the system in different scenarios with the application of a unified power flow controller is performed and the results will be analyzed in different performance indices (such as settling time, overshoot).

- ❖ **Result and Conclusion:** Conclusions and simulation results are stated based on the given results presented in the final report of the thesis. Finally, recommendations about the proposed method are forwarded in the thesis.

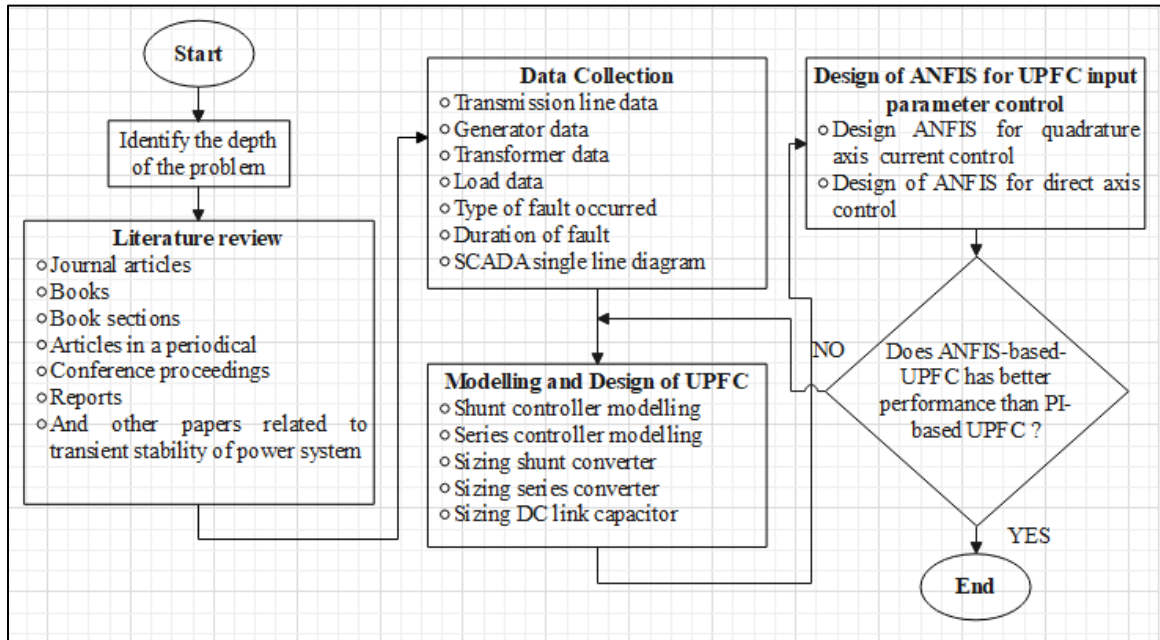


Figure 1. 2:Methodology of the overall system

1.9 Organization of The Thesis

This thesis is organised into six chapters, and each chapter description is presented as shown below:

Chapter One: This chapter focuses on the introduction, which consists of the background of the study, motivation, a statement of the problem, general and specific objectives, the significance of the study, the scope of the study, the methodology used to complete the work, and the organisation of the thesis.

Chapter Two : This chapter is about reviewing the different literature that has been done related to this work and the theoretical background of the study area.

Chapter Three : This chapter discusses the modelling and design of a unified power flow controller, which includes an overview of the FACTS device, an overview of unified power flow controller operation principles, and the mathematical modelling of a unified power flow controller. The mathematical modelling of a unified power flow controller comprises shunt converter modeling, series converter modeling, and DC link capacitor modeling.

Chapter Four : This chapter deals with the design of an adaptive neuro-fuzzy-based unified power flow controller and its optimal location, which includes the design of a shunt converter, the design of a series converter, the optimal location of the unified power flow controller using modified particle swarm optimization integrated with the Newton Raphson algorithm, the sizing of the unified power flow controller, the design of PI-based unified power controller, and the design of an adaptive neuro-fuzzy-based unified power controller.

Chapter Five : This chapter mainly discusses simulation result and discussion. This includes performance evaluation of the system at steady state (the "base case"), the performance evaluation of the system without UPFC, with PI-based UPFC, and with ANFIS-based UPFC when different faults are applied at different sections of the transmission line. Finally, it compares the total loss reduced before and after incorporating UPFC, the transient stability enhancement with different performance indices, the voltage profile before and after series injected voltage.

Chapter Six : This chapter deals with the main research findings that lead to a conclusion as well as recommendations and future work.

CHAPTER TWO

2. LITERATURE REVIEW AND THEORETICAL BACKGROUND

2.1 Background of The Case Study Area

Ethiopian Electric Power Corporation (EEPCO), a state-owned monopoly that generates, transmits, and distributes and sells electric power nationwide. The company was formed in 1956 E.C as the Ethiopian Electric Light and Power Authority (EELPA), which bundled all Ethiopian activities around electricity in a single organization. This company have served over 50 years. Now a days, the corporation has about 2 million customers in the country and has also recently started exporting power to neighbouring Djibouti and Kenya for a monthly fee of 1.5 million dollars for 35 megawatts of power. It plans to expand the foreign market to other countries such as Sudan and Eritrea in the near future [15].

Tis abay and Tana beles are the primary electrical energy sources for EELPA from the NWR side. Tana Beles is used as a base load next to Gibe III. This thesis area is the NWR high-voltage interconnected transmission system, which contains power lines incoming from Tana Beles and Tis Abay. From the Tisabay side, 132 kV is coming to the Bahirdar II substation and being converted to 230 kV. From Tana Beles's side, a double line of 400 kV is coming to Bahrdar Substation II and stepping down to 230kV. The 230kV from both sides is connected via bus bar coupler and feeds Alamata (230kV), Gondar-1 (230kV), Gondar-2 (230kV), Mota (230kV), Dangila (66kV), and Bahir Dar-1 (66kV). On the other hand, 400 kV is directly outgoing to Debremarkos after getting into the Bahir Dar switching station [16].



Figure 2. 1:North-West region 400kV and 230kV transmission line route

The Beles Hydroelectric Power Plant is a run-of-river hydroelectric power plant in Ethiopia near Lake Tana. The power plant receives water from the lake through the Tana-Beles interbasin transfer and after utilizing it to produce electricity, the water is then discharged into the Beles River. The plant has a capacity of 460 MW and is the country's third-largest power plant, next to Gibe III and GERD. It was inaugurated in May 2010 and the last generator was operational in February 2012. Its construction was negatively perceived by downstream Egypt.

Tis Abay II hydropower plant has a capacity of 73MW. Tis Abay I hydropower plant has a capacity of 11.4MW. It is located on the Abay River Basin 32.2 km apart from Bahir Dar. It has been developed in single phase. The Tis Abay II hydropower plant began commercial operation in 2001, while the Tis Abay I hydropower plant began commercial operation in 1964 [17].

The single-line diagram of a North-West region power system, which shows the main connections of the system components above 66 kV, is depicted as shown below.

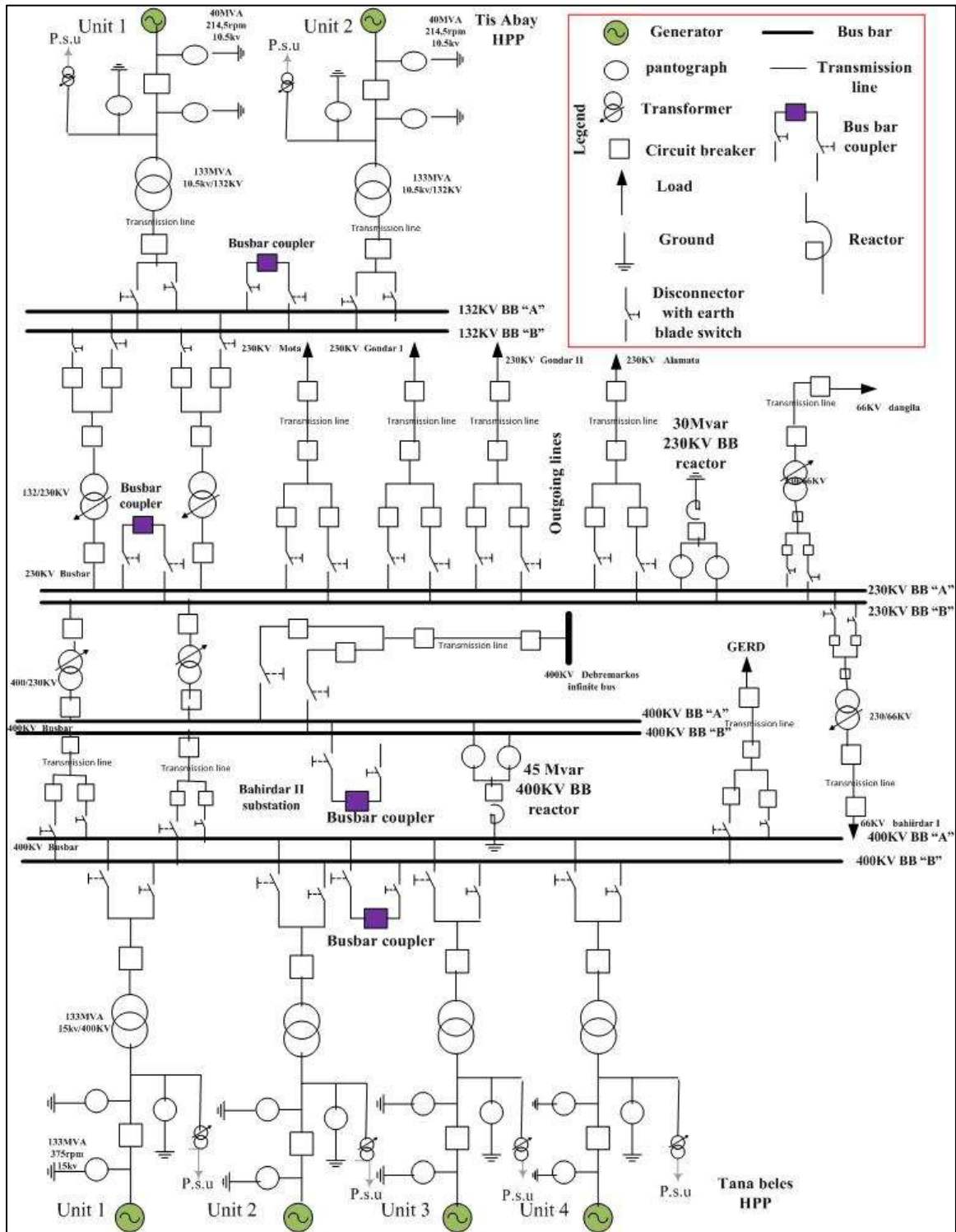


Figure 2. 2:Single line diagram of North West region power system above 66kV

2.2 Literature Review

This section provides an overview of previous related efforts about transient stability enhancement. The knowledge gained in reviewing different papers is extremely useful in the preliminary design and simulation of this thesis i.e Neuro-fuzzy-based unified power flow controller for transient stability enhancement of high voltage transmission power system.

I.Muzaffer and M. Uddin Mufti [18] in 2017 advocated modeling of a multi-machine system aided with power system stabilizers and shunt compensator for transient stability enhancement. The aim of this study is to investigate the collective effects of two diverse techniques (i.e power system stabilizers and shunt compensation) on improving both rotor angle stability and voltage stability. The compact and user-friendly design is intended to be helpful in real-world application. A power system stabiliser assigned to each generator achieves damping of rotor angle oscillations, and a shunt compensator achieves bus voltage stability. The system can also able to withstand sudden unprecedented changes in load without any adverse effects on stability. However, it focuses on improving transient stability at the generation level only. Further work can be done to determine what will be the response of the generator at generation level when a disturbance happens at transmission line level so that transient stability can be investigated both at generation level and transmission line level.

S.Siddula et al [19] in 2020 examined improvement of power quality using fuzzy based unified power flow controller. The Fuzzy logic controller is introduced, developed by the Mamdani type inference method replacing PI controller on a transmission line under different power system operating conditions. It was observed that the UPFC with the Fuzzy logic based control technique in improving voltage stability has superior transient oscillation damping performance than that of UPFC with the PI controller. However, the accuracy of the systems are completely dependant on human knowledge and expertise and compromised as the system mostly works on inaccurate data and inputs. If the expert assigns the wrong rules, then fuzzy logic controller may provide poor performance even than PID controller.

R. Kumar and M. Kumar [20] in 2015 suggested improvement of power system stability using unified power flow controller based on hybrid fuzzy logic-PID tuning in SMIB system. In order to providing stabilizer signal, the output of obtained model reference of power system is compared with output of real power system and the error signal is fed to a fuzzy controller. The suggested controller has better performance in damping low frequency oscillations. However, to study power system stability over a wide range of the system, this work focuses on a single machine infinite bus system rather than a multimachine power system.

S. Hadjeri et al [21] in 2016 investigated the impact of PSS and SVC on the power system transient stability. The findings show that a system for the stability of transients in a two-machine transmission system with PSS and SVC has been successfully developed. The basic structure of power system stabilizer is operating under typical control of generator while the basic structure of static var compensator is operating under typical bus voltage control. The results of these studies demonstrate that the selective of (PSS) are capable of providing sufficient damping to the steady state oscillation and transient stability voltages performance over a wide range of operating conditions and the SVC has an excellent capability in damping power system oscillations and enhances the dynamic stability of the power system. However, SVC responds slower than other voltage source converter-based FACTS devices, such as an unified power flow controller.

B. V. Khurana and L. S. Titare [22] in 2020 examined improvement of power flow and voltage stability using UPFC with artificial neural network in Matlab. The basic UPFC system uses two separate system model architectures, STATCOM AND SSSC to compensate for high voltage power transmission line voltage and current. Both are reusing higher voltage power transmission and consume more time period for power stabilization. Hence generating transmission impedance mismatching. This problem is solved by designing a UPFC using ANN algorithm simulation model. Artificial neural network gives a better result and compared to previous UPFC controller like PID and fuzzy logic in terms of reducing settling time. ANN learning duration is higher in case of huge training data or complicated systems.

K.B.Mohanty and S.Pati [23] in 2016 suggested fuzzy logic controller based STATCOM for voltage profile improvement in a micro-grid. The voltage profile of the single alternator based radial microgrid system is improved using a STATCOM. The controllers used for the control of STATCOM i.e. PI and fuzzy logic controller are designed. It is found that the steady state error is more with PI controller where as fuzzy logic controller gives better results with small steady state error. Overshoots and settling time are also less with fuzzy logic controllers. The voltage deviation due to load change with fuzzy logic controllers is much less than conventional PI controllers. These all performances prove that fuzzy logic controller gives robust performance as compared to conventional PI controller in all types of load conditions. However, fuzzy logic controller performance depends on the expert. If the expert assigns the wrong rules, then fuzzy logic controller may provide poor performance even than PID controller.

M.Roy and A.K.Kori [24] in 2021 developed fuzzy logic based improvement of UPFC performance in power system. The observation and investigation of Fuzzy based UPFC system gives a better stability, lower transient, lower damping and lower value of percentage of total harmonic distortion (THD). The developed model results lower THD for both nonlinear load and linear load. Hence this is applicable to HVAC power transmission system because reduced of transmission loss and gives a proper impedance matching transmitter end to receiver end. However, the controller's performance is insignificant in terms of improving transient stability compared with neuro-fuzzy based unified power flow controller.

P.Das et al [25] in 2016 examined the voltage stability improvement by using fuzzy logic controller in multimachine power system. The SVC with fuzzy logic controller has been tested in a 2- machines 3-bus power system where several parameters including the difference of rotor angle between the machines, speed of the machines, terminal voltage and the transmission line active power have been observed. The performance of the system implemented with the fuzzy based SVC controller. The system implemented with the fuzzy-SVC controller show better performance in damping oscillations, maintain terminal voltage, and controlling the power after the system is subjected to disturbance. However, in this work, the fuzzy based SVC controller has a deliberate dynamic response since its

highly nonlinearity property causes the system to be uncertain to improve transient stability.

H.Rahman et al [26] in 2012 examined the Stability Improvement of Power System by Using SVC With PID Controller. They present the stability improvement of voltage level, machine oscillation damping, real and reactive power in a power system model of SVC with and without properly tuned PID controller for different types of faulted conditions. The result shows PID is a very efficient controller for SVC to enhance the power system stability. However, in this work PID controller have inadequacy of providing robust control over a wide range of power system operating conditions.

V.S.krishna et al [27] in 2015 have studied the enhancement of transient stability in a multimachine power system using adaptive neuro-fuzzy controller for FACTs devices. In this paper, Transient Stability improvement and Power Oscillation damping of a three-machine power system by various FACTs devices such as SSSC and UPFC is analyzed. It is clear from the simulation results that there is a considerable improvement in the system performance with the presence of UPFC for which the settling time and amplitude of LFO is reduced when compared to SSSC and lead-lag, which shows that the proposed UPFC-based neuro-fuzzy controller provides efficient damping to power system oscillations and greatly improves the system voltage profile. But the system have large overshoot to damp the oscillation compared to ANFIS based UPFC.

L. Vetoshkin et al [28] in 2019 studied improvement of transient stability using STATCOM combined with optimization. It clearly presents an approach to improvement of transient stability through utilization FACTs devce, particularly STATCOM(Static Synchronous Compensators) combined with optimization. The authors applied optimization technique to determine controllers gains. The examinations of results yield that third definition of objective functions is probably better for the improvement of transient stability. However, it may be valid only for STATCOM in the midpoint of the transmission between a generator and an electric grid. Definitely, more case studies must be done, and they have to include different types of FACTS devices.

S. Khan and S. Bhowmick [29] in 2015 examined a fuzzy TCSC Controller for transient stability improvement. In this work, the effectiveness of a FLC-based-TCSC damping controller in improving the transient stability of a SMIB system is analysed. At first, the SMIB system is analysed. without the TCSC. The clearing time of the system was observed to be 0.086 sec. Subsequently, a FLC-based-TCSC damping controller was employed. The rotor speed deviation and rotor angle deviation were taken as the two inputs to the FLC. The firing angle deviation of the TCSC is obtained as the output signal. It is observed that with the FLC-based-TCSC damping controller, the clearing time of the system increases to a value of 0.18 sec. It is observed that the transient stability of the system is markedly improved. However, TCSC is a series compensator only, and it is investigated in SMIB only.

All the above researchers have done effective work regarding transient stability enhancement using different FACTS devices. This understandably paves the way to this thesis work. This thesis is going to enhance transient stability of North West region 400 kV system using ANFIS based UPFC. Shunt and series converters have been designed, and optimal placement of UPFC using particle swarm optimization has been selected. Finally, the performance of the selected controller is compared with a conventional controller such as a PI-based UPFC controller. Also, the power transfer capability of UPFC and the reduced total loss have been investigated.

CHAPTER THREE

3. MODELLING AND DESIGN OF UNIFIED POWER FLOW CONTROLLER

3.1 Overview of FACTs Device

A system made up of static equipment used for the transmission of electrical energy using alternating current (AC) is known as a flexible alternating current transmission system (FACTS). Among several techniques for improving transient stability, the FACTS device is essential as it is a fast and soft switching power electronics-based device. This helps to enhance the controllability and power transmission capacity of the network. Power electronics are typically the basis of the system. This static power-electronic device is installed in AC transmission networks to increase power transfer capability, stability, and controllability of the networks through series or shunt compensation [30].

These issues were resolved using mechanical switches to connect capacitors, reactors, or synchronous generators long before the advent of power electronics switches. However, there are numerous problems with using mechanical switches. It responds quite slowly, and mechanical switches are susceptible to wear and strain. In order to make the transmission line more stable and controllable, these methods are not reliable. Power electronics-based FACTs controllers were developed following the invention of power electronics switches such as the thyristor, which can be used for high-voltage applications [31].

Based on the arrangement to be installed in the transmission line and its converter, FACTs devices can be classified into three categories.

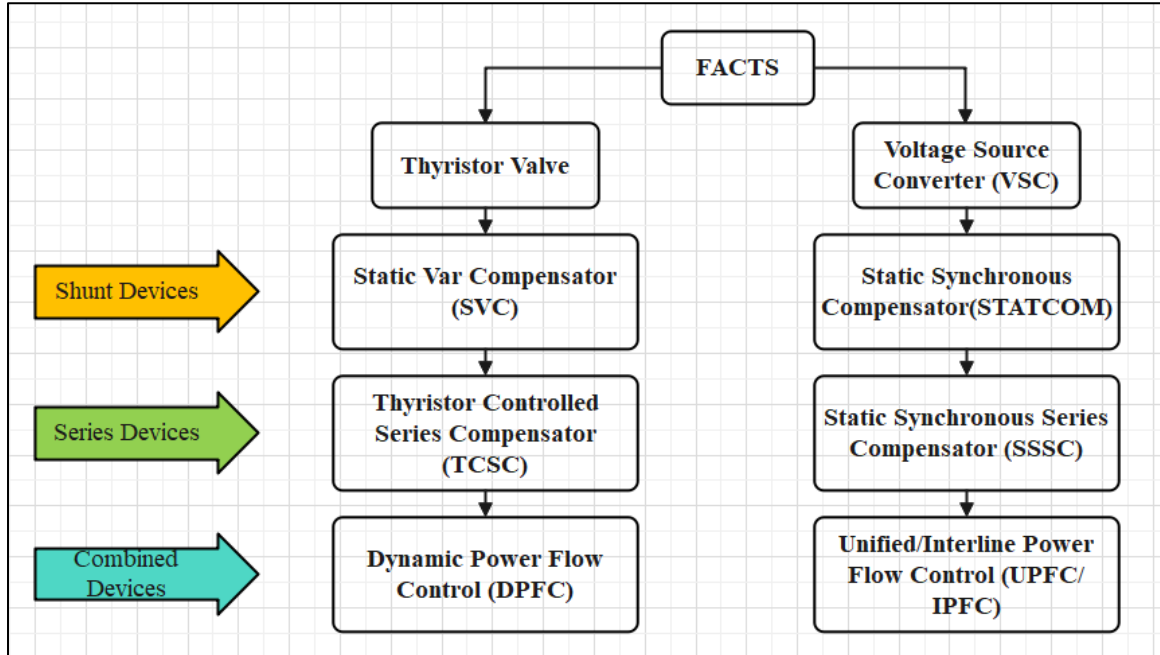


Figure 3. 1:Classification of FACTS device

3.2 Overview of the UPFC and its Operation Principle

3.2.1 Introduction

The UPFC concept was proposed by Gyugyi in 1991. It is able to control, simultaneously or selectively, all the parameters affecting power flow in the transmission line (i.e., voltage, impedance, and phase angle). UPFC is a combined series-shunt controller consisting of two switching converters operated by a common DC link [32].

UPFC consists of two back-to-back converters named VSC1 and VSC2, which are operated from a DC link provided by a DC storage capacitor. These arrangements operate as an ideal AC-to-DC converter in which real power can freely flow in either direction between the AC terminals of the two converters and each converter can independently generate or absorb reactive power at its own AC output terminal [33].

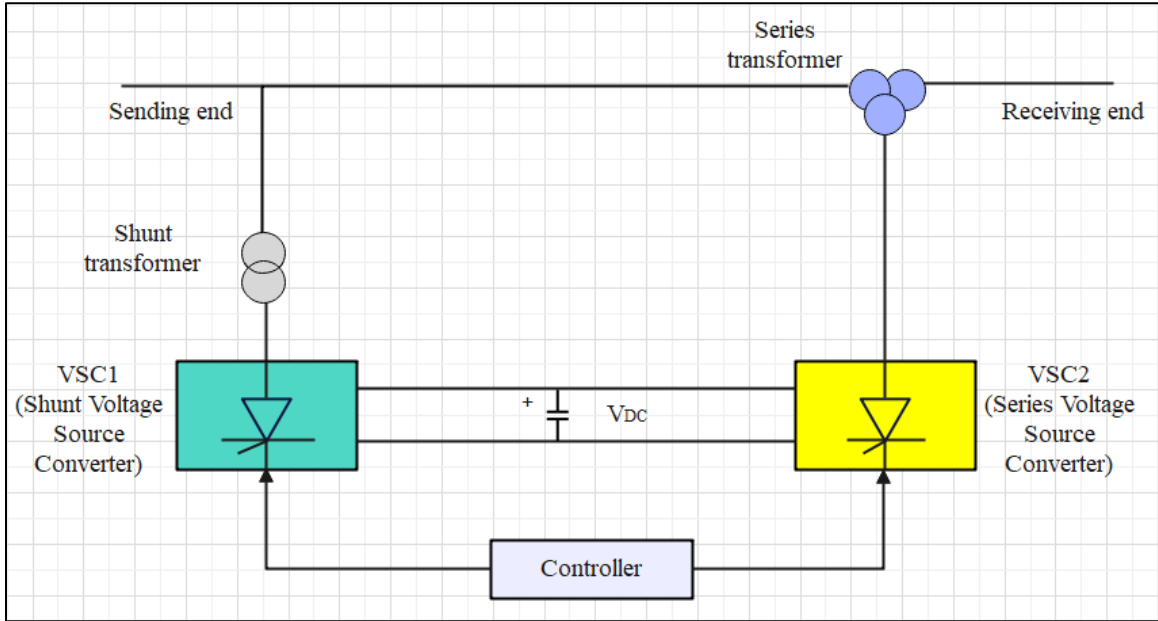


Figure 3. 2: Basic UPFC schematic diagram

VSC1 is connected to the transmission line in shunt via a shunt transformer, while VSC2 is connected in series via a series transformer. Two VSCs are linked by DC terminals, forming a path for active power exchange between the converters. The major function of UPFC is performed by VSC, which injects a voltage with controlled magnitude and phase angle in series with the line via an injection transformer. This injected voltage operates as a synchronous AC voltage source [34].

The transmission line current flows through this voltage source resulting in reactive and active power exchange between it and the AC system. The reactive power exchanged at the DC terminal is generated internally by the converter. The real power exchanged at the AC terminal is converted into DC power which appears at the DC-link as real power demand. VSC1 is to supply or absorb the real power demanded by VSC2 at the common DC link to support real power exchange resulting from the series voltage injection. This DC link power demand of VSC2 is converted back to AC by VSC1 and coupled to the transmission line bus via a shunt-connected transformer. In addition, VSC1 can also generate or absorb controllable reactive power if it is required and thereby provide independent shunt reactive compensation for the line. Thus, VSC1 can be operated at a unity power factor or to be controlled to have a reactive power exchange with the line

independent of the reactive power exchanged by VSC1. Obviously, there can be no reactive power flow through the UPFC DC link [35].

3.2.2 Operation Principle of Unified Power Flow Controller

The voltage sources V_{sh} and V_{se} mentioned in Section 3.2.1 are obtained by converting DC voltage to AC voltage. The conversion from DC voltage to AC voltage is obtained by using standard bridge circuits. These bridge circuits use GTO as their building blocks. Since these circuits convert DC voltage to AC voltage, they are termed "voltage source converters (VSC). The control system associated with VSC allows it to adjust its magnitude and phase angle. The term "inverter" has also been used to denote the VSC. Inverter 1 (VSC1) can charge the DC link capacitor [9]. To understand the unified power flow concept, consider a power system with two machines connected by a transmission line of reactance X_t (purely inductive) along with two voltage sources (V_{sh} and V_{se}) that represent UPFC as shown in figure 3.3. The voltage sources denoted by V_{sh} and V_{se} are connected in shunt and series, respectively, at the midpoint of the transmission line.

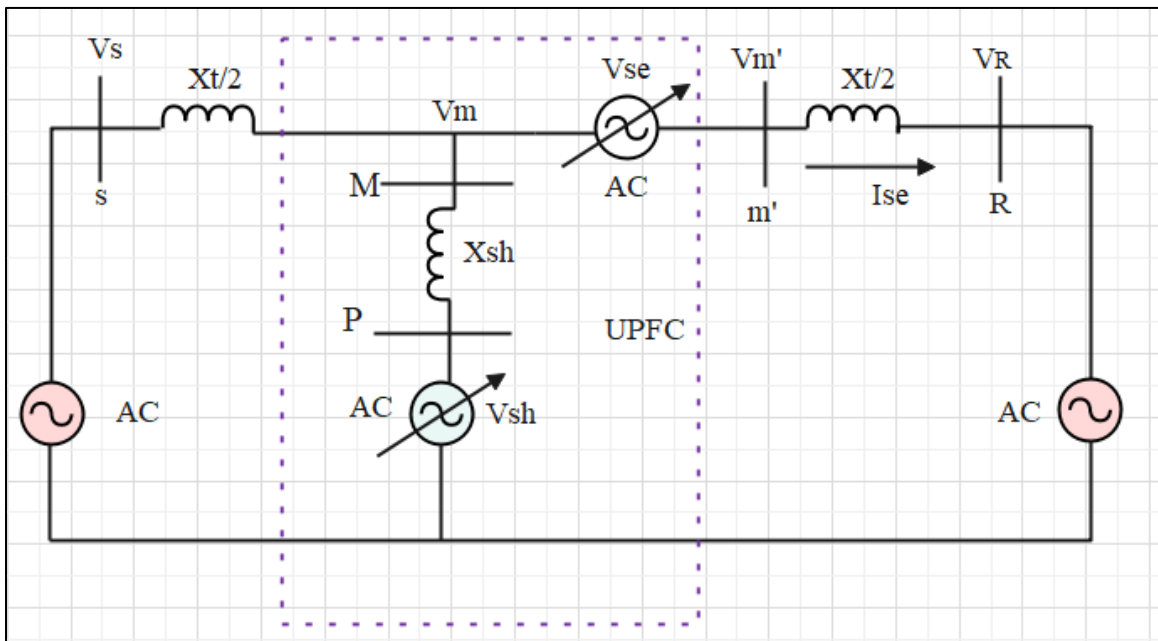


Figure 3. 3:A power system with two machines connected by a transmission line with voltage sources v_{sh} and v_{se} representing the UPFC

A voltage source (V_{sh}) is connected to the transmission line through a transformer represented by a reactance (X_{sh}). It is assumed that the voltage sources denoted by V_{sh} and V_{se} have the capability of varying their magnitude and their phase angle. To understand the operation of the source voltage V_{sh} , the source voltage V_{se} is disconnected. Reactive power flows from the voltage source V_{sh} to bus M if the magnitude of the voltage source V_{sh} is greater than the mid-point voltage V_m and the phases of them are the same. If the phase angle of the voltage source V_{sh} leads the phase angle of the mid-point voltage V_m and the magnitude of V_{sh} is greater than V_m , then real and reactive power will flow from the voltage source V_{sh} to the bus M [36].

Conversely, if the magnitude of the shunt voltage V_{sh} is less than the midpoint voltage V_m but the phase angle difference between them is zero, then only reactive power will flow from the bus M to the bus P. In this process, the voltage source V_{sh} is consuming reactive power. If the phase angle of V_{sh} lags the phase angle of V_m , then both real and reactive power will flow from bus M to bus P, and the voltage source is said to be consuming both real and reactive power [36].

In summary, by controlling the magnitude and phase angle of the shunt voltage source V_{sh} , the direction of real and reactive power flow to the bus M can be controlled. Alternatively, the voltage source V_{sh} can be made to function as a load or as a generator for the power system. In the above operation, if the phase angle difference between the voltage at bus M and that of V_{sh} is maintained at zero, then by varying the magnitude of V_{sh} , reactive power can either be consumed or generated by V_{sh} . This operation can be compared with that of a thyristor controller reactor with a fixed capacitor (shunt compensator) that generates or absorbs reactive power by altering its shunt reactive impedance.

Now consider only the operation of a series voltage source V_{se} with the shunt voltage source V_{sh} disconnected. It is assumed that the magnitude and phase angle of the series voltage source V_{se} can be varied. The transmission line current I_{se} interacts with the series voltage source V_{se} , causing real and reactive power to be exchanged between the series voltage source and the transmission line. If the voltage source V_{se} and the transmission line current I_{se} have a phase angle difference of 90° and the voltage phasor of V_{se} leads

the line current, the voltage source V_{se} then generates only reactive power. The phasor diagram has been shown in the figure 3.4 below.

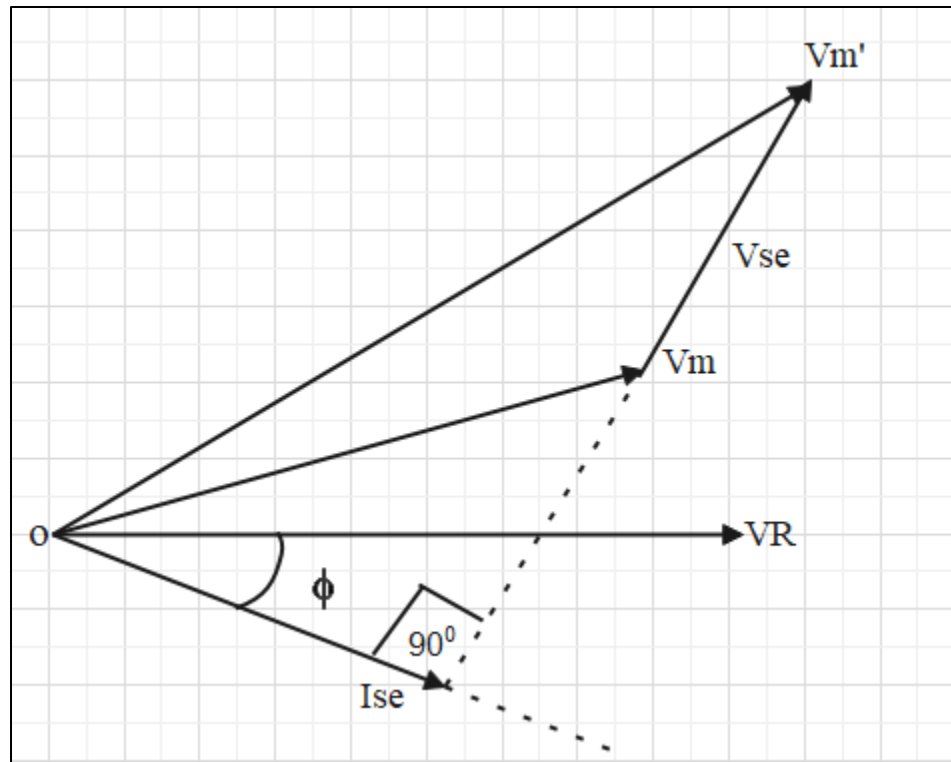


Figure 3. 4:Phasor relationship between the voltage source V_{se} and the line current I_{se} for series compensation

Conversely, if the voltage source V_{se} phasor lags the transmission line current I_{se} phasor by 90° , then the voltage source V_{se} will consume reactive power. The above operation should be compared as analogy with that of a series capacitor or series inductor in the transmission line. When capacitors placed in series with the transmission line, it generates reactive power. The amount of reactive power generated depends on the amount of series compensation and the line current. When inductors placed in series with the transmission line, it consumes reactive power. Generally, the function of series capacitor could be performed by the series voltage source V_{se} by maintaining its phase to lead the transmission line current I_{se} phasor by 90° . Conversely, the function of a series inductor could be performed by the series voltage source V_{se} by adjusting its phase angle to be lagging the line current I_{se} phasor by 90° [36].

By properly adjusting the phase angle of the series voltage source V_{se} , the operation of a phase shifter has obtained. In the case of a phase shifter, the phase angle of the series voltage source V_{se} leads or lags the voltage of the bus to which it is attached by 90° . This causes the voltage phasor to shift depending on the magnitude of the injected voltage. In this case, if the series voltage source V_{se} has 90° leading or lagging phase relationship with the bus voltage V_m , then a phase shift $\alpha = \tan^{-1} \left(\frac{V_{se}}{V_m} \right)$ could be obtained. In summary, by adjusting the phase angle of the series voltage source V_{se} to be either leading or lagging the bus voltage M by 90° , a phase shifter operation could be obtained. In order to vary the magnitude of phase shift, the magnitude of the series voltage source V_{se} could be varied. The above illustration has shown all the possible functions of shunt compensation, series compensation and phase angle compensation that could be obtained by manipulating the series and the shunt voltage sources magnitude and phase angle of a UPFC [36].

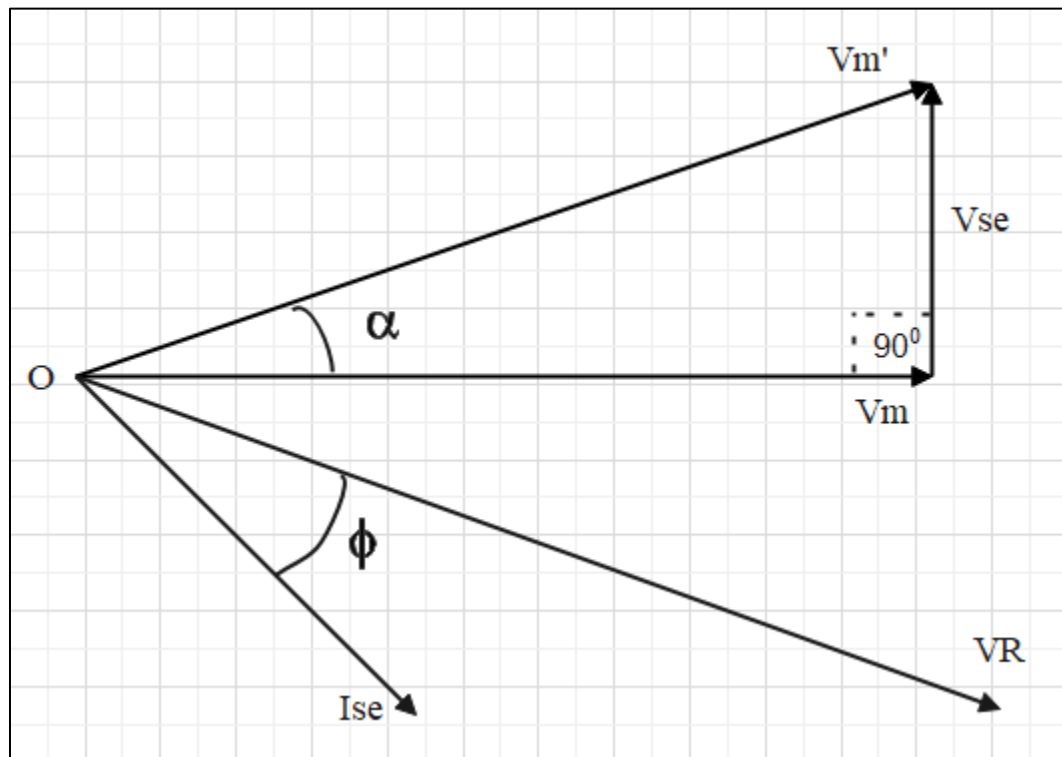


Figure 3. 5: Phasor relationship between the midpoint voltage V_m and the series voltage source V_{se} , for phase shifter operation

3.3 Mathematical Modeling of Unified Power Flow Controller

A typical unified power flow controller circuit is depicted as in figure 3.6. Control objectives in the system are the voltage magnitude $|v_1|$ and the transmission line real and reactive power flow P and Q which enhances transient stability. $|v_1|$ is controlled by the shunt device by injecting a leading or lagging current into the point of connection. System power flow P and Q are controlled by the series device by injecting proper voltage into the transmission line. The series device exchanges real and reactive power with the system. The reactive power is exchanged locally with the DC capacitor bank. The active power in the series device injected into the line is drawn from the shunt device via the DC capacitor bank.

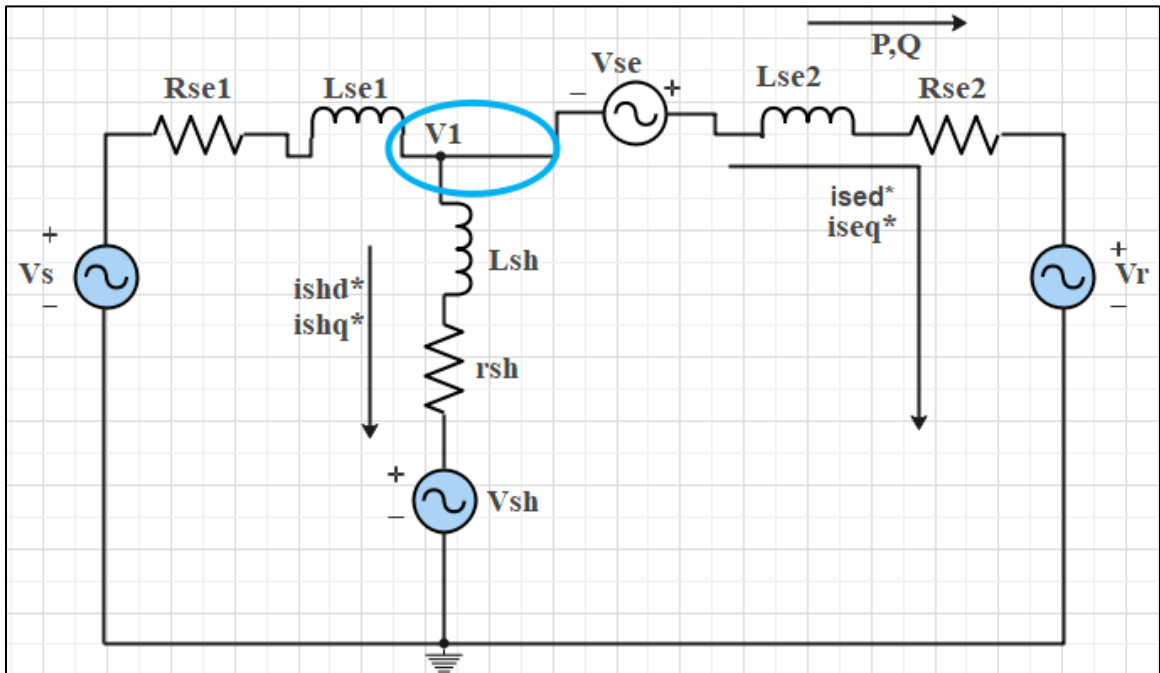


Figure 3. 6:Single phase circuit representation of a power flow in UPFC [37]

3.3.1 Mathematical Modeling of Shunt Converter

A shunt device model is depicted in the figure 3.7 below, with voltage source V_1 , shunt resistance r_{sh} and shunt inductance L_{sh} .

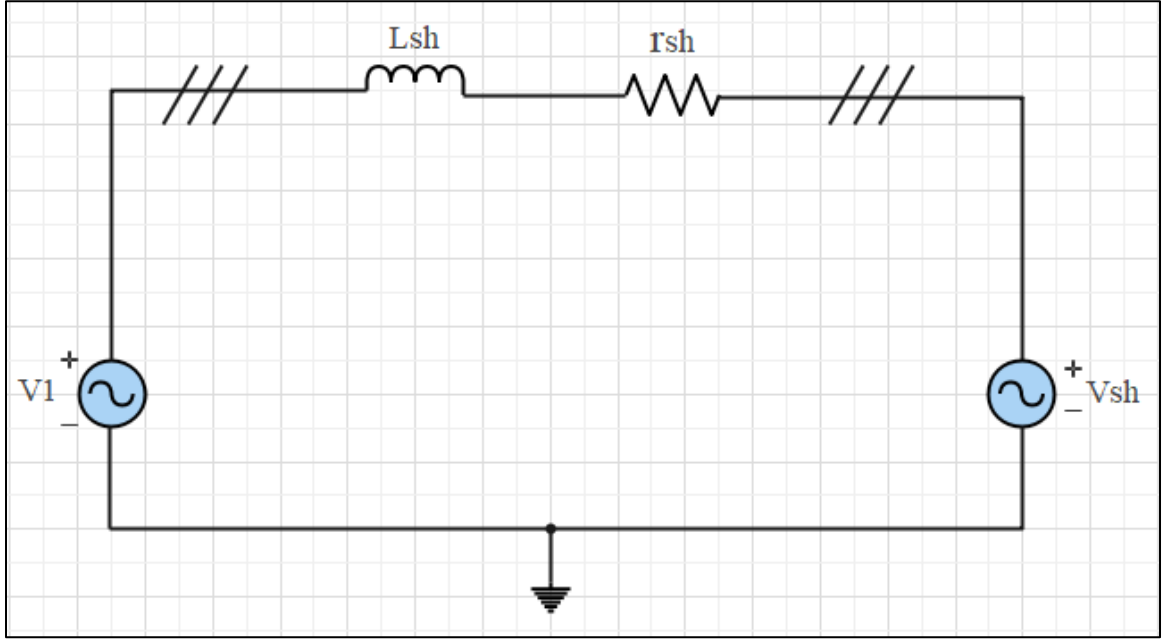


Figure 3. 7:Shunt device model of UPFC

From figure 3.7 the differential equation obtained for shunt converter in a-b-c reference axis system. The differential equation from the circuit is written as :

$$\begin{cases} V_{1a} - V_{sha} = r_{sh}i_{sha} + L_{sh} \frac{d}{dt} i_{sha} \\ V_{1b} - V_{shb} = r_{sh}i_{shb} + L_{sh} \frac{d}{dt} i_{shb} \\ V_{1c} - V_{shc} = r_{sh}i_{shc} + L_{sh} \frac{d}{dt} i_{shc} \end{cases} \quad (3.1)$$

Rearranging equation (3.1) can be written as:

$$\begin{cases} \frac{d}{dt} i_{sha} = \frac{V_{1a} - r_{sh}i_{sha} - V_{sha}}{L_{sh}} \\ \frac{d}{dt} i_{shb} = \frac{V_{1b} - r_{sh}i_{shb} - V_{shb}}{L_{sh}} \\ \frac{d}{dt} i_{shc} = \frac{V_{1c} - r_{sh}i_{shc} - V_{shc}}{L_{sh}} \end{cases} \quad (3.2)$$

In matrix format, the equation (3.2) can be organized as:

$$\frac{d}{dt} \begin{bmatrix} i_{sha} \\ i_{shb} \\ i_{shc} \end{bmatrix} = \begin{bmatrix} -\frac{r_{sh}}{L_{sh}} & 0 & 0 \\ 0 & -\frac{r_{sh}}{L_{sh}} & 0 \\ 0 & 0 & -\frac{r_{sh}}{L_{sh}} \end{bmatrix} \begin{bmatrix} i_{sha} \\ i_{shb} \\ i_{shc} \end{bmatrix} + \frac{1}{L_{sh}} \begin{bmatrix} V_{1a} - V_{sha} \\ V_{1b} - V_{shb} \\ V_{1c} - V_{shc} \end{bmatrix} \quad (3.3)$$

Where, V_{sha} , V_{shb} and V_{shc} are the phase a, phase b and phase c shunt voltage respectively. V_{1a} , V_{1b} and V_{1c} are the phase a, phase b and phase c of the node voltage respectively. i_{sha} , i_{shb} and i_{shc} are the phase a, phase b and phase c shunt current respectively. r_{sh} and L_{sh} are the shunt resistance and inductance respectively.

Using Park's transformation rule three-phase system can be transformed to d-q axis. The Park transform converts the time-domain components of a three-phase system in an a-b-c reference frame to direct, quadrature, and zero components in a rotating reference frame and make computations much easier. Let Park's transformation ratio be $T(\omega t)$ [38].

$$T(\omega t) = \frac{2}{3} \begin{bmatrix} \cos(\omega t) & \cos(\omega t - 120^\circ) & \cos(\omega t + 120^\circ) \\ -\sin(\omega t) & -\sin(\omega t - 120^\circ) & -\sin(\omega t + 120^\circ) \\ \frac{1}{2} & \frac{1}{2} & \frac{1}{2} \end{bmatrix} \quad (3.4)$$

Three phase voltage parks transformation from three phase abc to $dq0$ using Park's transformation ratio be $T(\omega t)$ can be written as $V_{dq0} = T(\omega t) * V_{abc}$.

$$\begin{bmatrix} Vd \\ Vq \\ V0 \end{bmatrix} = \frac{2}{3} \begin{bmatrix} \cos(\omega t) & \cos(\omega t - 120^\circ) & \cos(\omega t + 120^\circ) \\ -\sin(\omega t) & -\sin(\omega t - 120^\circ) & -\sin(\omega t + 120^\circ) \\ \frac{1}{2} & \frac{1}{2} & \frac{1}{2} \end{bmatrix} \begin{bmatrix} Va \\ Vb \\ Vc \end{bmatrix} \quad (3.5)$$

Likewise, for three phase current parks transformation from three phase a-b-c to d-q-0 using Park's transformation ratio be $T(\omega t)$ can be written as $i_{dq0} = T(\omega t) * i_{abc}$.

$$\begin{bmatrix} id \\ iq \\ i0 \end{bmatrix} = \frac{2}{3} \begin{bmatrix} \cos(\omega t) & \cos(\omega t - 120^\circ) & \cos(\omega t + 120^\circ) \\ -\sin(\omega t) & -\sin(\omega t - 120^\circ) & -\sin(\omega t + 120^\circ) \\ \frac{1}{2} & \frac{1}{2} & \frac{1}{2} \end{bmatrix} \begin{bmatrix} ia \\ ib \\ ic \end{bmatrix} \quad (3.6)$$

Using calculus derivative product rule:

$$\frac{d}{dt} \begin{bmatrix} id \\ iq \\ i0 \end{bmatrix} = \frac{d}{dt} \left(T(\omega t) \begin{bmatrix} ia \\ ib \\ ic \end{bmatrix} \right) = \frac{d}{dt} T(\omega t) * \begin{bmatrix} ia \\ ib \\ ic \end{bmatrix} + T(\omega t) * \frac{d}{dt} \begin{bmatrix} ia \\ ib \\ ic \end{bmatrix} \quad (3.7)$$

Substituting equation (3.3) into equation (3.7) for shunt converter will be:

$$\frac{d}{dt} \begin{bmatrix} i_{shd} \\ i_{shq} \\ i_{sh0} \end{bmatrix} = T'(\omega t) * \begin{bmatrix} i_{sha} \\ i_{shb} \\ i_{shc} \end{bmatrix} + T(\omega t) * \frac{d}{dt} \begin{bmatrix} i_{sha} \\ i_{shb} \\ i_{shc} \end{bmatrix} \quad (3.8)$$

Then transform the equation (3.3) into d-q-0 system. In this case, the zero axis is assumed to be symmetric. Therefore, neglecting zero axis component only d-q reference can be written as follows :

$$\frac{d}{dt} \begin{bmatrix} i_{shd} \\ i_{shq} \end{bmatrix} = \begin{bmatrix} -\frac{r_{sh}}{L_{sh}} & \omega \\ -\omega & -\frac{r_{sh}}{L_{sh}} \end{bmatrix} * \begin{bmatrix} i_{shd} \\ i_{shq} \end{bmatrix} + \frac{1}{L_{sh}} \begin{bmatrix} V_{1d} - V_{shd} \\ V_{1q} - V_{shq} \end{bmatrix} \quad (3.9)$$

Where, V_{shd} , V_{shq} and V_{sh0} are direct axis, quadrature axis and zero axis shunt voltage respectively. V_{1d} , V_{1q} and V_{10} are direct axis, quadrature axis and zero axis of the node voltage respectively. i_{shd} , i_{shq} and i_{sh0} are direct axis, quadrature axis and zero axis shunt current respectively. r_{sh} and L_{sh} are the shunt resistance and inductance respectively.

From equation (3.9), the d and q components of first order time varying currents can be written as follows.

❖ The d-component of shunt current is:

$$\frac{d}{dt} [i_{shd}] = -\frac{r_{sh}}{L_{sh}} * i_{shd} + \omega i_{shq} + \frac{1}{L_{sh}} (V_{1d} - V_{shd}) \quad (3.10)$$

❖ The q-component of shunt converter is:

$$\frac{d}{dt} [i_{shq}] = -\omega i_{shd} - \frac{r_{sh}}{L_{sh}} * i_{shq} + \frac{1}{L_{sh}} (V_{1q} - V_{shq}) \quad (3.12)$$

Where, $\omega=2\pi f$, f is the fundamental frequency of the supply voltage.

3.3.2 Shunt Converter Control Variable Reference

This section describes how the system control block uses operator inputs and the power system data to compute the reference signals for the functional control block. Magnitude of the sending end bus voltage $|v_1|$ is controlled by shunt device reactive power injection. So, the reactive injection power Q_{sh} can be controlled by a PI controller. Reference value of shunt reactive power represented by star symbol (*) as superscript [39].

$$Q_{sh}^* = \left(\frac{k_{iv}}{s} + k_{pv} \right) (|v_1|^* - |v_1|) \quad (3.13)$$

Where, $|v_1|^*$ is the sending end reference voltage magnitude. $|v_1|$ is the real time voltage magnitude. k_{iv} and k_{pv} are the integral and the proportional gain for the PI controller.

If the rotating axis is synchronous with the sending end voltage, the d-axis component of the voltage is the instant magnitude of the voltage. So, $|v_1| = v_{1d}$. Then, the q-axis reference current in the shunt branch should be:

$$i_{shq}^* = \frac{Q_{sh}^*}{v_{1d}} \quad (3.14)$$

Substituting equation (3.13) into equation (3.14) will give:

$$i_{shq}^* = \frac{\left(\frac{k_{iv}}{s} + k_{pv} \right) (|v_1|^* - |v_1|)}{v_{1d}} \quad (3.15)$$

The d-axis reference current for the shunt branch has taken from the active power drawn by the series converter. At the same time, the real component of the shunt converter current is responsible of providing power losses in the switching devices and the DC capacitor. This is reflected by keeping the DC capacitor voltage constant. So,

$$i_{shd}^* = \frac{P_{se}^*}{v_{1d}} + \left(k_{pDC} + \frac{k_{iDC}}{s} \right) (v_{DC}^* - v_{DC}) \quad (3.16)$$

where v_{1d} is the d-axis component of the voltage at the point of connection. $P_{se}^* = v_{sed}i_{sed} + v_{seq}i_{seq}$ is the instantaneous real power injected into the transmission line by the series converter. v_{sed} and v_{seq} is the real and reactive component of the injected voltage respectively. i_{sed} and i_{seq} are the real and reactive components of the line current respectively. k_{pDC} and k_{iDC} are the integral and the proportional gain for the PI controller. The real power drawn by the series converter is supplied by the shunt converter through the DC capacitor.

The real power drawn by the series converter is supplied by the shunt converter through the DC capacitor. The shunt current reference computation process is illustrated in figure 3.8 below:

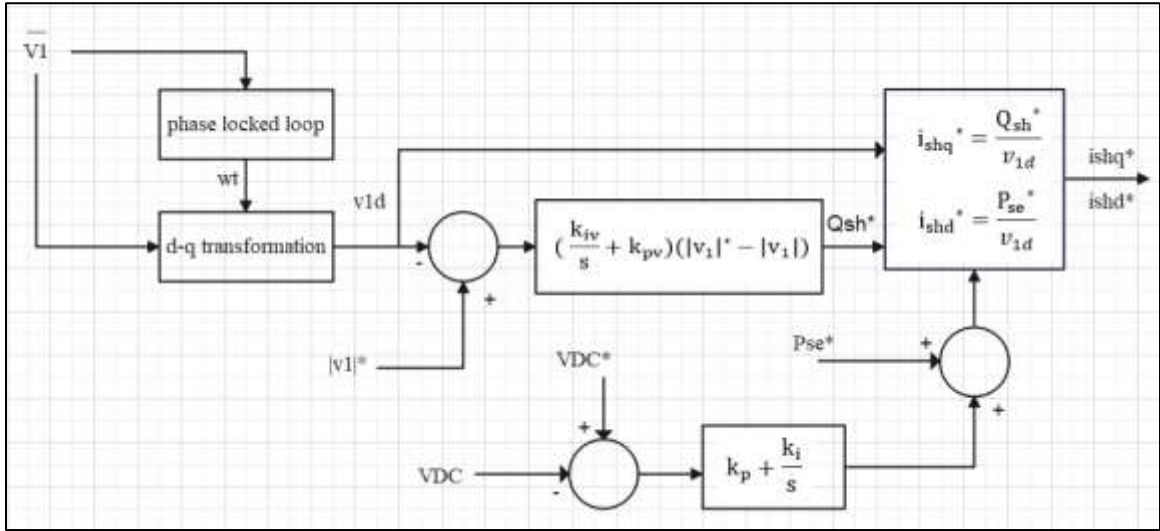


Figure 3. 8:Shunt current reference computation

3.3.3 Mathematical Modeling of Series Converter

Formulating the mathematical modelling of the series converter is the same procedure as the shunt converter. Using KVL, the dynamic modelling of a series converter for a balanced three-phase system is modelled on a per-phase basis as a voltage source with series resistance R_{se} and inductance L_{se} , as shown in figure 3.9 below:

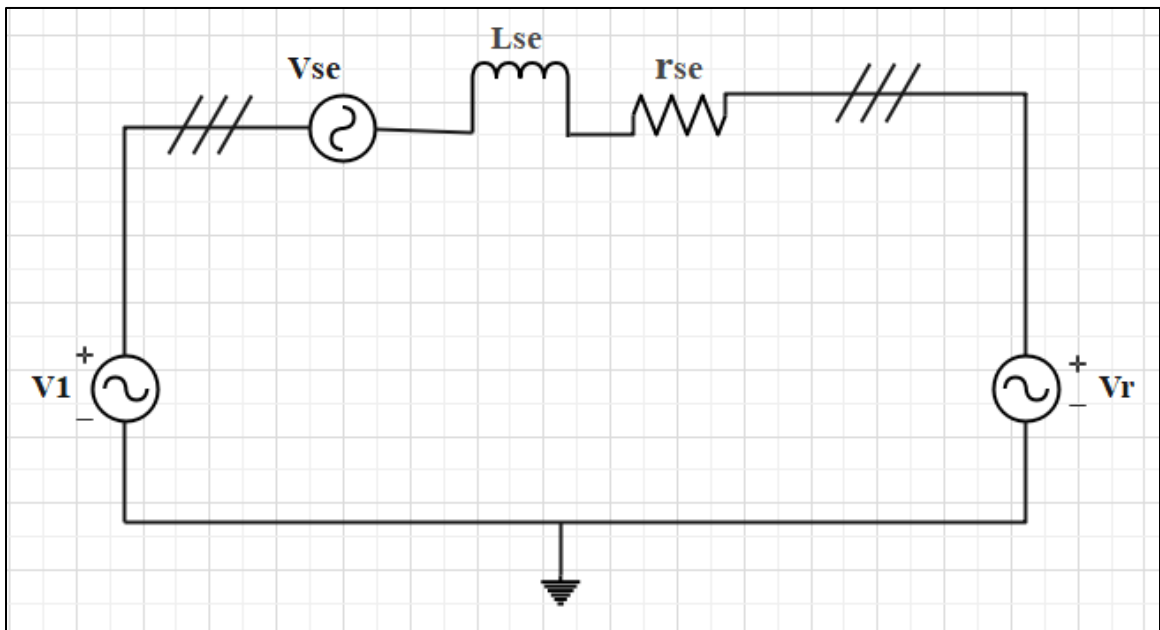


Figure 3. 9:Series device model of UPFC

From figure 3.9 the differential equation obtained for series converter in a-b-c axis system, resulting three-phase circuit equation set can be written as:

$$\begin{cases} V_{1a} + V_{sea} - V_{ra} = R_{se}i_{sea} + L_{se} \frac{d}{dt} i_{sea} \\ V_{1b} + V_{seb} - V_{rb} = R_{se}i_{seb} + L_{se} \frac{d}{dt} i_{seb} \\ V_{1c} + V_{sec} - V_{rc} = R_{se}i_{sec} + L_{se} \frac{d}{dt} i_{sec} \end{cases} \quad (3.17)$$

Rearranging equation (3.17), it can be written as:

$$\begin{cases} \frac{d}{dt} i_{sea} = \frac{V_{1a} + V_{sea} - V_{ra} - R_{se}i_{sea}}{L_{sh}} \\ \frac{d}{dt} i_{seb} = \frac{V_{1b} + V_{seb} - V_{rb} - R_{se}i_{seb}}{L_{sh}} \\ \frac{d}{dt} i_{sec} = \frac{V_{1c} + V_{sec} - V_{rc} - R_{se}i_{sec}}{L_{sh}} \end{cases} \quad (3.18)$$

In matrix format, the equation (3.18) can be organized as:

$$\frac{d}{dt} \begin{bmatrix} i_{sea} \\ i_{seb} \\ i_{sec} \end{bmatrix} = \begin{bmatrix} -\frac{R_{se}}{L_{se}} & 0 & 0 \\ 0 & -\frac{R_{se}}{L_{se}} & 0 \\ 0 & 0 & -\frac{R_{se}}{L_{se}} \end{bmatrix} \begin{bmatrix} i_{sea} \\ i_{seb} \\ i_{sec} \end{bmatrix} + \frac{1}{L_{se}} \begin{bmatrix} V_{1a} + V_{sea} - V_{ra} \\ V_{1b} + V_{seb} - V_{rb} \\ V_{1c} + V_{sec} - V_{rc} \end{bmatrix} \quad (3.19)$$

Where, V_{sea} , V_{seb} and V_{sec} are the phase a, phase b and phase c series voltage respectively. V_{1a} , V_{1b} and V_{1c} are the phase a, phase b and phase c of the node voltage respectively. V_{ra} , V_{rb} and V_{rc} are the phase a, phase b and phase c receiving end voltage respectively. i_{sha} , i_{shb} and i_{shc} are the phase a, phase b and phase c current respectively. R_{sh} and L_{sh} are the shunt resistance and inductance respectively.

Following the same procedure of shunt converter, transform equation (3.19) into d-q-0 system. In this case, the zero axis is assumed to be symmetric. Therefore, neglecting zero axis component only d-q reference can be written as follows :

$$\frac{d}{dt} \begin{bmatrix} i_{sed} \\ i_{seq} \end{bmatrix} = \begin{bmatrix} -\frac{R_{se}}{L_{se}} & \omega \\ -\omega & -\frac{R_{se}}{L_{se}} \end{bmatrix} * \begin{bmatrix} i_{sed} \\ i_{seq} \end{bmatrix} + \frac{1}{L_{se}} \begin{bmatrix} V_{1d} + V_{sed} - V_{rd} \\ V_{1q} + V_{seq} - V_{rq} \end{bmatrix} \quad (3.20)$$

Where, V_{sed} , V_{seq} and V_{se0} are direct axis, quadrature axis and zero axis series voltage respectively. V_{1d} , V_{1q} and V_{10} are direct axis, quadrature axis and zero axis of the node voltage respectively. V_{rd} , V_{rq} and V_{r0} are direct axis, quadrature axis and zero axis of the receiving end voltage respectively. i_{sed} , i_{seq} and i_{se0} are direct axis, quadrature axis and zero axis current respectively. R_{se} and L_{se} are the series resistance and inductance respectively. From equation (3.20), the d and q components of first order time varying currents can be written as follows.

❖ The d-component of series converter current is:

$$\frac{d}{dt}[i_{sed}] = -\frac{R_{se}}{L_{se}} * i_{sed} - \omega i_{seq} + \frac{1}{L_{se}}(V_{1d} - V_{sed} - V_{rd}) \quad (3.21)$$

❖ The q-component of series converter current is:

$$\frac{d}{dt}[i_{seq}] = \omega i_{sed} - \frac{R_{se}}{L_{se}} * i_{seq} + \frac{1}{L_{se}}(V_{1q} - V_{seq} - V_{rq}) \quad (3.22)$$

3.3.4 Series Converter Control Variable Reference

By d-q transformation, the transmitted real and reactive power to the receiving end bus is controlled independently. The rotating axis is synchronous with the receiving end voltage V_{rd} . Therefore, $P_{se}^* = V_{rd} i_{sed}^*$, $Q_{se}^* = V_{rd} i_{seq}^*$. where, V_{rd} is the d-axis component of the receiving end voltage. i_{sed}^* and i_{seq}^* are reference real and reactive components of the line current respectively. So, the d-axis and q-axis reference current in the transmission line are calculated as equation (3.23). The computation process is depicted as figure 3.10.

$$\begin{cases} i_{sed}^* = \frac{P_{se}^*}{V_{rd}} \\ i_{seq}^* = \frac{Q_{se}^*}{V_{rd}} \end{cases} \quad (3.23)$$

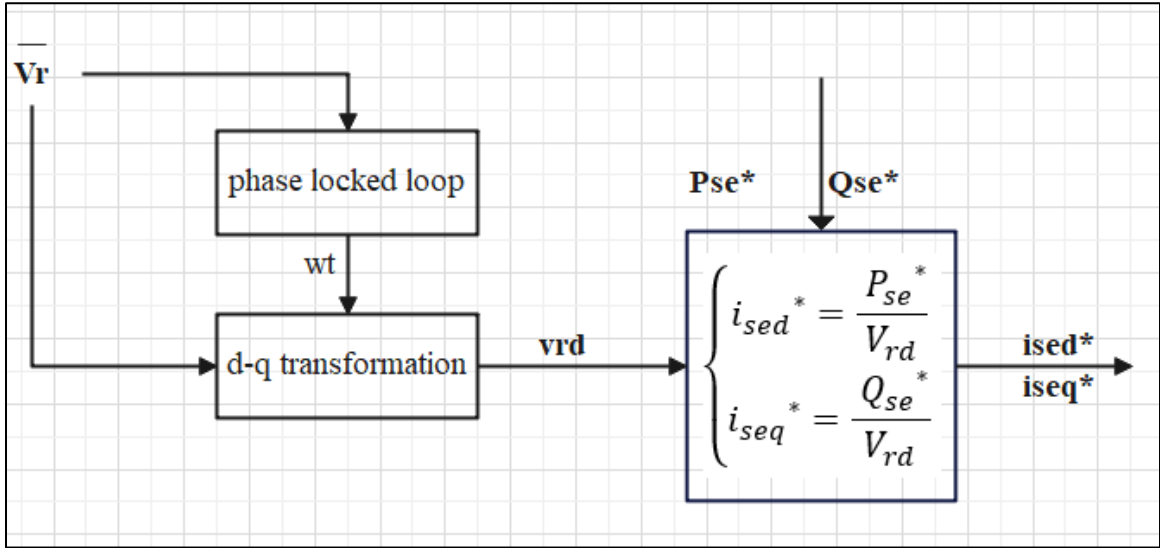


Figure 3. 10:Series current reference computation

3.3.5 Mathematical Modelling of DC Link Capacitor

The model is shown in figure 3.11. The voltage of the DC capacitor bank is decided by the real power drawn and injected by the shunt and series devices.

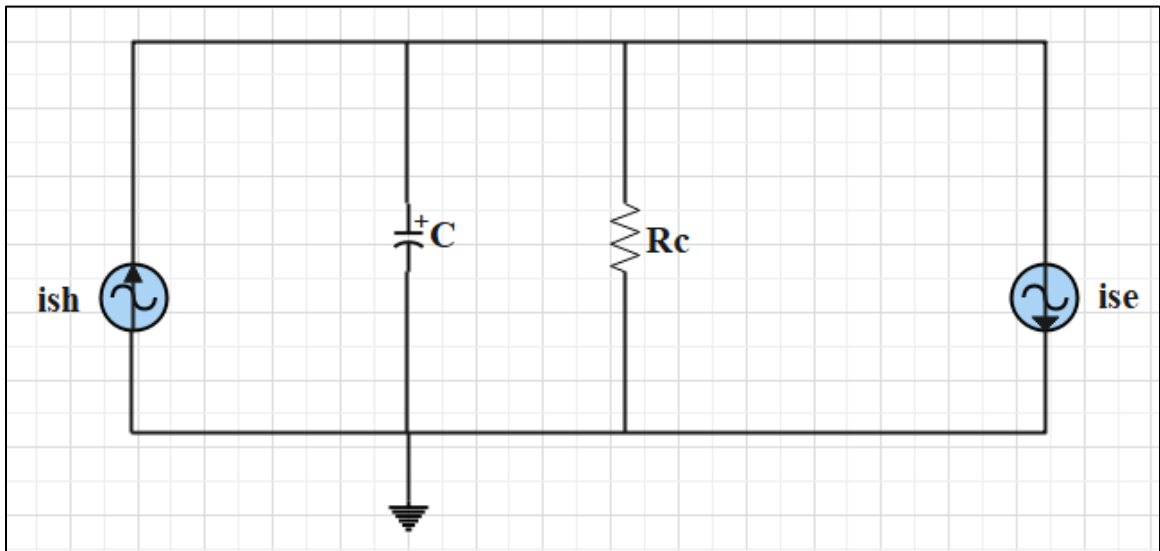


Figure 3. 11:DC link capacitor voltage control model

R_c is losses of the shunt device, series device, and the DC capacitor which are modeled as a shunt connected resistance with the DC capacitor. The node current at the positive side of the capacitor can be written as:

$$i_{sh} - i_{se} = C \frac{d}{dt} V_{dc} + \frac{V_{dc}}{R_c} \quad (3.24)$$

where i_{sh} and i_{se} are the currents drawn by the shunt and series converter respectively. The currents are decided by the real power drawn or provided by the shunt and series devices. So, equation (3.24) can be revised as:

$$\frac{P_{sh} - P_{se}}{V_{dc}} = C \frac{d}{dt} V_{dc} + \frac{V_{dc}}{R_c} \quad (3.25)$$

The real power provided by the shunt converter is expressed as equation (3.26):

$$P_{sh} = V_{shd} i_{shd} + V_{shq} i_{shq} \quad (3.26)$$

The real power drawn by the series converter is written as in equation (3.27):

$$P_{se} = V_{sed} i_{sed} + V_{seq} i_{seq} \quad (3.27)$$

Substitute equations (3.26) and (3.27) into equation (3.25):

$$\frac{V_{shd} i_{shd} + V_{shq} i_{shq} - V_{sed} i_{sed} - V_{seq} i_{seq}}{V_{dc}} = C \frac{d}{dt} V_{dc} + \frac{V_{dc}}{R_c} \quad (3.28)$$

Reorganize the equation (3.28), it can be written as:

$$\frac{d}{dt} V_{dc} = \frac{V_{shd} i_{shd} + V_{shq} i_{shq} - V_{sed} i_{sed} - V_{seq} i_{seq}}{C V_{dc}} - \frac{V_{dc}}{C R_c} \quad (3.29)$$

Neglecting the voltage harmonics due to the inverter switching, the shunt and series converter output voltage d-q components can be expressed as:

$$\begin{bmatrix} V_{shd} \\ V_{shq} \\ V_{sed} \\ V_{seq} \end{bmatrix} = V_{dc} \begin{bmatrix} k_{sh} \cos \delta_{sh} \\ k_{sh} \sin \delta_{sh} \\ k_{se} \cos \delta_{se} \\ k_{se} \sin \delta_{se} \end{bmatrix} \quad (3.30)$$

Where k_{sh} and k_{se} are the constants for the relationship of the shunt and series converter versus the DC voltage. It integrates the transformer turns ratio and the modulation index of the shunt and series converter. δ_{sh} and δ_{se} are the phase angle of the shunt and series converter output fundamental voltage with respect to reference voltage, normally the sending or receiving end bus voltage [39].

Substitute equation (3.30) into (3.29), will give (3.31):

$$\frac{dV_{dc}}{dt} = \frac{k_{sh} \cos \delta_{sh} i_{shd} + k_{sh} \sin \delta_{sh} i_{shq} - k_{se} \cos \delta_{se} i_{sed} - k_{se} \sin \delta_{se} i_{seq}}{C} - \frac{V_{dc}}{CR_c} \quad (3.31)$$

3.4 Controller Design of Unified Power Flow Controller

As observed from the complete circuit of UPFC in figure 3.2, it has a controller used for switching of the two converters (i.e., a shunt and a series controller). The controllers regulate the two converters, determining when and what remedial action has to be taken. Therefore, proper design of the series and shunt converter control systems in the UPFC has to be established. so that proper coordination of real and reactive power in the UPFC is maintained and the transient stability problems that occur during disturbances will be solved.

There are two parameters to determine the action of the converters. These are the set value (reference) and actual measured values of the system. The reference or initial set value is the value of power system parameters (voltage, current, and power) at steady state conditions from the connection point of the UPFC and the system network. The measured value is the value of power system parameters at any instant of time at the connection point of UPFC with the system network. The standard synchronous D-Q frame is used for UPFC modelling and controller design. The output voltages of UPFC converters that are used to develop firing pulses are the control variables or input signals of a pulse width modulator. Combining equations (3.9), (3.20), and (3.31), the state space representation of the shunt converter model, series converter model, and DC link capacitor model can be written as:

$$\begin{cases} \dot{x} = Ax + Bu \leftarrow \text{state equation} \\ y = Cx + Du \leftarrow \text{output equation} \end{cases} \quad (3.32)$$

Where $[x]$ is the state variable that determines the state of the system, n variables ($x_1, x_2, x_3, \dots, x_n$) are needed to completely describe the behaviour of a dynamic system. $[u]$ is the input variable. $[A]$ is a state matrix, which represents how the system dynamics depend on the other state variables. $[B]$ is the input matrices, which represent how the state dynamics depend on the input variables. $[C]$ is an output matrix, which represents how the output equation depends on the state variables. $[D]$ is a direct transition matrix, which represents how much the output depends on the input variables.

This helps for a concise representation of a dynamic system by introducing state variables. The state space equation of the UPFC is nonlinear. To simplify the problem, assume DC capacitor voltage can be seen as a constant. Then the state equation can be simplified into a fourth-order system. For transient stability enhancement, the series and shunt converter controls have to be dealt with separately by decoupling from the state-space equation [39].

3.4.1 Controller Design of Shunt Converter

In the transformation of shunt controller to state space representation, the rotary d-q axis is synchronized to the connection point voltage V_1 . So, $V_{1d} = |V_1|$, $V_{1q} = 0$. Reorganize equation (3.9) into the following form [39]:

$$\frac{d}{dt} \begin{bmatrix} i_{shd} \\ i_{shq} \end{bmatrix} = \begin{bmatrix} -\frac{r_{sh}}{L_{sh}} & 0 \\ 0 & -\frac{r_{sh}}{L_{sh}} \end{bmatrix} * \begin{bmatrix} i_{shd} \\ i_{shq} \end{bmatrix} + \frac{1}{L_{sh}} \begin{bmatrix} V_{1d} - V_{shd} + \omega L_{sh} i_{shq} \\ -V_{shq} - \omega L_{sh} i_{shd} \end{bmatrix} \quad (3.33)$$

$$\text{Where, } \dot{x} = \frac{d}{dt} \begin{bmatrix} i_{shd} \\ i_{shq} \end{bmatrix}, x = \begin{bmatrix} i_{shd} \\ i_{shq} \end{bmatrix}, A = \begin{bmatrix} -\frac{r_{sh}}{L_{sh}} & 0 \\ 0 & -\frac{r_{sh}}{L_{sh}} \end{bmatrix}, B = \begin{bmatrix} 1 & 0 \\ 0 & 1 \end{bmatrix}, Y = \begin{bmatrix} Y1 \\ Y2 \end{bmatrix}$$

$$C = \begin{bmatrix} 1 & 0 \\ 0 & 1 \end{bmatrix} \text{ and } u = \begin{bmatrix} u1 \\ u2 \end{bmatrix} = \frac{1}{L_{sh}} \begin{bmatrix} V_{1d} - V_{shd} + \omega L_{sh} i_{shq} \\ -V_{shq} - \omega L_{sh} i_{shd} \end{bmatrix}$$

Equation (3.33) can be written as:

$$\frac{d}{dt} \begin{bmatrix} i_{shd} \\ i_{shq} \end{bmatrix} = \begin{bmatrix} -\frac{r_{sh}}{L_{sh}} & 0 \\ 0 & -\frac{r_{sh}}{L_{sh}} \end{bmatrix} * \begin{bmatrix} i_{shd} \\ i_{shq} \end{bmatrix} + \begin{bmatrix} u1 \\ u2 \end{bmatrix} \quad (3.34)$$

Lets assume the following equation to integrate control variables u with PI [39]:

$$\begin{cases} u1 = \frac{1}{L_{sh}} \left(k_{psh} + \frac{k_{ish}}{s} \right) (i_{shd}^* - i_{shd}) \\ u2 = \frac{1}{L_{sh}} \left(k_{psh} + \frac{k_{ish}}{s} \right) (i_{shq}^* - i_{shq}) \end{cases} \quad (3.35)$$

Now substitute equation (3.35) into (3.32) and equate it with (3.33) and solving for reference of the output of the shunt converter V_{shd}^* and V_{shq}^* will give:

$$\begin{bmatrix} V_{shd}^* \\ V_{shq}^* \end{bmatrix} = \begin{bmatrix} k_{psh} + \frac{k_{ish}}{s} & 0 \\ 0 & k_{psh} + \frac{k_{ish}}{s} \end{bmatrix} * \begin{bmatrix} i_{shd}^* - i_{shd} \\ i_{shq}^* - i_{shq} \end{bmatrix} + \begin{bmatrix} V_{1d} + \omega i_{shq} \\ -\omega i_{shd} \end{bmatrix} \quad (3.36)$$

Where, i_{shd}^* is the d-axis reference, thus the active component reference of the UPFC shunt current. i_{shq}^* is the reactive component of the shunt reference current. Then combining equation (3.15), (3.16) from shunt current reference computation and equation (3.36) above, the shunt converter control diagram is shown in the figure below:

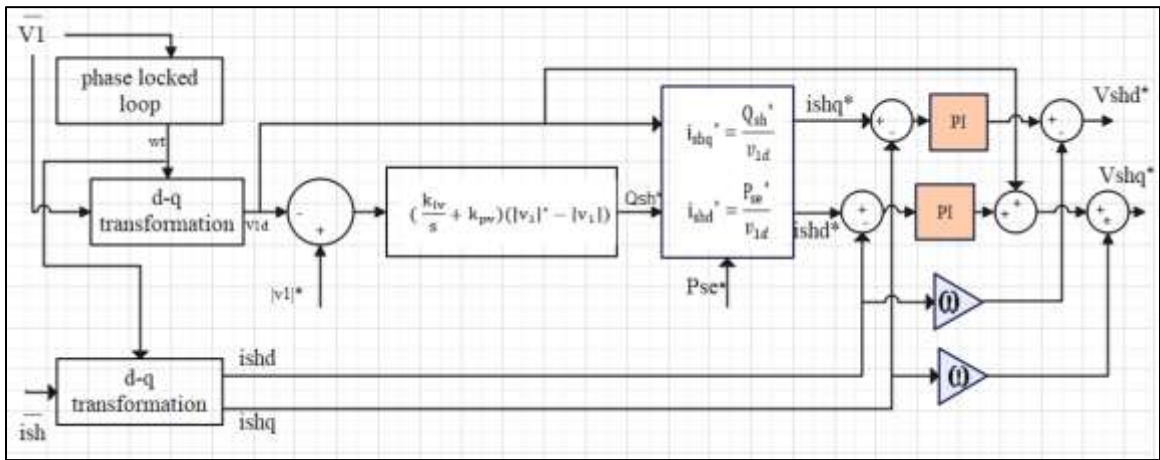


Figure 3. 12:D-Q frame shunt converter control of UPFC

3.4.2 Simulink Model of Shunt Converter Controller

Taking the mathematical modeling of shunt converter controller, MATLAB/SIMULINK model has been designed. The overall Simulink model of shunt controller is as depicted below:

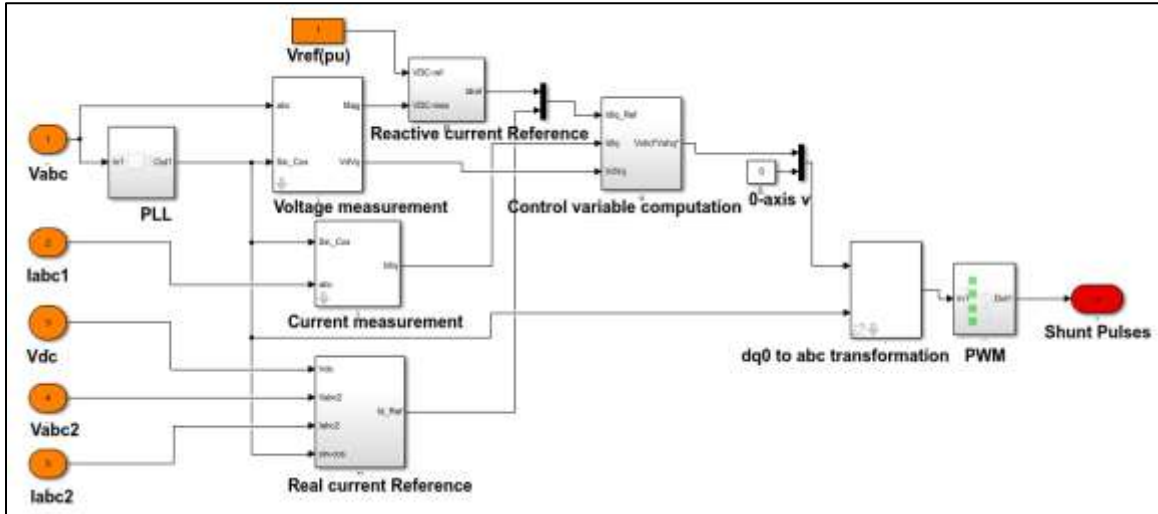


Figure 3. 13:SIMULINK model of shunt converter controller

Each block in the Simulink model is described below:

- ❖ The PLL block model is a Phase Lock Loop (PLL) closed-loop control system that tracks the frequency and phase of a sinusoidal signal by using an internal frequency oscillator. The control system adjusts the internal oscillator frequency to keep the phase difference of voltage and current zero.
- ❖ The voltage and current measurement block measures the voltage and current on the line and transforms it to a dq0 frame using the Parks transformation. The fundamental reason to transform the three-phase instantaneous voltages and currents into the synchronously rotating reference dq0 frame is to make computations much easier. Secondly, it allows the system operator to independently control the active (d-axis) and reactive (q-axis) components of the currents.
- ❖ Reactive reference current contains voltage regulator for i-qref block ensures a steady constant voltage supply through all operational conditions. It regulates the AC voltage during power fluctuations and variations in different disturbances. Its Simulink model is depicted as follows:

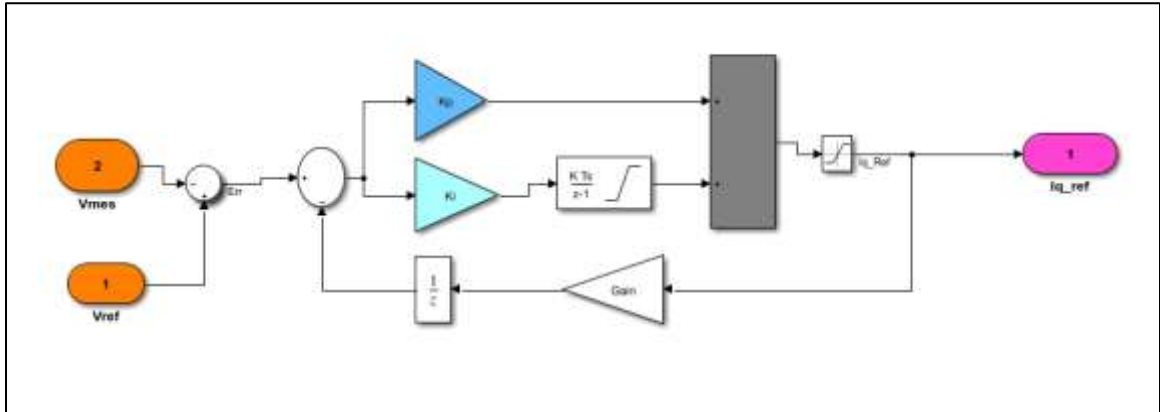


Figure 3. 14:PI based AC voltage regulator for iq-ref

- ❖ Control variable computation block computes the necessary d-axis reference voltage and q-axis reference voltage.

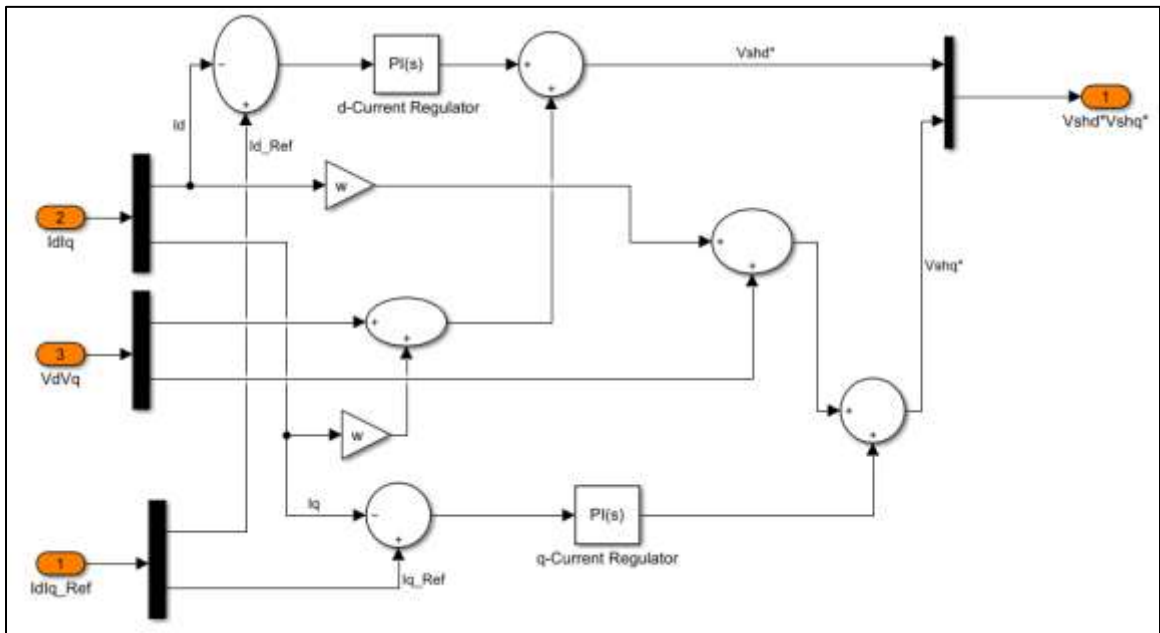


Figure 3. 15:Control variable computation for vshd* and vshq*

- ❖ Real reference current block consists of voltage regulator for id-ref. It ensures a steady constant voltage supply through all operational conditions. It regulates the DC link voltage during power fluctuations and variations in different disturbances. Its Simulink model is depicted as follows:

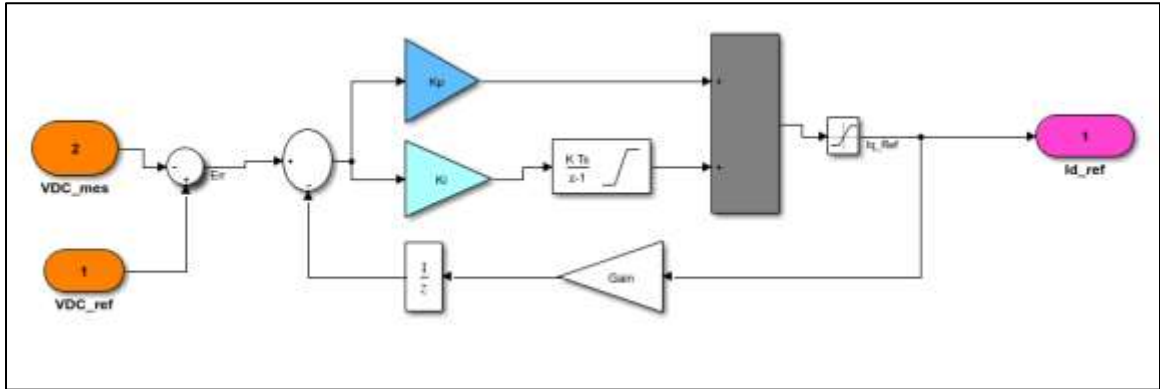


Figure 3. 16:PI based DC voltage regulator for id-ref

- ❖ dq0 to abc transformation block transforms the dq0 to abc using the following equations:

$$V_a = V_d * \sin \omega t + V_q * \cos \omega t + V_0 \tag{3.37}$$

$$V_b = V_d * \sin \left(\omega t - \frac{2\pi}{3} \right) + V_q * \cos \left(\omega t - \frac{2\pi}{3} \right) + V_0 \tag{3.38}$$

$$V_c = V_d * \sin \left(\omega t + \frac{2\pi}{3} \right) + V_q * \cos \left(\omega t + \frac{2\pi}{3} \right) + V_0 \tag{3.39}$$

- ❖ Discrete PWM generator block generates the PWM signal to control the switching condition of power converter to regulate the output voltage.

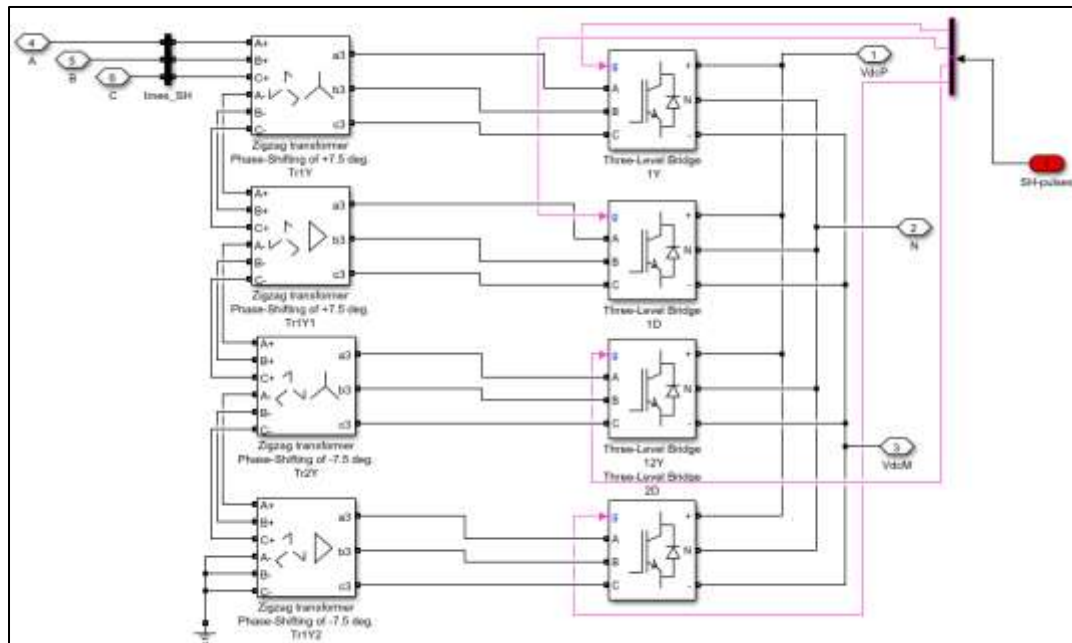


Figure 3. 17:Shunt voltage source converter (switches)

- ❖ Shunt voltage source converter block is the main part of the converter at which voltage is converted either from AC to DC or DC to AC via a common DC link Capacitor. It consists of four identical zigzag transformer and four identical three-level bridge GTO to turn on and off system parameters based on predetermined set values. The Zigzag transformer is selected because of its iron core design to limit the harmonic fluxes. Zigzag transformers are smaller in size than wye-delta transformers for the same zero sequence impedance, which makes them less costly than wye-delta transformers. The tasks that has to be done by three-level bridge GTO depends on the input pulses coming from the shunt controller.

3.4.3 Controller Design of Series Converter

In the transformation of the series controller to state space equation, the rotating axis is synchronous with the receiving end voltage V_r . So, $V_{rd} = |V_r|, V_{rq} = 0$. Equation (3.20) can be reorganized as the following form:

$$\frac{d}{dt} \begin{bmatrix} i_{sed} \\ i_{seq} \end{bmatrix} = \begin{bmatrix} -\frac{R_{se}}{L_{se}} & 0 \\ 0 & -\frac{R_{se}}{L_{se}} \end{bmatrix} * \begin{bmatrix} i_{sed} \\ i_{seq} \end{bmatrix} + \frac{1}{L_{se}} \begin{bmatrix} V_{1d} + V_{sed} - V_{rd} + \omega L_{se} i_{seq} \\ V_{1q} + V_{seq} - \omega L_{se} i_{sed} \end{bmatrix} \quad (3.40)$$

Where, $\dot{x} = \frac{d}{dt} \begin{bmatrix} i_{sed} \\ i_{seq} \end{bmatrix}$, $x = \begin{bmatrix} i_{sed} \\ i_{seq} \end{bmatrix}$, $A = \begin{bmatrix} -\frac{R_{se}}{L_{se}} & 0 \\ 0 & -\frac{R_{se}}{L_{se}} \end{bmatrix}$, $B = \begin{bmatrix} 1 & 0 \\ 0 & 1 \end{bmatrix}$, $Y = \begin{bmatrix} Y1 \\ Y2 \end{bmatrix}$

$C = \begin{bmatrix} 1 & 0 \\ 0 & 1 \end{bmatrix}$, and $u = \begin{bmatrix} u1 \\ u2 \end{bmatrix} = \frac{1}{L_{se}} \begin{bmatrix} V_{1d} + V_{sed} - V_{rd} + \omega L_{se} i_{seq} \\ V_{1q} + V_{seq} - \omega L_{se} i_{sed} \end{bmatrix}$

Equation (3.40) can be written as:

$$\frac{d}{dt} \begin{bmatrix} i_{sed} \\ i_{seq} \end{bmatrix} = \begin{bmatrix} -\frac{R_{se}}{L_{se}} & 0 \\ 0 & -\frac{R_{se}}{L_{se}} \end{bmatrix} * \begin{bmatrix} i_{sed} \\ i_{seq} \end{bmatrix} + \begin{bmatrix} u_1 \\ u_2 \end{bmatrix} \quad (3.41)$$

Lets assume the following equation to integrate control variables u with PI:

$$\begin{cases} u1 = \frac{1}{L_{sh}} \left(k_{psh} + \frac{k_{ish}}{s} \right) (i_{shd}^* - i_{shd}) \\ u2 = \frac{1}{L_{sh}} \left(k_{psh} + \frac{k_{ish}}{s} \right) (i_{shq}^* - i_{shq}) \end{cases} \quad (4.42)$$

Where, i_{sed}^* is the d- component reference current of series converter and i_{seq}^* is the q- component reference current of series converter. Then, substitute (4.42) into (4.41) and equate it with (3.40) and solving for reference of the output of the series converter V_{sed}^* and V_{seq}^* will give:

$$\begin{bmatrix} V_{sed}^* \\ V_{seq}^* \end{bmatrix} = \begin{bmatrix} k_{pse} + \frac{k_{ise}}{s} & 0 \\ 0 & k_{pse} + \frac{k_{ise}}{s} \end{bmatrix} * \begin{bmatrix} i_{sed}^* - i_{sed} \\ i_{seq}^* - i_{seq} \end{bmatrix} + \begin{bmatrix} V_{rd} - V_{1d} - \omega i_{seq} \\ -V_{1q} + \omega i_{sed} \end{bmatrix} \quad (4.43)$$

The series converter control diagram is shown in the figure below:

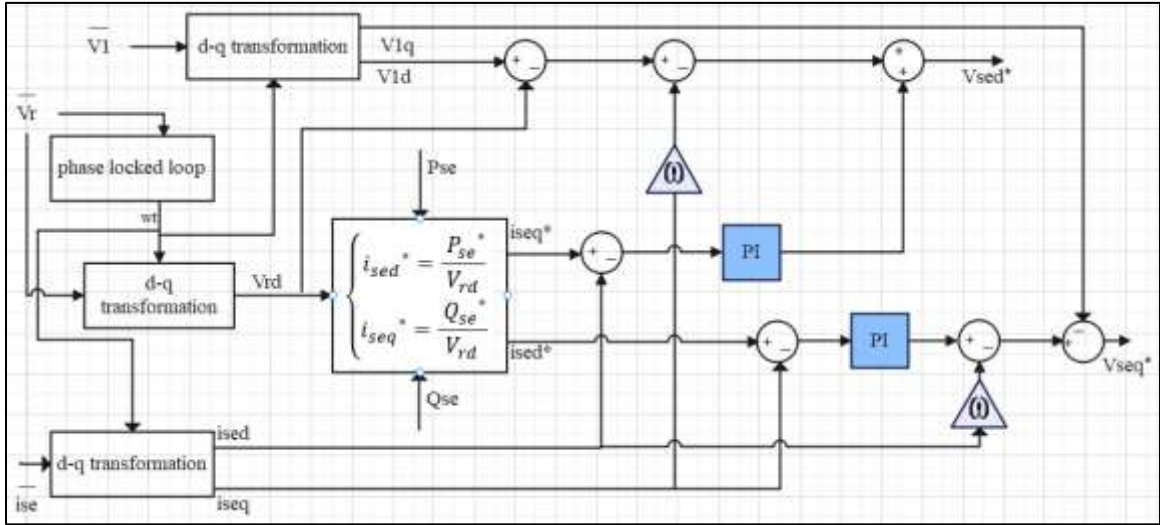


Figure 3. 18:D-Q frame of series converter control of UPFC

3.4.4 Simulink Model of Series Converter Controller

Taking the mathematical modeling of series converter controller, MATLAB/SIMULINK model has been designed. The overall Simulink model of series controller is as depicted below:

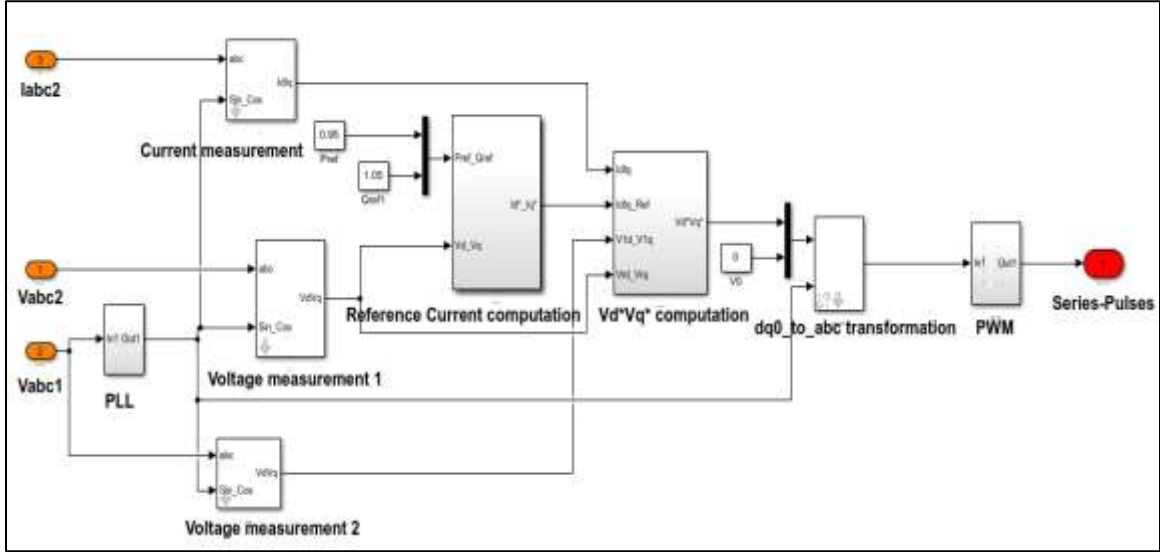


Figure 3. 19:SIMULINK models of series converter controller

Each block in the Simulink model is described below:

- ❖ The PLL block models is a Phase Lock Loop (PLL) closed-loop control system, which tracks the frequency and phase of a sinusoidal signal by using an internal frequency oscillator. The control system adjusts the internal oscillator frequency to keep the phase difference to zero.
- ❖ Voltage measurement and current measurement block measures the line voltage and current, and transforms to d-q-0 frame using parks transformation. The fundamental reason to transform the three-phase instantaneous voltages and currents into the synchronously rotating reference d-q-o frame is to make computations much easier. Secondly, it allows the system operator to independently control the active (d-axis) and reactive (q-axis) components of the currents.
- ❖ Reference computation block computes the instantaneous reactive and active reference current as follows:

$$i_d^* = \frac{P * V_d + Q * V_q}{V_d^2 + V_q^2} \quad (3.44)$$

$$i_q^* = \frac{P * V_q - Q * V_d}{V_d^2 + V_q^2} \quad (4.45)$$

From equation (4.44) and (4.45), the Simulink model of reference computation block is shown in the figure below.

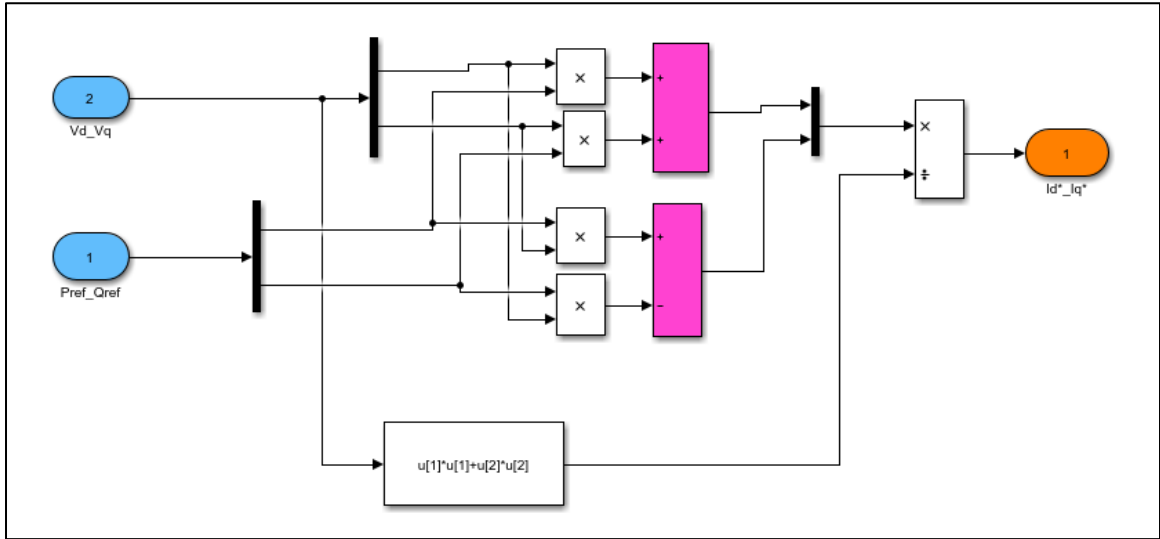


Figure 3. 20: Simulink model of d-axis and q-axis reference current computation of series controller of UPFC

- ❖ Control variable computation block computes the d-axis and q-axis reference voltage based on the given input (i.e d-axis and q-axis reference current, d-axis and q-axis current, and source voltage). Its Simulink model is represented as shown below:

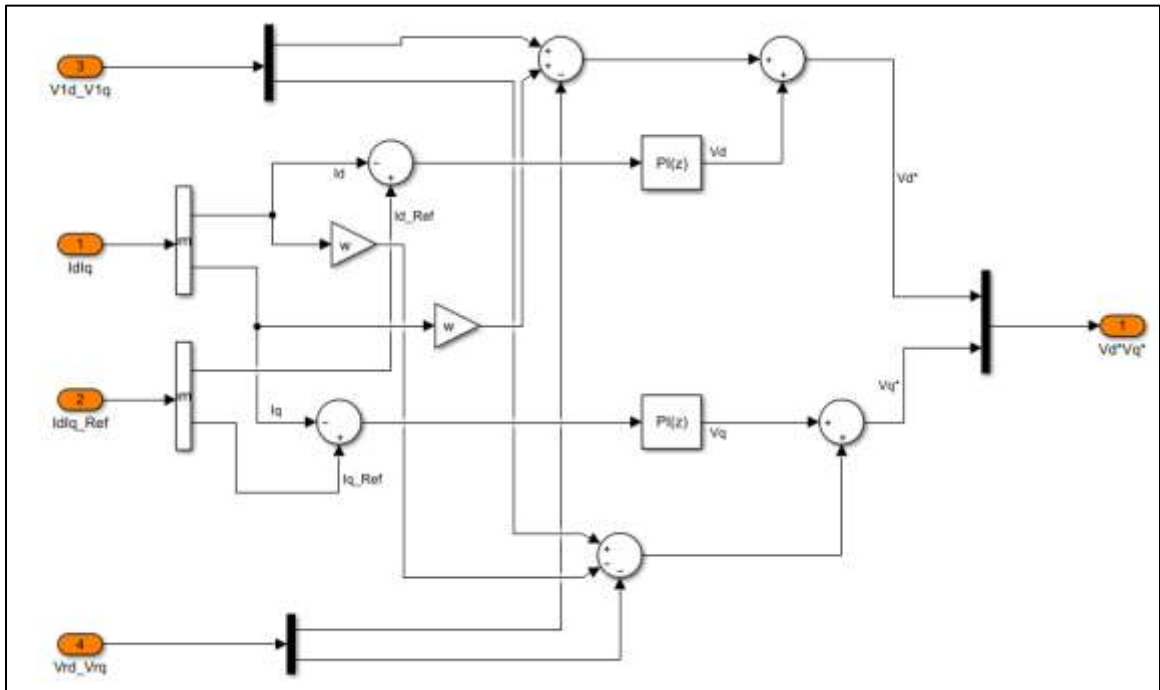


Figure 3. 21: D-axis and Q-axis reference voltage of series converter

- ❖ dq0 to abc Transformation block transforms the dq0 to abc as follows:

$$V_a = V_d * \sin wt + V_q * \cos wt + V_0 \quad (3.46)$$

$$V_b = V_d * \sin\left(wt - \frac{2\pi}{3}\right) + V_q * \cos\left(wt - \frac{2\pi}{3}\right) + V_0 \quad (3.47)$$

$$V_c = V_d * \sin\left(wt + \frac{2\pi}{3}\right) + V_q * \cos\left(wt + \frac{2\pi}{3}\right) + V_0 \quad (3.48)$$

- ❖ Discrete PWM generator block generates the PWM signal to control the switching condition of power convertor to regulate the output voltage .

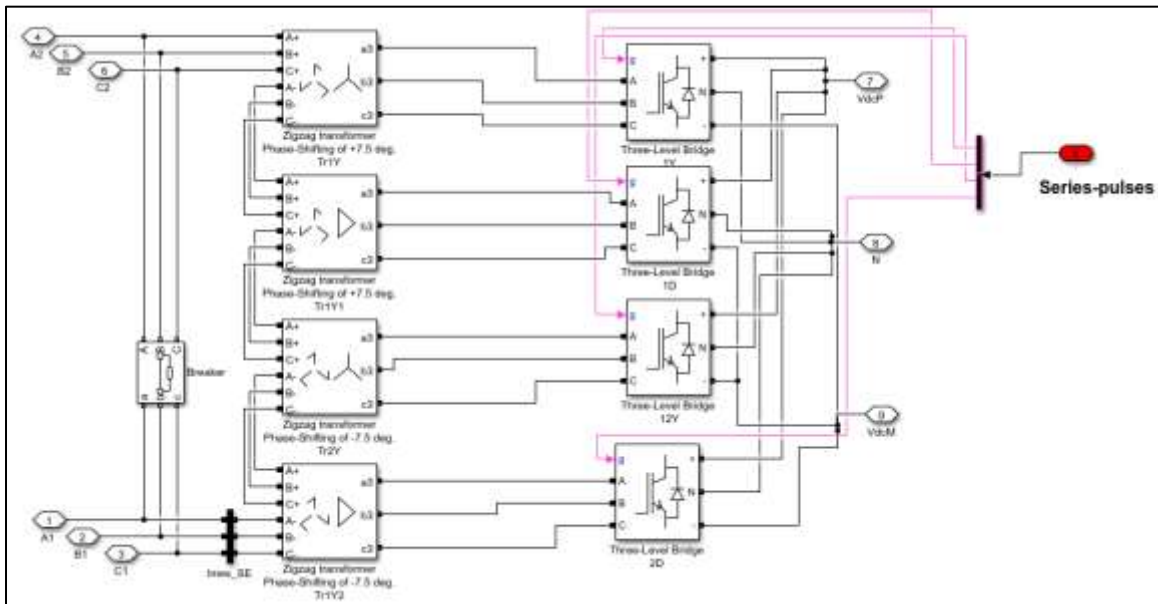


Figure 3. 22:Series voltage source converter (switches)

- ❖ Series voltage source converter block is the main part of the converter at which voltage is converted either from AC to DC or DC to AC via a common DC link Capacitor. It consists of four identical zigzag transformer and four identical three-level bridge GTO to turn on and off system parameters based on pulse signals. The Zigzag transformer is selected because of its iron core design to limit the harmonic fluxes. Zigzag transformers are smaller in size than wye-delta transformers for the same zero sequence impedance, which makes them less costly than wye-delta transformers. A gate turn-off thyristor (GTO) is a high-power semiconductor device. It works by acting as a switch in high-voltage circuits. Like a thyristor (SCR Silicon-Controlled Rectifier), it has 3 terminals; anode, cathode, and a gate terminal. The tasks that has to be done by three-level bridge GTO depends on the input pulses coming from the series controller.

CHAPTER FOUR

4. DESIGN OF ADAPTIVE NEURO-FUZZY-BASED UNIFIED POWER FLOW CONTROLLER AND ITS OPTIMAL LOCATION

4.1 Optimal Location of Unified Power Flow Controller Using Modified PSO Integrated With Newton Raphson Algorithm

4.1.1 Power Flow Study using Newton Raphson Algorithm

Power flow studies are crucial for planning and operation of power system. The magnitude and angle of the voltage at each bus are obtained by a power flow analysis. Once the bus voltage magnitudes and angles are determined, system losses can be determined by calculating the real and reactive power flow through each line. Power flow studies are a steady state analysis of a power system. These studies are known as load flow studies. Since the loads are specified in terms of power, the resulting equations are non-linear algebraic which need to be solved iteratively [40]. Newton-Raphson power flow analysis is an iterative technique for solving a set of various nonlinear equations with an equal number of unknowns. Load flow solution by Newton's method is mathematically superior to the Gauss-Seidel method and it is less prone to divergence with ill-conditioned problems [41].

4.1.2 Power Flow Problem

Figure below shows a typical i^{th} bus of a power system. The relation between voltage and current is obtained by the application of KCL to this bus.

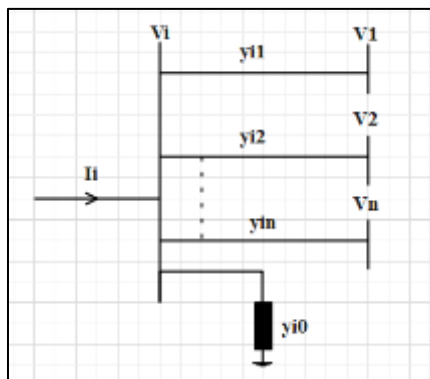


Figure 4. 1:A typical bus of power system

The net current injected into the network at the i^{th} bus is:

$$I_i = Y_{i1}V_1 + Y_{i2}V_2 + \dots + Y_{iN}V_N = \sum_{n=1}^N Y_{in}V_n \quad (4.1)$$

Where N be the total number of buses in the network. Let P_i and Q_i be the net real and reactive power entering the network at the i^{th} bus.

$$P_i + jQ_i = V_i I_i^* \quad (4.2)$$

By substituting equation (4.1) into equation (4.2) will give (4.3) :

$$P_i - jQ_i = V_i^* \sum_{n=1}^N Y_{in}V_n \quad (4.3)$$

Equating the real and imaginary parts:

$$P_i = \sum_{n=1}^N |Y_{in}| |V_i| |V_n| \cos(\theta_{in} + \delta_n - \delta_i) \quad (4.4)$$

$$Q_i = - \sum_{n=1}^N |Y_{in}| |V_i| |V_n| \sin(\theta_{in} + \delta_n - \delta_i) \quad (4.5)$$

Equations (4.4) and (4.5) form a set of nonlinear algebraic equations in terms of independent variables. Expanding equations (4.4) and (4.5) in Taylor's series, results in set of linear equations as given below.

$$\begin{bmatrix} \Delta P_2^{(k)} \\ \vdots \\ \Delta P_n^{(k)} \\ \Delta Q_2^{(k)} \\ \vdots \\ \Delta Q_n^{(k)} \end{bmatrix} = \begin{bmatrix} \frac{\partial P_2^{(k)}}{\partial \delta_2^{(k)}} & \dots & \frac{\partial P_2^{(k)}}{\partial \delta_n^{(k)}} & \frac{\partial P_2^{(k)}}{\partial |V_2|^{(k)}} & \dots & \frac{\partial P_2^{(k)}}{\partial |V_n|^{(k)}} \\ \vdots & \ddots & \vdots & \vdots & \ddots & \vdots \\ \frac{\partial P_n^{(k)}}{\partial \delta_2^{(k)}} & \dots & \frac{\partial P_n^{(k)}}{\partial \delta_n^{(k)}} & \frac{\partial P_n^{(k)}}{\partial |V_2|^{(k)}} & \dots & \frac{\partial P_n^{(k)}}{\partial |V_n|^{(k)}} \\ \frac{\partial Q_2^{(k)}}{\partial \delta_2^{(k)}} & \dots & \frac{\partial Q_2^{(k)}}{\partial \delta_n^{(k)}} & \frac{\partial Q_2^{(k)}}{\partial |V_2|^{(k)}} & \dots & \frac{\partial Q_2^{(k)}}{\partial |V_n|^{(k)}} \\ \vdots & \ddots & \vdots & \vdots & \ddots & \vdots \\ \frac{\partial Q_n^{(k)}}{\partial \delta_2^{(k)}} & \dots & \frac{\partial Q_n^{(k)}}{\partial \delta_n^{(k)}} & \frac{\partial Q_n^{(k)}}{\partial |V_2|^{(k)}} & \dots & \frac{\partial Q_n^{(k)}}{\partial |V_n|^{(k)}} \end{bmatrix} \begin{bmatrix} \Delta \delta_2 \\ \vdots \\ \Delta \delta_n \\ \Delta |V_2|^{(k)} \\ \vdots \\ \Delta |V_n|^{(k)} \end{bmatrix} \quad (4.6)$$

The Jacobian matrix gives the linearized relationship between small changes in the voltage angle $\Delta\delta_i^{(k)}$ and $\Delta|V_i^k|$ voltage magnitude with the small changes in real $\Delta P_i^{(k)}$ and reactive power $\Delta Q_i^{(k)}$. Equation 4.6 can be written in short form as:

$$\begin{bmatrix} \Delta P \\ \Delta Q \end{bmatrix} = \begin{bmatrix} J1 & J2 \\ J3 & J4 \end{bmatrix} \begin{bmatrix} \Delta\delta \\ \Delta|V| \end{bmatrix} \quad (4.7)$$

The diagonal and the off diagonal elements of J_1 are:

$$\frac{\partial P_i}{\partial \delta_i} = \sum_{j \neq i}^n |Y_{ij}| |V_i| |V_j| \sin(\theta_{ij} - \delta_i + \delta_j) \quad (4.8)$$

$$\frac{\partial P_i}{\partial \delta_j} = -|Y_{ij}| |V_i| |V_j| \sin(\theta_{ij} - \delta_i + \delta_j) \quad j \neq i \quad (4.9)$$

The diagonal and the off-diagonal elements of J_2 are:

$$\frac{\partial P_i}{\partial |V_i|} = 2|Y_{ii}| |V_i| \cos(\theta_{ii}) + \sum_{j \neq i}^n |Y_{ij}| |V_j| \cos(\theta_{ij} - \delta_i + \delta_j) \quad (4.10)$$

$$\frac{\partial P_i}{\partial |V_j|} = |Y_{ij}| |V_i| \cos(\theta_{ij} - \delta_i + \delta_j) \quad j \neq i \quad (4.11)$$

The diagonal and the off-diagonal elements of J_3 are:

$$\frac{\partial Q_i}{\partial \delta_i} = \sum_{j \neq i}^n |Y_{ij}| |V_i| |V_j| \cos(\theta_{ij} - \delta_i + \delta_j) \quad (4.12)$$

$$\frac{\partial Q_i}{\partial \delta_j} = -|Y_{ij}| |V_i| |V_j| \cos(\theta_{ij} - \delta_i + \delta_j) \quad j \neq i \quad (4.13)$$

The diagonal and off-diagonal elements of J_4 are:

$$\frac{\partial Q_i}{\partial |V_i|} = -2|Y_{ii}| |V_i| \sin(\theta_{ii}) - \sum_{j \neq i}^n |Y_{ij}| |V_j| \cos(\theta_{ij} - \delta_i + \delta_j) \quad (4.14)$$

$$\frac{\partial Q_i}{\partial |V_j|} = -|Y_{ij}| |V_i| \sin(\theta_{ij} - \delta_i + \delta_j) \quad j \neq i \quad (4.15)$$

$\Delta P_i^{(k)}$ and $\Delta Q_i^{(k)}$ are the difference between the scheduled and calculated values, known as power residuals which is given by:

$$\Delta P_i^{(k)} = P_i^{(sch)} - P_i^{(k)} \quad (4.16)$$

$$\Delta Q_i^{(k)} = Q_i^{(sch)} - Q_i^{(k)} \quad (4.17)$$

The new updated bus voltages and angles are:

$$|V_i^{(k+1)}| = |V_i^{(k)}| + \Delta|V_i^{(k)}| \quad (4.18)$$

$$\delta_i^{(k+1)} = \delta_i^{(k)} + \Delta\delta_i^{(k)} \quad (4.19)$$

The iteration will continue until the magnitude of power residuals $\Delta P_i^{(k)}$ and $\Delta Q_i^{(k)}$ are less than the specified accuracy. Rather than using the Newton Raphson alone, integrating PSO algorithm with Newton Raphson provides accurate convergence and reduced computational time. This algorithm is applied to the computational achievement of the load flow solution, based on the power minimization of the power mismatches in the power system. The minimum voltage magnitude observed among the given bus voltage magnitudes is considered the worst case at which a FACTS compensator needs to be placed [42].

4.1.3 Modified Particle Swarm Optimization

PSO is a population-based optimization technique that was originally developed in 1995 by Drs. James Kennedy and Russell Eberhart. It was inspired by the graceful behaviour of a school of fish and a flock of birds. This artificial intelligence technique can be used to find approximate solutions to extremely difficult numeric maximization and minimization problems. A population-based search method with the position of a particle represents a solution with a swarm of particles as the searching agent. It uses a number of particles (agents) that constitute a swarm moving around in the search space looking for the best solution. Unlike other intelligent optimization techniques, PSO allows for global and local exploration of solutions. PSO is more robust in finding optimal control parameters and it is computationally efficient [42].

In PSO, each single solution is viewed as a particle. The position of each particle can be expressed as $X_i = (X_{i1}, X_{i2}, X_{i3}, \dots, X_{im})$. The initial solutions in PSO are randomly selected and then PSO will continually search for optimal value by updating the solutions in each iteration. The fitness value of the particle is related to the objective function and the velocity of the particles $V_i = (V_{i1}, V_{i2}, V_{i3}, \dots, V_{im})$ is related to its previous velocity, global best known position, and local best-known position. The velocity indicates the directions of all the particles in the next iteration [43].

The local best-known position is the best solution that achieved by each particle so far. The global best-known position is the best solution among all the achieved solutions. The inertia velocity part, local best-known position part (cognitive component), and global best-known position (social component) are part of the velocity which reflects the cooperation and competition mechanism in PSO. PSO starts with a group of randomly generated solutions and updates the solutions in each iteration. The behavior of all the particles appears to be managed by a control center [44].

Each particle in the search space tries to modify its velocity and position using the following equation. In PSO search scheme there are two best positions.

1. Personal best (P^{best}): The best particle achieved so far by that particle.
2. Global best (G^{best}): The best value obtained so far by any particle in the neighbourhood of that particle.

$$V^{t+1} = w * V^t + c1r1(P^{best} - X^t) + c2r2(G^{best} - X^t) \quad (4.20)$$

$$X^{t+1} = X^t + V^{t+1} \quad (4.21)$$

Where; V^t is velocity of the particle at time t .

X^t is Particle position at time t .

W is Inertia weight.

$c1$ and $c2$ are learning factor or accelerating coefficient.

$r1$ and $r2$ are uniformly distributed random number between 0 and 1.

P^{best} and G^{best} are particles best position and global best position respectively.

Acceleration coefficients are essential parameters of particle swarm optimization, which helps to control the movement of particles by modifying their cognitive and social components. It handles the step sizes of the particles in the next iteration. If the acceleration coefficients are too small, the particles may not have enough velocity to reach the target point. If the acceleration coefficients are too large, the particles may go beyond the optimal value. Appropriate selection of acceleration coefficients could avoid trapping in local minima and reduce the computation time. Inertia weight is used to control the influence of previous velocity on the new velocity. A large inertia weight facilitates a global search, while a small inertia weight facilitates a local search.

4.1.4 Problem formulation for Particle Swarm Optimization

I. Objective Function

The objective function is to minimize the transmission loss by changing control variables within their limits. Hence, the system constraints, which are to be formed as equality and inequality constraints, are shown below. The objective function is to minimise the real power loss to find the optimal location of UPFC by integrating the PSO algorithm with the Newton Raphson load flow algorithm. PSO was selected as an optimization method due to its popularity as a successful algorithm in solving non-smooth optimization problems.

Objective function = Min $F(P_{loss})$

The real power loss of the system equals the sum of the real power loss on each branch, and it can be described as [45]:

$$F: P_{loss} = \sum_{i \in j}^N G_{ij} (V_i^2 + V_j^2 - 2V_i V_j \cos \theta_{ij}) \quad (4.22)$$

Where: N is the number of the branches.

G_{ij} is the conductance of the branch between bus i and bus j.

V_i is the voltage magnitude of bus i.

V_j is the voltage magnitude of bus j.

θ_{ij} is the difference of phase angle between bus i and bus j.

II. Equality Constraints

The equality constraints are the power balance equations, which can be described by the equations as follows.

$$P_{gi} - P_{di} - V_i \sum_{j=1}^{NP} V_j (G_{ij} \cos\theta_{ij} + B_{ij} \sin\theta_{ij}) = 0 \quad (4.23)$$

$$Q_{gi} - P_{di} - V_i \sum_{j=1}^{NQ} V_j (G_{ij} \sin\theta_{ij} - B_{ij} \cos\theta_{ij}) = 0 \quad (4.24)$$

Where: P_{gi} is the real power generation at bus i.

P_{di} is the real power demand at bus i.

Q_{gi} is the real power generation at bus i.

Q_{di} is the real power demand at bus i.

III. Inequality Constraints

The inequality constraints taken is bus voltage magnitude.

$$V_i^{min} < V_i < V_i^{max} \quad (4.25)$$

The per unit bus voltage value should be within the prescribed limit (i.e. with $\pm 5\%$ in the range of $(0.95 \leq v_i \leq 1.05)$).

IV. The Penalty Functions

These are added to the objective function. The main goal of penalty function is to maintain the system security. When power flow problem has too many constraints, sometimes a feasible solution cannot be obtained. To avoid this situation, some constraints are not enforced completely. In this study, bus voltages, was chosen as penalty functions. Although constraints at penalty function can be violated, this violation should be very small and when violation at constraint increases, penalty function should increase quickly. Thus, quadratic penalty functions more suitable for optimal power flow problems are used in this study. The most significant advantage of quadratic penalty function is to control importance of

constraint in optimal power flow by simply changing value of penalty factor [46]. The equations are depicted as follows:

$$\Omega_v = \rho \sum_{i=1}^{N_B} \{\max(0, |V_i| - |V_i^{max}|)\}^2 + \rho \sum_{i=1}^{N_B} \{\max(0, |V_i^{min}| - |V_i|)\}^2 \quad (4.26)$$

Where;

Ω_v is the penalty function for bus voltages.

ρ is the penalty factor.

V_i^{max} is upper limit of voltage magnitude at bus i.

V_i^{min} is lower limit of voltage magnitude at bus i.

If the bus voltage value is greater than or less than the prescribed limit, it will be penalized by simply changing value of penalty factor based equation (4.26). To identify the weakest bus ,PSO integrated with Newton Raphson is applied in three different scenarios. Its result is shown in the table 4.1 below.

- I. PSO at peak load
- II. PSO at average load
- III. PSO at light load

Table 4. 1: PSO parameters used for UPFC placement

PSO parameter	Value
Cognitive factor min (C1)	1.5
Cognitive factor max (C1)	2.5
Social factor min (C2)	1.5
Social factor max (C2)	2.5
Inertia weight min (Wmin)	0.4
Inertia weight max (Wmax)	0.9
Maximum number of iteration	50
Population size	100

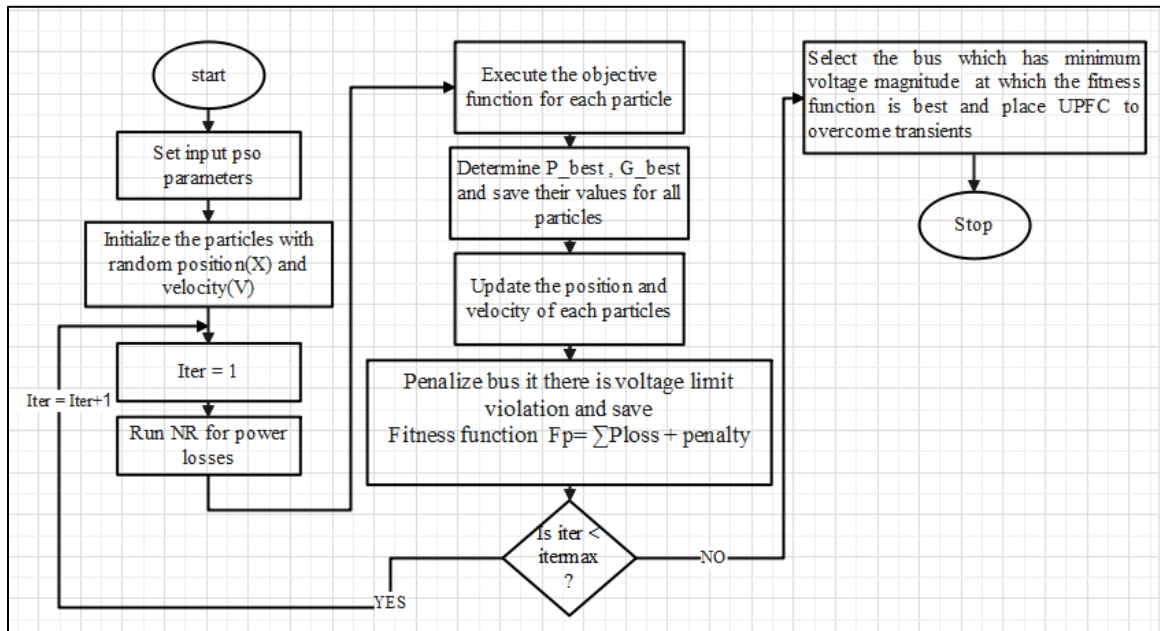


Figure 4. 2:Flow chart of the modified PSO for UPFC placement

Table 4. 2:Bus voltage magnitude using modified PSO at three different loading scenarios

Bus No	Bus location	Voltage magnitude (p.u) at peak load	Voltage magnitude (p.u) at average load	Voltage magnitude (p.u) at light load
1	Tana Beles	1.0200	1.0200	1.0200
2	Tis Abay II	1.0100	1.0100	1.0100
3	Bahir Dar 400kV	0.9365	0.9421	0.9539
4	Bahir Dar 230kV	0.9365	0.9489	0.9549
5	Bahir Dar 132kV	0.9532	0.9549	0.9563
6	D/markos 400kV	0.9532	0.9569	0.9683
7	D/markos 230kV	0.9432	0.9559	0.9682
8	Mota 230kV	0.9532	0.9579	0.9683
9	Alamata 230kV	0.9432	0.9529	0.9533
10	Gonder I 230kV	0.9570	0.9608	0.9631
11	Gonder II 230kV	0.9548	0.9612	0.9634

According to the PSO result, the bus with the lowest magnitude of voltage at peak load, average load, and light load is taken as the optimal location for UPFC placement. Based on the proposed algorithm, the Bahir Dar 400 kV bus bar is the selected bus to place UPFC, as its magnitude is 0.9365, 0.9421, and 0.9539 (i.e., a low voltage magnitude bus with the lowest value, which is ranked as the weakest bus) for peak load, average load, and light load, respectively. The convergence characteristics for 50 iterations are as follows:

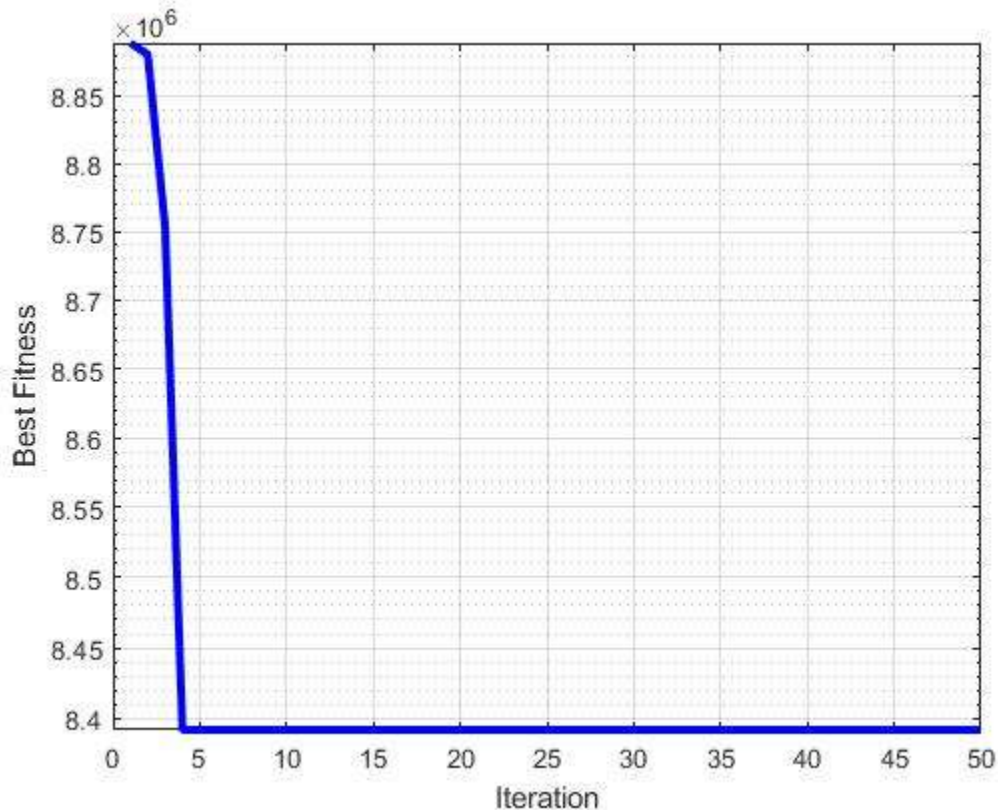


Figure 4. 3:Convergence characteristics at peak load for 50 iteration

4.2 UPFC Converter Sizing

Based on power flow analysis using newton Raphson, the weakest bus selected for UPFC allocation is Bahirdar 400kV substation bus bar. Sizing errors are detrimental to both the UPFC and the power network. Shunt converter rating, series converter rating, and capacitor rating are all included in sizing. The line voltage and power where the UPFC is connected serve as the input to the primary side transformers of both converters. The bus bar voltage,

which is 400kV, is the same as the primary side voltage of the transformers used in the shunt and series converters (i.e $V_{sh \text{ primary}} = V_{SE \text{ primary}} = 400 \text{ kV}$).

The transformer used in the convertor design is zigzag transformer. Due to its reduced cost and the iron core design's capacity to restrict the flow of the triple-harmonic fluxes, the zigzag transformer is the most widely used. For the same zero-sequence impedance, zigzag transformers are more compact than wye-delta transformers. Zigzag transformers are often used for high voltage lines when connecting three phase inverters to the grid to provide a stable neutral voltage and prevent excessive phase to ground voltages. The nominal power, nominal voltage, and frequency of both shunt and series convertor primary side are similar with the transmission line i.e. 133MVA, 400KV, and 50HZ respectively. Transformer impedance and magnetizing branch is selected from zig zag transformer catalogue. Three level bridge convertor (GTO) implements a three-level bridge of selected forced-commutated power electronics devices which is directly connected with zigzag transformer.

UPFC is placed between two buses named UPFC sending end bus and the UPFC receiving end bus. It consists of two Voltage-Sourced Converters (VSCs) with a common DC link. For the fundamental frequency model, the VSCs are replaced by two controlled voltage sources. The voltage source at the sending bus is connected in shunt and will therefore be called the shunt voltage source. The second source, the series voltage source, is placed between the sending and the receiving buses. The UPFC is placed on high-voltage transmission lines. This arrangement requires step-down transformers in order to allow the use of power electronics devices for the UPFC [7].

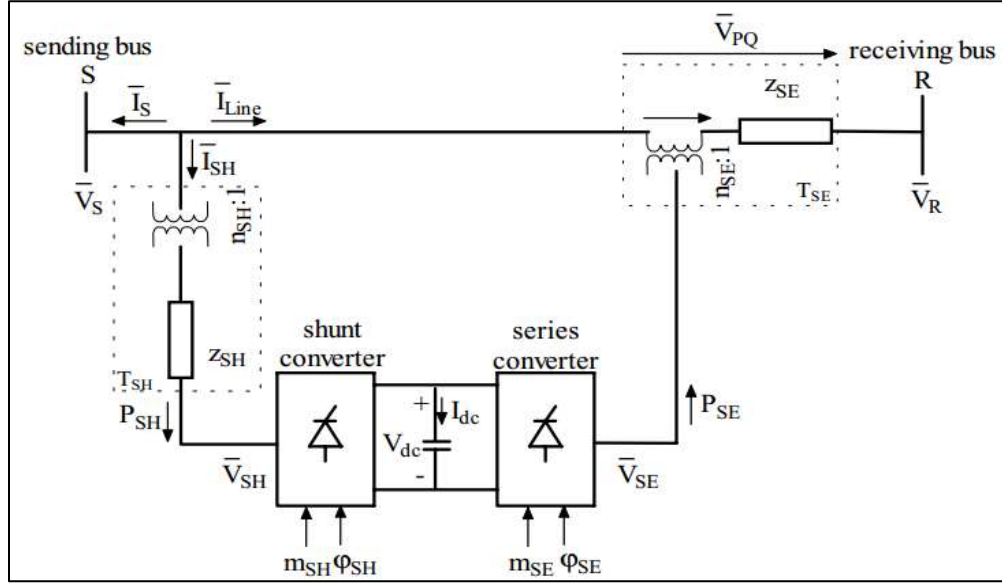


Figure 4. 4:Fundamental frequency model of UPFC

To calculate capacitance of capacitor the rated KVAR of the line must be known, then actual KVAR of the capacitor can be calculated as follows.

$$\text{Actual KVAR} = \text{Rated KVAR} * \frac{\text{Minimum operating frequency of the system}}{\text{Rated frequency of the system}} \quad (4.27)$$

Rated KVAR of the line where UPFC is connected = 45.69 KVAR (i.e Bahir Dar 400kV)

Rated frequency=50 Hz

Operating frequency recorded = minimum 49 Hz

$$\text{Actual KVAR} = 45.69 * \frac{49}{50} = 44.776\text{KVAR}$$

Then capacitance of capacitor can be obtained from the actual KVAR using equation (4.28):

$$C = \frac{\text{Actual KVAR} * 10^3}{2\pi V^2} \quad (4.28)$$

Where V= 400 kV (The bus bar voltage) at which UPFC is connected .

$$C = \frac{44.77 * 10^3}{2 * \pi * 400 \text{ kV}^2} = 4.455\text{mF}$$

For a given surface areas of electrode (A) to design a capacitor , the corresponding distance between the electrodes (D) can be obtained using the equation (4.29).

$$C = \varepsilon_0 \varepsilon_r \frac{A}{D} \quad (4.29)$$

Where, ε_0 : absolute permittivity (8.854 pF/m).

ε_r : relative permittivity of the material (1 for vacuum) .

D : distance of the space between the plates.

A: area of the plate.

The energy stored in a capacitor is proportional to the capacitance of the capacitor and the supply voltage to it. The maximum amount of energy that can be stored by DC link capacitor is 475 joules with charge time range 1 to 10 second [47].

$$E = \frac{CV_{DC}^2}{2} \quad (4.30)$$

Now solving for DC link voltage:

$$V_{DC} = \frac{2E}{C} = \frac{2 * 475}{4.455} = 213.243V(\sim 230V \text{ Standard})$$

Applying the Pulse Width Modulation (PWM) technique to the two VSCs the following equations helps to obtain magnitudes of shunt and series injected voltages at the secondary side of the transformer [48].

$$V_{SH \text{ secondary}} = m_{SH} \frac{V_{DC}}{2\sqrt{2} n_{SH} V_B} \quad (4.31)$$

$$V_{SE \text{ secondary}} = m_{SE} \frac{V_{DC}}{2\sqrt{2} n_{SE} V_B} \quad (4.32)$$

where: m_{SH} – Amplitude modulation index of the shunt VSC control signal

m_{SE} – Amplitude modulation index of the series VSC control signal

n_{SH} – Shunt transformer turn ratio.

n_{SE} – Series transformer turn ratio

V_B – Base voltage in kV

V_{DC} – DC link voltage

According to IEEE specifications of UPFC details, the amplitude modulation index of the shunt VSC and series VSC control signal is in the range of 0.01 to 0.1. Now solving for V_{SH} and V_{SE} :

$$\begin{aligned} V_{SH \text{ secondary}} &= m_{SH} \frac{V_{DC}}{2\sqrt{2} n_{SH} V_B} = 0.9 * \frac{230}{2\sqrt{2} * 0.0037 * 400} \\ &= 50 \text{ kV} \end{aligned}$$

$$\begin{aligned} V_{SE \text{ secondary}} &= m_{SE} \frac{V_{DC}}{2\sqrt{2} n_{SE} V_B} = 0.9 * \frac{230}{2\sqrt{2} * 0.0045 * 400} \\ &= 40 \text{ kV} \end{aligned}$$

The winding resistance, inductance, magnetizing branch resistance, and magnetizing branch inductance of UPFC are selected from UPFC IEEE catalogue based on the above calculated corresponding values. Then UPFC will have the following necessary block parameters of shunt and series transformer with a common dc link capacitor value.

Table 4. 3:Block parameters of shunt and series transformer

UPFC parameters	Shunt values	Series values
Nominal power (Sn)	133MVA	133MVA
Nominal frequency (fn)	50Hz	50Hz
Primary nominal voltage (Vp)	400kV	400kV
Secondary nominal voltage (Vs)	50kV	40kV
Primary winding resistance (R1)	0.0016pu	0.0012pu
Primary winding inductance (L1)	1pu	0.9pu
Secondary winding resistance (R2)	0.0016pu	0.0012pu
Secondary winding inductance (L2)	30pu	25pu
Magnetizing branch resistance (Rm)	1pu	1pu
Magnetizing branch inductance (Lm)	1pu	1pu

4.3 Design of Adaptive Neuro-Fuzzy Inference System for Unified Power Flow Controller

4.3.1 Background of Neuro Fuzzy Inference System

A neuro-fuzzy system is a fuzzy system that learns its parameters (fuzzy sets and fuzzy rules) by processing data samples using a learning algorithm developed from or inspired by neural network theory, proposed by Jang in 1993, which generates a fuzzy rule base and membership functions automatically [49]. The combination of fuzzy control and neural networks had acknowledged a significant role in improving controller performances. Fuzzy logic has proven effective for complex, non-linear and imprecisely defined systems. The common barrier in fuzzy logic is the derivation of fuzzy rules and the parameter tuning for the controller. The neural networks have powerful learning abilities, optimization abilities and adaptation. Separately, each one of these techniques possess advantages and disadvantages that, when mixed together, their cooperation provides better results than the ones achieved with the use of each isolated technique. An adaptive network-based connectionist fuzzy logic controller can be created by combining neural networks and fuzzy logic. The attributes of the rules, the topology of fuzzy sets, and the structure of the control system are modified by this integrated adaptive system [50]. The drawback of the neural network inability to explain decision and drawback of learning inability of fuzzy logic controller have been conquered by adaptive neuro fuzzy inference system.

4.3.2 Significance of Adaptive Neuro Fuzzy Inference System

The Fuzzy Inference System (FIS) is a method for interpreting the values of an input vector and assigning corresponding values to the output vector using a set of fuzzy rules. This is a technique for employing fuzzy logic to map an input to an output. The system makes decisions and determines patterns based on this mapping process. Fuzzy inference systems generally are divided into two categories:

- I. Mamdani FIS and
- II. Sugeno FIS.

The Mamdani fuzzy inference system was proposed by Ebrahim Mamdani. Firstly it was designed to control a steam engine and boiler combination by a set of linguistic control

rules obtained from the experienced human operators. In the Mamdani inference system, the output of each rule is a fuzzy logic set.

The second fuzzy inference system was proposed by Takagi, Sugeno, and Kang to develop a systematic approach for generating fuzzy rules from a given input-output dataset. A rule R_k can be stated as follows:

$$R_k: \text{IF } \mu_{A_i}(x) \text{ AND } \mu_{B_i}(y) \text{ THEN } F = p_k x + q_k y + r_k \quad (4.33)$$

where k is the number of rules, A_i and B_i are n fuzzy membership functions of any shape i.e., Gaussian, triangular, trapezoidal, etc., denoted by μ in the antecedent part of the rule. R_k , and p_k, q_k, r_k are the linear parameters of consequent part of the k th rule. The parameters of membership functions (antecedent or premise parameters) and consequent part of the rule (consequent parameters) are tuned during the training process. F is a function that is the output of fuzzy membership functions. ANFIS uses the Sugeno Fuzzy Inference System due to the following features as compared with Mamdani:

- ❖ Non distribution of output, only mathematical combination of the output and the rules strength.
- ❖ Sugeno FIS possess more flexibility in the system design.
- ❖ The Sugeno inference system is well suited to mathematical analysis rather than human input.
- ❖ Work well with optimization and adaptive techniques.
- ❖ Guarantee output surface continuity.

4.3.3 Types of Membership Function

Membership function (MF) is a function that describes how much a given input belongs to a set. In the fuzzification and defuzzification stages of a FLS (fuzzy logic system), membership functions are employed to transform non-fuzzy input data into fuzzy linguistic terms and vice versa. In the first publication on fuzzy sets, Zadeh proposed membership functions (1965). In his theory of fuzzy sets, Zadeh suggested using a membership function that operates on the domain of all conceivable values and has a range covering the interval (0-1). Degree of membership function's output, which can only ever have a value between

0 and 1. It is also referred to as a membership grade or value. The membership function has different shapes, such as a triangular, Gaussian, generalized bell, and trapezoidal [51].

- ❖ **Triangular membership function:** One of the membership functions (MF) most frequently utilized and accepted in fuzzy logic controller design is triangular membership function. Three parameters, a , b , and c , can be used to define the triangle that fuzzes the input. Where a and c defining the base and b defining the height of the triangle.

$$\mu_{triangle}(x; a, b, c) = \begin{cases} 0, & x \leq a \\ \frac{x-a}{b-a}, & a \leq x \leq b \\ \frac{c-x}{c-b}, & b \leq x \leq c \\ 0, & x \geq c \end{cases} \quad (4.34)$$

- ❖ **Trapezoidal membership function:** defined by four parameters: a , b , c and d . Span b to c represents the highest membership value that element can take. And if x is between (a, b) or (c, d) , then it will have membership value between 0 and 1.

$$\mu_{trapezoidal}(x; a, b, c, d) = \begin{cases} 0, & x \leq a \\ \frac{x-a}{b-a}, & a \leq x \leq b \\ 1, & b \leq x \leq c \\ \frac{d-x}{d-c}, & c \leq x \leq d \\ 0, & d \leq x \end{cases} \quad (4.35)$$

- ❖ **Gaussian membership function:** is specified by two parameters $\{m, \sigma\}$ and can be defined as follows. In this function, m represents the mean or center of the Gaussian curve and σ represents the spread of the curve. This is more natural way of representing the data distribution, but due to mathematical complexity it is not much used for fuzzification.

$$\mu_{gaussian}(x; m, \sigma) = e^{-0.5\left(\frac{x-m}{\sigma}\right)^2} \quad (4.36)$$

- ❖ **Generalized bell shaped membership function:** It is also called Cauchy membership function. A generalized bell MF is specified by three parameters $\{a, b, c\}$ and can be defined as follows. It is called generalized MF, because by changing the parameters a , b and c , we can produce a family of different membership functions.

$$\mu_{bell}(x; a, b, c) = \frac{1}{1 + \left| \frac{x-c}{a} \right|^{2b}} \quad (4.37)$$

4.3.4 Architecture of Adaptive Neuro-Fuzzy Inference System

The architecture of the Adaptive Neuro-Fuzzy Inference System (ANFIS) is shown in figure 4.5 below. Consider a first-order sugeno fuzzy model with two input x and y and one output with fuzzy IF-THEN rules. ANFIS architecture consists of five-layers which comprises of two types of nodes: fixed and adaptable. The nodes in membership function layer and consequent layer are tunable, the rest of the nodes are fixed.

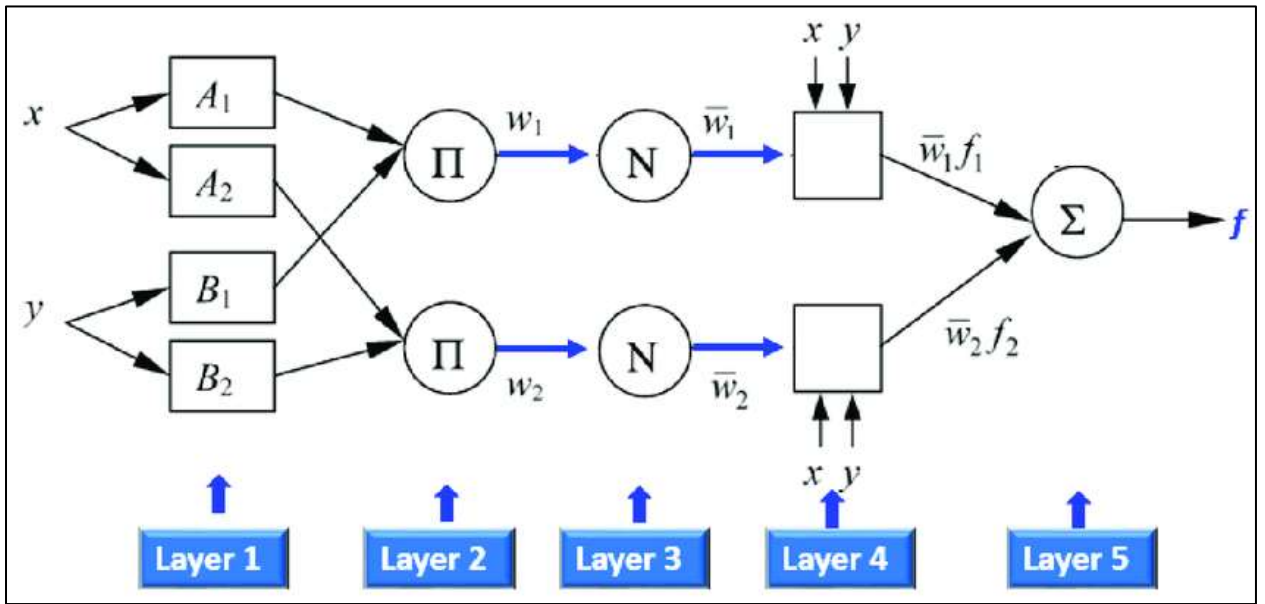


Figure 4. 5:Architecture of adaptive neuro fuzzy inference system

Standard structure of ANFIS w_1, w_2 and w_3 are the weight of the neurons and \bar{w}_1, \bar{w}_2 and \bar{w}_3 are the normalized weight of neurons.

- ❖ **Layer 1:** It is the fuzzification layer where each neuron is an adaptive node and holds the fuzzy value of the crisp inputs. The node output is calculated as follows:

$$O_i^1 = \begin{cases} \mu_{A_i}(x) & \forall i = 1,2, \\ \mu_{B_i}(y) & \forall i = 2,3, \end{cases} \quad (4.38)$$

Where μ is a membership function for the fuzzy sets A_i, B_i .

- ❖ **Layer 2:** This is an implication layer where the neurons contain the product of inputs, i.e., the weight of premise parameters. The node output is calculated as follows:

$$O_i^2 = w_i = \mu_{A_i}(x) * \mu_{B_i}(y), \forall i = 1,2, \quad (4.39)$$

Where w_i is the weight of the neuron.

- ❖ **Layer 3:** It is normalizing Layer where the neurons are fixed and are normalized by the sum of weights of all neurons in this layer. The node output is calculated as follows:

$$O_i^3 = \bar{w} = \frac{w_i}{\sum w_i}, \forall i = 1,2 \quad (4.40)$$

Where \bar{w} is the normalized weight of the neuron.

- ❖ **Layer 4:** This is the defuzzification layer where each neuron is also an adaptive node and holds the consequent parameters of the architecture. The node output is calculated as follows:

$$O_i^4 = \bar{w}fx + q_ky + r_k, \forall i = 1,2 \quad (4.41)$$

- ❖ **Layer 5:** It is an output layer where a single neuron is present for output, which computes the overall output as the summation of all incoming signals. The node output is calculated as follows:

$$O_i^5 = f(x,y) = \sum \bar{w}f = \frac{\sum w_i f_i}{\sum w_i} \quad \forall i = 1,2 \quad (4.42)$$

ANFIS learns by fine-tuning each of its tunable parameters (p_k , q_k , and r_k) in order to accurately map input to desired output with minimum error. Gradient descent (GD) is used by default in the ANFIS learning algorithm to fine-tune membership functions, and least square estimation (LSE) is used to train the consequent parameters. The two pass learning algorithm updates membership functions using gradient descent while back-propagating error back to the first layer and tunes subsequent parameters by least square estimation in the forward pass.

4.3.5 Design of Neuro Fuzzy Based Unified Power Flow Controller

Adaptive Neuro-Fuzzy Inference System (ANFIS) developed by Takagi-Sugeno blends advantages of both Artificial Neural Networks (ANNs) and Fuzzy Logic (FL) in a single framework. It provides accelerated learning capacity and adaptive interpretation capabilities to model complex patterns and apprehends nonlinear relationships.

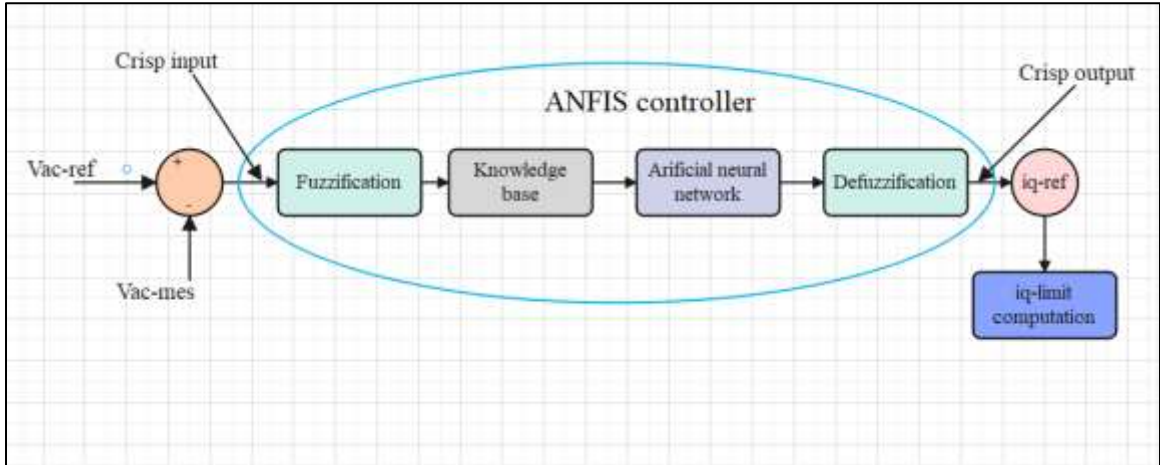


Figure 4. 6:Block diagram of adaptive neuro fuzzy inference system for iq-reference
 Vac-mes and Vac-ref is taken as the input to the AC voltage regulator of shunt controller ,which is used to calculate the q-axis current (Iq) value. These q-axis current value will be an input to the current regulator ,which is used to calculate the voltage and phase angle required for the transmission line. Vref is set to a constant value of 1pu. If the measured voltage is less than 1 pu, then PI adjusts the UPFC to inject current to the transmission line. If the measured voltage is greater than 1pu, then PI adjusts the UPFC to absorb current from the transmission line. Neither injection of current nor absorbtion is performed by UPFC ,If the measured voltage is equal to 1 pu.

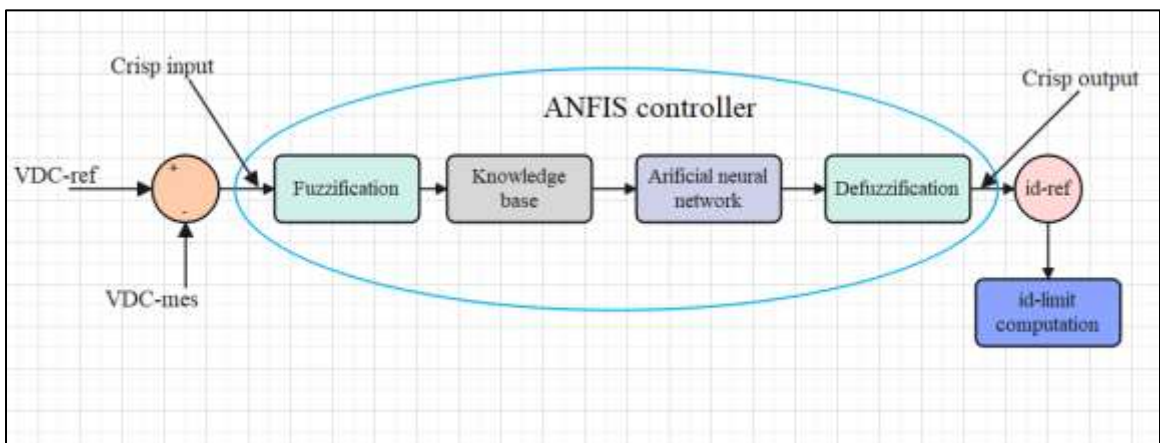


Figure 4. 7:Block diagram of adaptive neuro fuzzy inference system for id-reference
 VDC-mes and VDC-ref is taken as the input to the DC voltage regulator of shunt controller ,which is used to calculate the d-axis current (Id) value. These d-axis current value will be

an input to the d-axis current regulator ,which is used to calculate the voltage and phase angle required for series converter.

Table 4. 4:Characterstics of PID controller

Parameter	Rise time	Overshoot	Settling time	S-S error
Kp increase	Decrease	Increase	Small change	Decrease
Ki increase	Decrease	Increase	Increase	Eliminate
Kd increase	Small change	Decrease	Decrease	Small change

Since ANFIS-based UPFC provides a minimum overshoot and a low settling time when a disturbance is applied to a high-voltage transmission network, PI-based UPFC should be replaced by ANFIS-based UPFC [52].

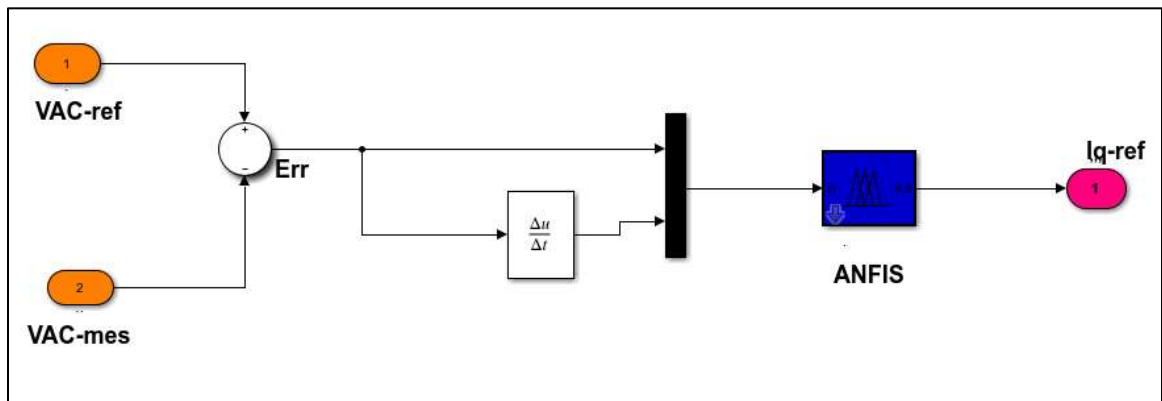


Figure 4. 8:ANFIS based iq-reference computation

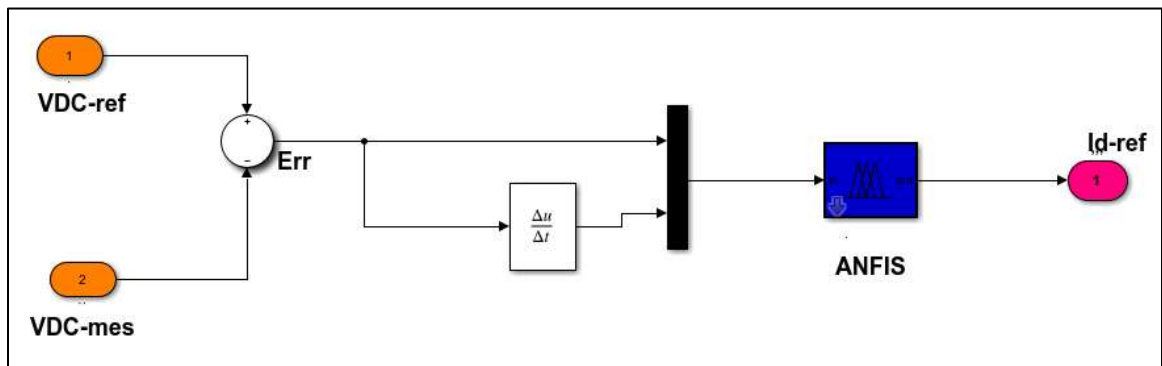


Figure 4. 9:ANFIS based id-reference computation

The input to the ANFIS controller is error (e) and derivative of error (de/dt) with a single output (I_{qref}). The choice of quadrature component current from real error is based upon the fact that when the quadrature reference current by UPFC is at right angle to line current it directly affects the reactance of the line hence regulates the real power flow. Further, the error and derivative of error being an input to the controller helps to design the rule base more effectively from the physical behavior of the power system following a transient disturbance such as fault.

Using a given input and output data set, the MATLAB toolbox function ANFIS constructs a Takagi Sugeno fuzzy inference system (FIS) whose membership function parameters are tuned (adjusted). This adjustment allows fuzzy systems to learn from the data they are modeling. Fuzzy inference system is a model that maps input characteristic to input membership function. Rule structure is effectively predetermined by the user's assessment of the characteristic of the variables in the model. ANFIS uses Takagi Sugeno approach to data modeling. We can select membership function parameters automatically using ANFIS tool in MATLAB. Using ANFIS we can apply fuzzy inference to a system for which we already have a collection of input and output data sets of parameters [53].

Some error measures are reduced via gradient vector. Typically, the sum of the squared differences between the desired and actual outputs is applied to determine this error measurement. Collect input and output data in a form that will be usable by ANFIS for training. You can create, train and test sugeno type fuzzy systems using the ANFIS editor GUI. GUI includes four distinct areas to support a typical work flow (i.e Loading data ,Generating or loading the initial FIS structure ,training the FIS, and Validating the trained FIS).

4.3.6 Accuracy of ANFIS Training Data

The coefficient of determination (R^2) is a statistical measure in a regression model that determines the proportion of variance in the dependent variable that can be explained by the independent variable. It is a measure of the goodness of fit of a model and how well the accuracy of training approximate the real data points. An R^2 of 0.94643 indicates that the regression predictions more than 90 % best fit the data.

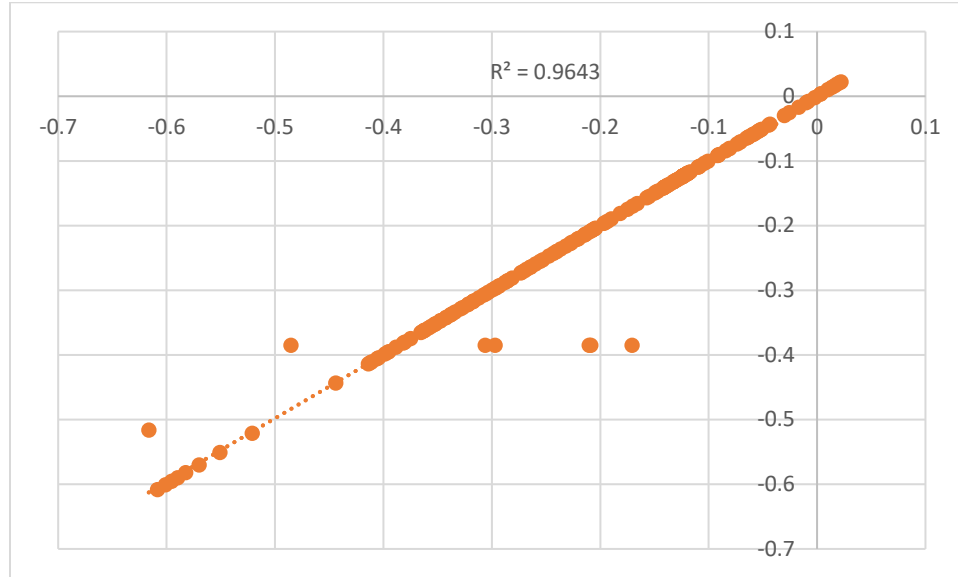


Figure 4. 10:Accuracy of ANFIS training data for UPFC model

4.3.7 ANFIS Rule Base

The ANFIS rule base is a set of IF-THEN statements that store the practical knowledge of human operators about the process. A rule that describes the relationship between input and output of neuro fuzzy can be set up using accessible knowledge in designing UPFC. The input to neuro fuzzy is voltage error and its derivative. 7 membership functions are selected for both voltage error and its derivative and result in 49 rules for the input-output relationship.

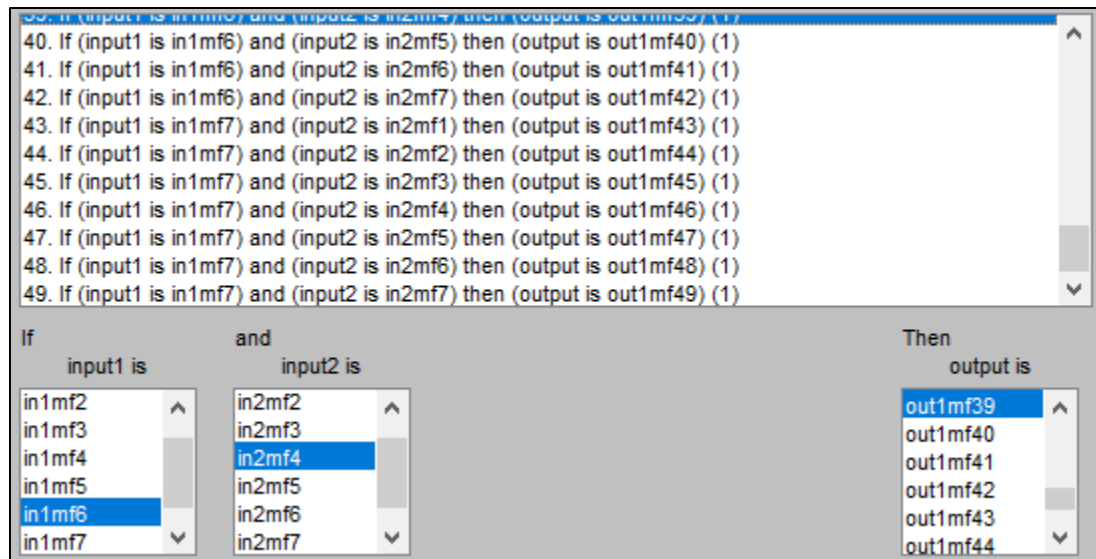


Figure 4. 11:Fuzzy inference rules of ANFIS

4.3.8 ANFIS Inference System and its Architecture

ANFIS inference is the process of formulating the mapping from a given input to an output using fuzzy logic. The mapping then provides a basis from which decisions can be made or patterns discerned. ANFIS uses Sugeno fuzzy inference type. The defuzzification process for a Sugeno system is more computationally efficient compared to that of a Mamdani system, since it uses a weighted average or weighted sum of a few data points rather than compute a centroid of a two-dimensional area. Sugeno fuzzy inference, also referred to as Takagi-Sugeno-Kang fuzzy inference, uses singleton output membership functions that are either constants or a linear function of the input values. Sugeno fuzzy inference has the following advantage compared with Mamdani type inference:

- Computationally efficient
- Work well with linear techniques, such as PID control
- Work well with optimization and adaptive techniques
- Guarantee output surface continuity
- well-suited to mathematical analysis

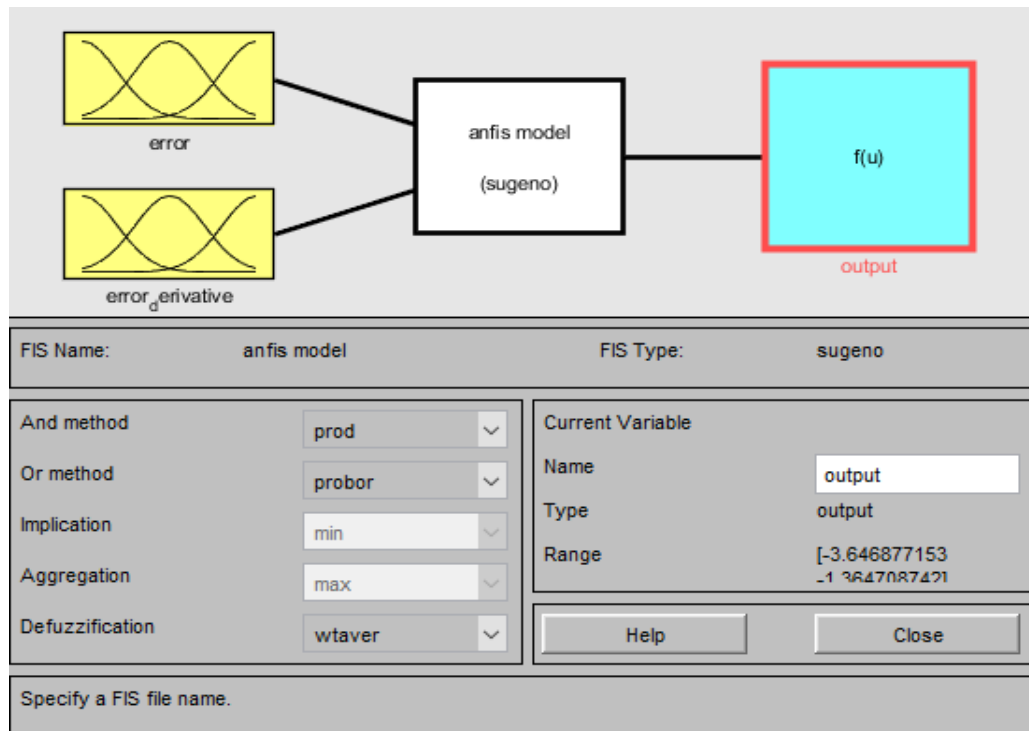


Figure 4. 12:ANFIS Sugeno inference system

The ANFIS structure consists of five layers, namely, the fuzzification layer, the product layer, the normalizing layer, the defuzzification layer, and the total output layer. Its MATLAB structure shown in the figure below. Voltage error and rate of change of voltage error are the two inputs to the ANFIS architecture.

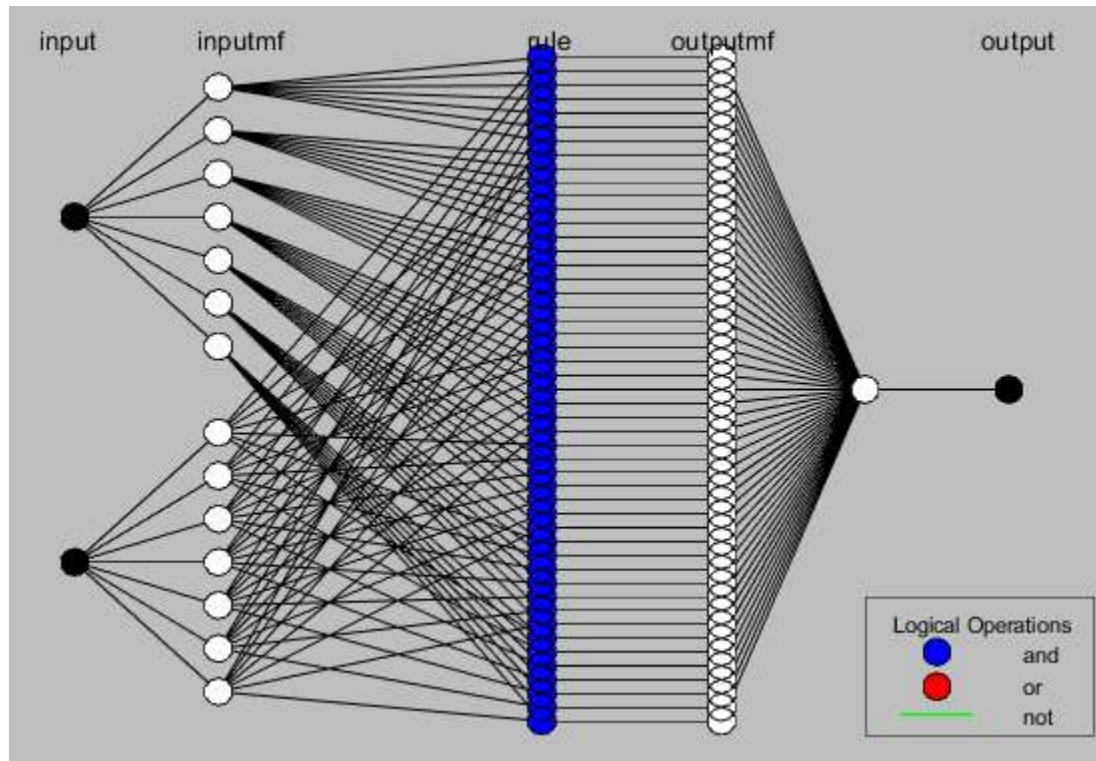


Figure 4. 13:Anfis model structure

4.4 Cost Analysis of Unified Power Flow Controller

UPFC is selected in this thesis since it provides fast-acting reactive power compensation on high-voltage electricity transmission networks compared with other compensation devices. Unified Power Flow Controller (UPFC), as a representative of the third generation of devices, is by far the most comprehensive FACTS device, in power system steady-state it can implement power flow regulation, reasonably controlling line active power and reactive power, improving the transmission capacity of power system, and in power system transient state it can realize fast-acting reactive power compensation, dynamically supporting the voltage at the access point and improving system voltage stability, moreover, it can improve the damping of the system and power angle stability.

The UPFC uses solid state devices, which provide functional flexibility, generally not attainable by conventional thyristor controlled systems. The UPFC is a combination of a static synchronous compensator (STATCOM) and a static synchronous series compensator (SSSC) coupled via a common DC voltage link. The main advantage of the UPFC is to control the active and reactive power flows in the transmission line. The UPFC operates only under balanced sine wave source. The controllable parameters of the UPFC are reactance in the line, phase angle and voltage. In this section, the cost analysis is done with and without ANFIS-based UPFC in three loading conditions. Different transient fault conditions are applied in the transmission line to see the synchronous generator response in the North-West region. Before cost analysis, determining the loss for each load is a prior task. The loss for each load is depicted in the table below.

Table 4. 5:Power loss from Beles to Bahir Dar line under various load

Loading condition	Without UPFC	With PI-based-UPFC	With ANFIS-based-UPFC
At minimum load	12.50	6.90	3.40
At average load	23.20	18.10	10.40
At peak load	40.00	19.50	11.40

Table 4. 6:Power loss from Bahir Dar to D/Markos line under various load

Loading condition	Without UPFC	With PI-based-UPFC	With ANFIS-based-UPFC
At minimum load	16.40	12.80	8.30
At average load	27.00	21.00	16.20
At peak load	48.00	40.00	25.00

Table 4. 7:Power loss from Bahir Dar to Mota line under various load

Loading condition	Without UPFC	With PI-based-UPFC	With ANFIS-based-UPFC
-------------------	--------------	--------------------	-----------------------

At minimum load	8.90	6.80	4.82
At average load	12.23	9.42	7.08
At peak load	15.00	10.60	8.40

Table 4. 8:Power loss from Bahir Dar to Alamata line under various load

Loading condition	Without UPFC	With PI-based-UPFC	With ANFIS-based-UPFC
At minimum load	12.61	9.45	7.31
At average load	15.38	12.39	10.29
At peak load	18.00	13.42	12.37

Table 4. 9:Power loss from Bahir Dar to Gonder I line under various load

Loading condition	Without UPFC	With PI-based-UPFC	With ANFIS-based-UPFC
At minimum load	11.54	8.34	6.22
At average load	14.26	11.28	9.18
At peak load	17.00	12.32	11.26

Table 4. 10:Power loss from Bahir Dar to Gonder II line under various load

Loading condition	Without UPFC	With PI-based-UPFC	With ANFIS-based-UPFC
At minimum load	10.11	7.55	5.31
At average load	13.05	10.38	8.29
At peak load	15.00	11.11	10.83

Table 4. 11:Power loss from D/Markos to Mota line under various load

Loading condition	Without UPFC	With PI-based-UPFC	With ANFIS-based-UPFC

At minimum load	6.82	4.24	2.21
At average load	10.23	7.87	5.03
At peak load	13.24	8.10	6.61

Table 4. 12:Power loss from Bahir Dar to Dangila line under various load

Loading condition	Without UPFC	With PI-based-UPFC	With ANFIS-based-UPFC
At minimum load	6.18	5.39	4.63
At average load	7.26	6.00	3.60
At peak load	8.98	7.54	4.83

4.4.1 Annual Energy Loss (MWh) for Each Line in Three Different Scenarios

The Annual energy of the power loss for all loads in three different scenarios can be evaluated as follows:

- I. The Annual energy loss from Beles to Bahir Dar line for the three scenarios evaluated in this study can be estimated as follows:

Case 1: Energy losses of the system without UPFC

Scenario 1: Annual MWh loss at minimum load

$$\text{Annual MWh loss} = (\text{Minimum loss in MW}) * 8760 \text{ h} = 12.5 \text{ MW} * 8760 \text{ h} = 109500 \text{ MWh}$$

Scenario 2: Annual MWh loss at an average load

$$\text{Annual MWh loss} = (\text{Average loss in MW}) * 8760 \text{ h} = 23.2 \text{ MW} * 8760 \text{ h} = 174000 \text{ MWh}$$

Scenario 3: Annual MWh loss at peak load

$$\text{Annual MWh loss} = (\text{Peak loss in MW}) * 8760 \text{ h} = 40 \text{ MW} * 8760 \text{ h} = 350400 \text{ MWh}$$

Case 2: Energy losses of the system with ANFIS-based-UPFC

Scenario 1: Annual MWh loss at minimum load

$$\text{Annual MWh loss} = (\text{Minimum loss in MW}) * 8760 \text{ h} = 3.4 \text{ MW} * 8760 \text{ h} = 29784 \text{ MWh}$$

Scenario 2: Annual MWh loss at an average load

$$\text{Annual MWh loss} = (\text{Average loss in MW}) * 8760 \text{ h} = 10.4 \text{ MW} * 8760 \text{ h} = 91104 \text{ MWh}$$

Scenario 3: Annual MWh loss at peak load

$$\text{Annual MWh loss} = (\text{Peak loss in MW}) * 8760 \text{ h} = 11.4 \text{ MW} * 8760 \text{ h} = 99864 \text{ MWh}$$

- II. Following the same procedure as above, the annual energy loss from Bahir Dar to the D/Markos line for the three scenarios evaluated in this study can be estimated as follows:

Table 4. 13: The Annual energy loss from Bahir Dar to D/Markos line without UPFC

Annual energy loss at different loading condition	Annual energy loss (MWh)
At minimum load	143664
At an average load	236520
At peak load	420480

Table 4. 14: The Annual energy loss from Bahir Dar to D/Markos line with ANFIS-based-UPFC

Annual energy loss at different loading condition	Annual energy loss (MWh)
At minimum load	72708
At an average load	141912
At peak load	219000

- III. The Annual energy loss from Bahir Dar to Mota line for the three scenarios evaluated in this study can be estimated as follows:

Table 4. 15: The Annual energy loss from Bahir Dar to Mota line without UPFC

Annual energy loss at different loading condition	Annual energy loss (MWh)
---	--------------------------

At minimum load	77964
At an average load	107134
At peak load	131400

Table 4. 16: The Annual energy loss from Bahir Dar to Mota line with ANFIS-based-UPFC

Annual energy loss at different loading condition	Annual energy loss (MWh)
At minimum load	42223.2
At an average load	62020.80
At peak load	73584

IV. The annual energy loss from Bahir Dar to Alamata line for the three scenarios evaluated in this study can be estimated as follows:

Table 4. 17: The Annual energy loss from Bahir Dar to Alamata line without UPFC

Annual energy loss at different loading condition	Annual energy loss (MWh)
At minimum load	110463
At an average load	134728.8
At peak load	157680

Table 4. 18: The Annual energy loss from Bahir Dar to Alamata line with ANFIS-based-UPFC

Annual energy loss at different loading condition	Annual energy loss (MWh)
At minimum load	64035.6
At an average load	90140.4
At peak load	108361.2

V. The annual energy loss from Bahir Dar to Gonder I line for the three scenarios evaluated in this study can be estimated as follows:

Table 4. 19: The Annual energy loss from Bahir Dar to Gonder I line without UPFC

Annual energy loss at different loading condition	Annual energy loss (MWh)
At minimum load	101090
At an average load	124917.6
At peak load	148920

Table 4. 20: The Annual energy loss from Bahir Dar to Gonder I line with ANFIS-based-UPFC

Annual energy loss at different loading condition	Annual energy loss (MWh)
At minimum load	54487
At an average load	80416.8
At peak load	98637.6

VI. The annual energy loss from Bahir Dar to Gonder II line for the three scenarios evaluated in this study can be estimated as follows:

Table 4. 21: The Annual energy loss from Bahir Dar to Gonder II line without UPFC

Annual energy loss at different loading condition	Annual energy loss (MWh)
At minimum load	88563.6
At an average load	114318
At peak load	131400

Table 4. 22: The Annual energy loss from Bahir Dar to Gonder II line with ANFIS-based-UPFC

Annual energy loss at different loading condition	Annual energy loss (MWh)
At minimum load	46515.6
At an average load	72620.4
At peak load	94870.8

- VII. The annual energy loss from D/Markos to Mota line for the three scenarios evaluated in this study can be estimated as follows:

Table 4. 23: The Annual energy loss from D/Markos to Mota line without UPFC

Annual energy loss at different loading condition	Annual energy loss (MWh)
At minimum load	59743.2
At an average load	89614.8
At peak load	115982.4

Table 4. 24: The Annual energy loss from D/Markos to Mota line with ANFIS-based-UPFC

Annual energy loss at different loading condition	Annual energy loss (MWh)
At minimum load	19359.6
At an average load	44062.8
At peak load	57903.6

- VIII. The annual energy loss from Bahir Dar to Dangila line for the three scenarios evaluated in this study can be estimated as follows:

Table 4. 25: The Annual energy loss from Bahir Dar to Dangila line without UPFC

Annual energy loss at different loading condition	Annual energy loss (MWh)
At minimum load	54136.8
At an average load	63597.6
At peak load	78664.8

Table 4. 26: The Annual energy loss from Bahir Dar to Dangila line with ANFIS-based-UPFC

Annual energy loss at different loading condition	Annual energy loss (MWh)
At minimum load	40558.8
At an average load	31536
At peak load	42310.83

Although FACTS controllers can offer high-speed control for enhancing electric power system, one significant disadvantage of power electronic based controllers is more expense per unit of rating than that of conventional equipment. Table 4.12 shows the typical investment cost for various FACTS controllers.

Table 4. 27: Typical investment cost for different FACTs controller [54]

FACTs Controller	Cost (US \$)
DSTATCOM	34 per KVAR
SVC	26 per KVAR
TCSC	47 per KVAR
UPFC	37 per KVAR

From chapter-3 UPFC rating calculated is 133MVA. The power factor at peak load at Bahir Dar 400kV bus is 0.87. MVAR rating of UPFC at peak load is calculated as ($MVAR = MVA * \sin\theta = 133 * 0.493046 = 65.57MVAR$).

The total cost is $65.57 * 1000 * 37\$ = 2426090\$$. Convert the dollar into Ethiopian birr: $1\$ = 53.44ETB$. The total investment cost for UPFC is $2426090 * 53.44ETB =$ **129,650,249.6ETB**. Energy tariff implementation for all consumer class adjusted by Ethiopian Electric Power and Ethiopian Energy Authority shown in the table 4.13.

Table 4. 28:Ethiopias energy tariff for all consumer levels

Consumer block	Consumption	Energy Tariff (Birr/kWh)
1 st Block	Up to 50kWh	0.2730
2 nd Block	Up to 100kWh	0.7670
3 rd Block	Up to 200kWh	1.6250
4 th Block	Up to 300kWh	2.0000
5 th Block	Up to 400kWh	2.2000
6 th Block	Up to 500kWh	2.4050
7 th Block	kWh> 500kWh	2.4810

Table 4. 29:Total energy saved annually for all transmission lines

Loading condition	Total MWh loss annually Without UPFC	Total MWh loss annually With ANFIS-based-UPFC	Total Energy (MWh) saved annually	Total ETB saved annually
At minimum load	745123	369671	375452	20064154.90
At average load	1035367	613810	421557	22528006.08
At peak load	1534926	772281	762645	40755748.81

4.4.2 Payback Period for UPFC Investment Cost

The payback period is the number of years it takes to recover the initial cash investment of UPFC. This method determines the period after which the initial investment is recovered. A project is only carried out if the payback time is lower than a certain threshold defined by the company. Typically used thresholds for the payback time vary between 2 to 6 years.

$$\text{Payback period} = \frac{\text{Initial UPFC investment cost}}{\text{Total ETB saved annually}} \quad (4.43)$$

$$\text{Payback period at Peak load} = \frac{129,650,249.6\text{ETB}}{40,755,748.81\text{ETB}} = 3.181 \text{ years}$$

CHAPTER FIVE

5. SIMULATION RESULT AND DISCUSSION

5.1 Introduction

In this chapter, the developed models are verified by simulation. The simulation result of the model reveals the transient stability of an ANFIS-based UPFC connected in the North West region to a 400 kV , 256.54 km interconnected long transmission power system that covers Tana Beles to Debre Markos with its equivalent transmission line impedances, transformer parameters, and loads. This demonstrates the transient stability enhancement of the NWR interconnected power system under different disturbance scenarios. PSO is used to identify the weakest bus of the test system for optimal placement of UPFC. Using this method, the Bahirdar substation's 400 kV bus bar is the appropriate place for UPFC to work effectively.

The simulation is conducted using MATLAB/SIMULINK software, and different performance indices are recorded to compare and validate the designed controller. To validate the designed controller, ANFIS data is extracted for training and testing from the PI input and output of the voltage regulator. The input is error and error derivatives of voltage regulator, while the output is direct and quadrature current output. The membership function used for the ANFIS set is the triangular membership function since it is effective to map the non-fuzzy input values to fuzzy linguistic terms in transient stability enhancement. 300,000 rows of data have been extracted from the PI-based UPFC.

To validate ANFIS, 30 percent of the extracted data is used for the ANFIS test, and the remaining 70 percent is for the ANFIS train. Finally, the effectiveness of ANFIS-based UPFC is tested by comparing its performance, such as its power transfer capacity, loss reduction, and voltage profile improvement.

5.2 Fault types and its percentage of occurrence in the North-West Region High Voltage Transmission Line

There are mainly two types of faults in the electrical power system. Those are symmetrical and unsymmetrical faults.

- I. **Symmetrical faults:** These are very severe faults that occur infrequently in power systems. These are also called balanced faults and are of two types: line-to-line-to-ground (L-L-L-G) and line-to-line-to-line (L-L-L). If these faults occur, the system remains balanced but suffers severe damage to its electrical and mechanical equipment.
- II. **Unsymmetrical faults:** These are very common and less severe than symmetrical faults. There are mainly three types, namely line-to-ground (L-G), line-to-line (L-L), and double line-to-ground (L-L-G) faults. These are also called "unbalanced faults," since their occurrence causes unbalance in the system. The system is unbalanced if the impedance values in each phase differ, causing unbalanced currents to flow between the phases.

The fault percentage of North-West region accounted for each type of fault in 2021 GC is shown in the pie chart below. To test the proposed method in this thesis, three-phase ground faults are applied from a severity perspective, and single-line ground faults are applied from a high probability of occurrence perspective.

Table 5. 1: Fault type occurring in NWR and its duration of interruption in 2021 G.C

Fault Type	Duration of interruption (hrs.)
Single phase with ground (L-G)	110
Double line with ground (L-L-G)	55
Line to line (L-L)	26
Triple line (L-L-L)	13
Triple line with ground (L-L-L-G)	6.92
Total =210.92hrs.	

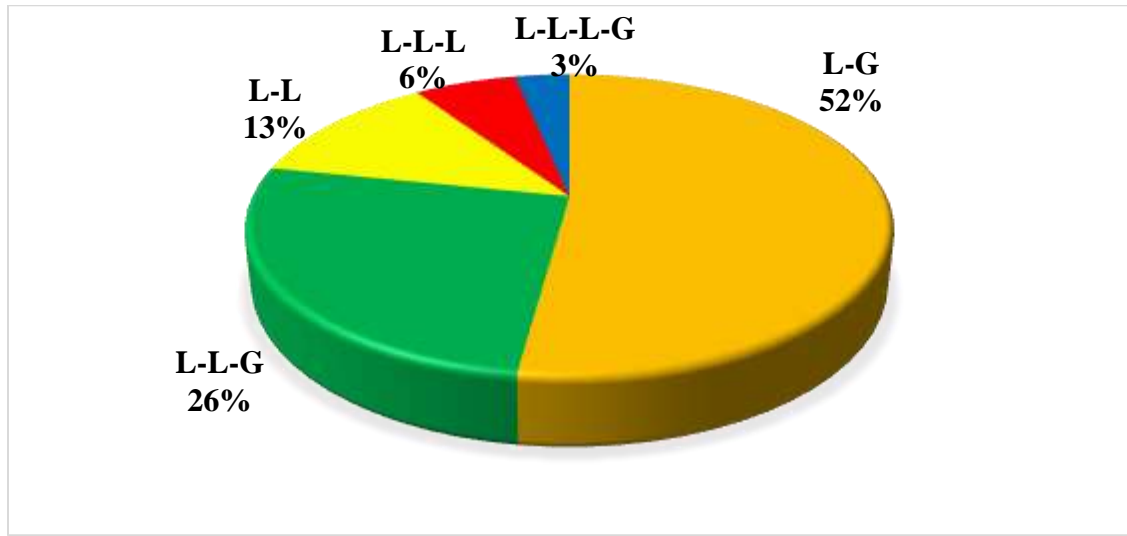


Figure 5. 1:Percentage of fault occurring in NWR recorded in 2021 G.C

5.3 System Performance at Base Case for an Average Load

This section shows the response of rotor speed deviation, rotor speed, rotor angle deviation, and output active power of the Tana Beles synchronous generators without compensator at both generation level and transmission line level for the average load on the transmission line. The simulation result shows the response of the system without imposing a fault on the system, which helps to analyse the existing behaviour of the North-West region synchronous generators. As illustrated in the figure below, due to switching surges, initially the system response oscillates. As time goes on, the arc occurs due to switching dieout, and the oscillating amplitude decreases and settles after a few seconds later.

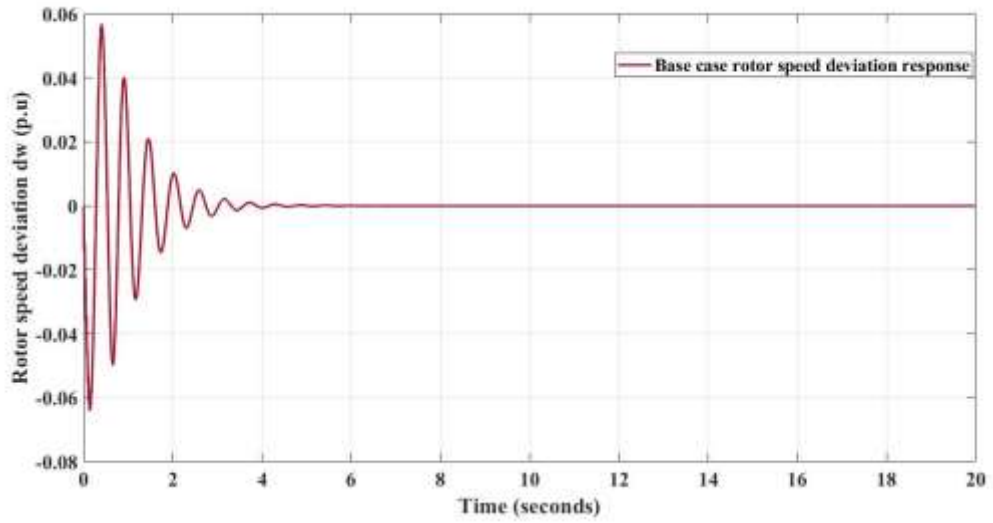


Figure 5. 2: Base case rotor speed deviation response without disturbance dw(pu)

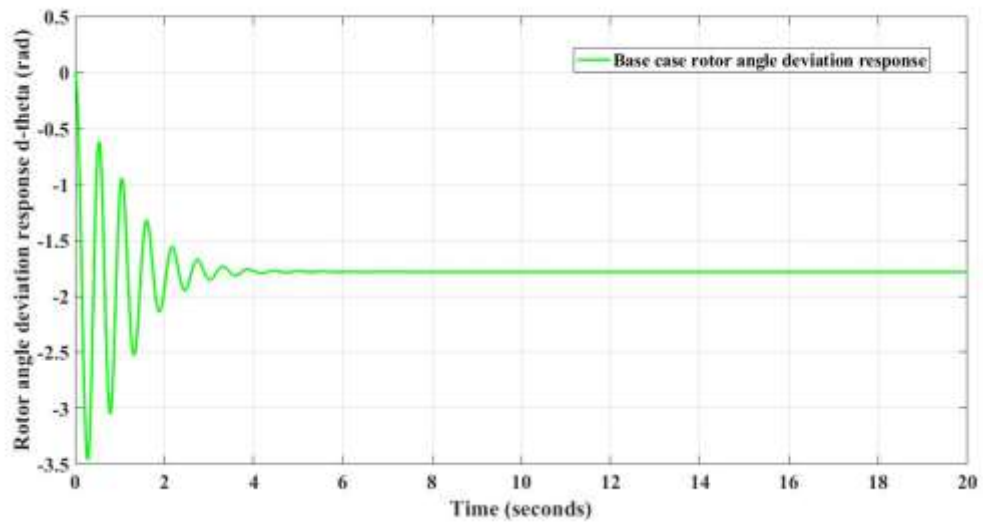


Figure 5. 3: Base case rotor angle deviation response (rad) without disturbance

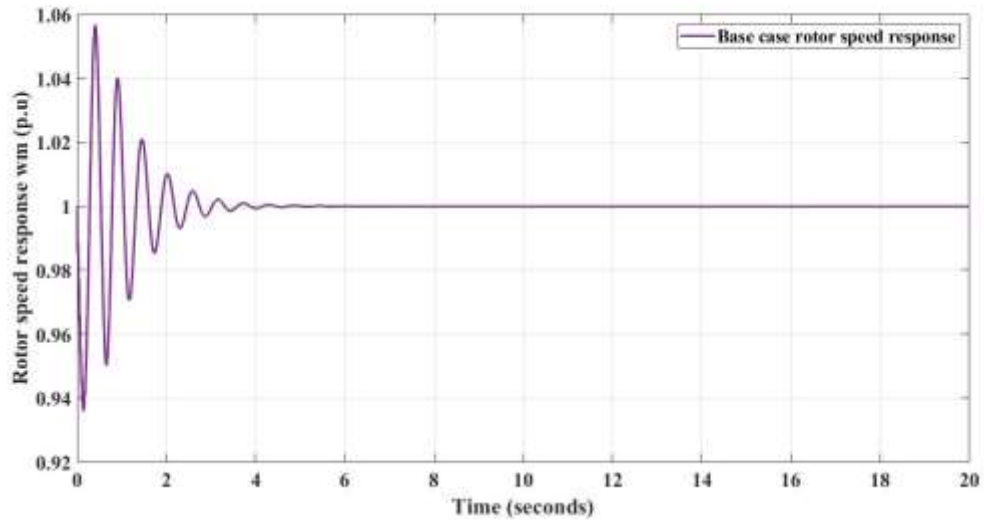


Figure 5. 4:Base case rotor speed response(pu) without disturbance

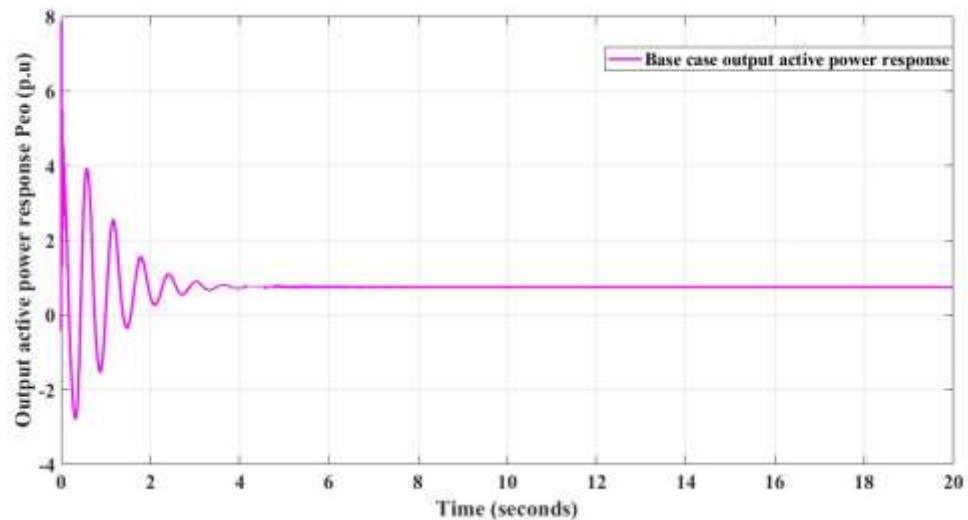


Figure 5. 5:Base case output active power P_{eo} (pu) response without disturbance

In the time domain simulation, the performance indices taken in this paper are percentage overshoot and settling time.

- I. Percentage overshoot:-**The ratio of the maximum value of the step excited output to the final output is called overshoot of the system.
- II. Settling time:-**The time taken by the system response to settle down and stay within 2 % tolerance of its final value.

From figures 5.2–5.5, the simulation result shows that in the base case for an average load, rotor speed deviation, rotor angle deviation, rotor speed, and the generator's output active power at normal operating conditions (without fault) have a low settling time of less than 4 seconds. Also, the simulation result shows that in the base case for an average load, rotor speed deviation, rotor angle deviation, rotor speed, and the generator's output active power at normal operating conditions (without fault) have a percentage overshoot of 6.1 %, 80.5 %, 105.9 %, and 100 %, respectively. This indicates that the system can sustain a stable operating condition without loss of synchronism in the base case at an average load without disturbance.

5.4 The Waveforms of NWR 400kV Transmission Line Before and After UPFC Series Voltage Injection

The waveforms before the series injected voltage and after the series injected voltage for both PI-based UPFC and ANFIS-based UPFC are presented in the figure 5.6. The peak voltage level before series injected voltage is 394kV. The peak voltage levels after series injected voltage for both PI-based UPFC and ANFIS-based UPFC are 401 kV and 418 kV, respectively. The result shows that the proposed ANFIS-based UPFC has better performance in improving line voltages than the PI-based UPFC. The percentages of voltage level improvement after series injection for both PI-based UPFC and ANFIS-based UPFC are 1.776 % and 6.09 %, respectively.

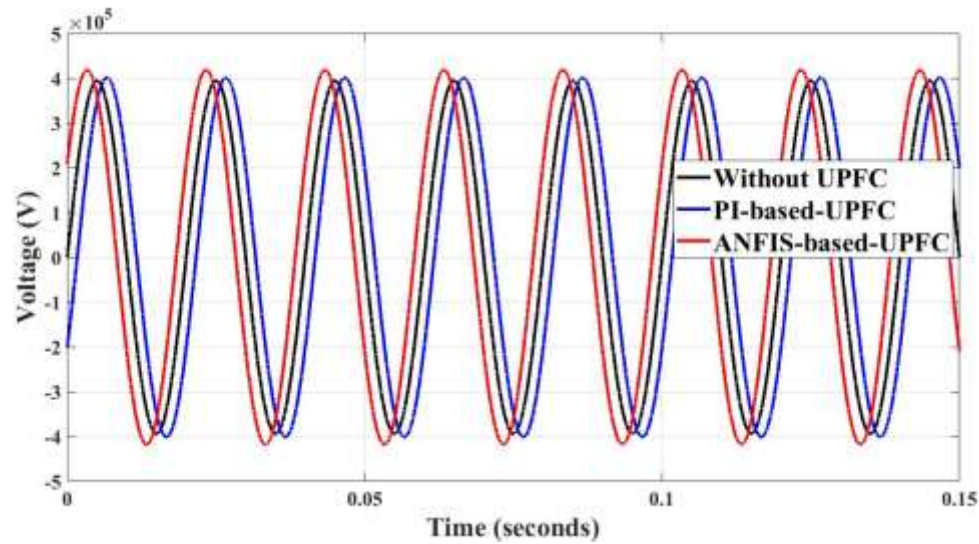


Figure 5. 6: The voltage waveforms of NWR 400kV transmission line before and after series injected voltage by UPFC

5.5 System Response for a Disturbance with and without UPFC

The system response is analysed without UPFC, with PI-based UPFC, and with ANFIS-based UPFC. The PI parameters found by autotuning are $K_p = 10$ and $K_i = 0.1$. In this section, the ability of the system to maintain synchronism at the generation level for a disturbance that occurred at the transmission line has been observed with different performance indices, such as settling time and maximum overshoot. If the problem persists and is not resolved within the short time period, it can cause serious damage to the equipment, which in turn can lead to a loss of power and a blackout.

5.5.1 System Response when a Fault Occurred at the Midpoint of the Tana Beles to Bahir Dar Transmission Line

In this section, the Simulink model is used to investigate the influence of incorporating UPFC on enhancing transient stability when a disturbance is applied at the midpoint of the Tana Beles to Bahir Dar 400 kV transmission line. When a three-phase ground fault and a single-phase ground fault are applied at the midpoint of the Tana Beles to Bahir Dar 400 kV transmission line, the responses of active power, rotor angle deviation, rotor speed, and rotor speed deviation of North-West region generators are examined, as shown below.

I. System response for a balanced three-phase with ground fault

The responses of rotor angle deviation, rotor speed, output active power, and rotor speed deviation of North-West region generators when a balanced three-phase fault occurred at the midpoint of the Tana Beles to Bahir Dar 400 kV transmission line at 6 seconds and cleared at 6.25 seconds are shown in the figure below.

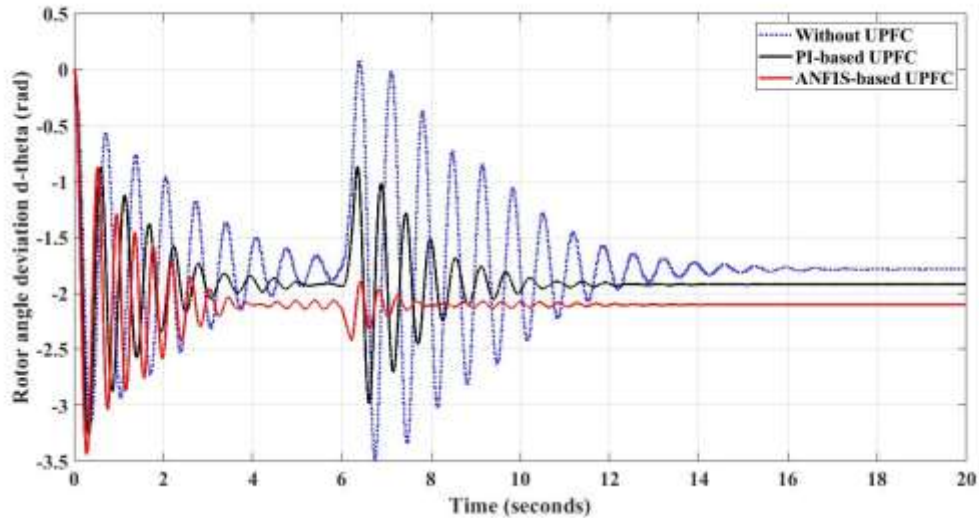


Figure 5. 7: Rotor angle deviation response for 3ph-G fault occurred at the midpoint of the Tana Beles to Bahir Dar transmission line with and without UPFC

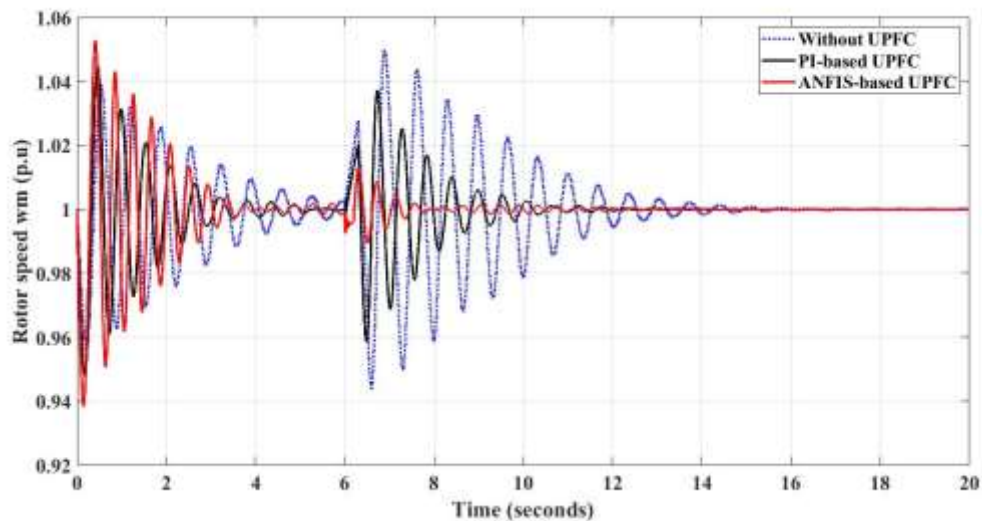


Figure 5. 8: Rotor speed response for 3ph-G fault occurred at the midpoint of the Tana Beles to Bahir Dar transmission line with and without UPFC

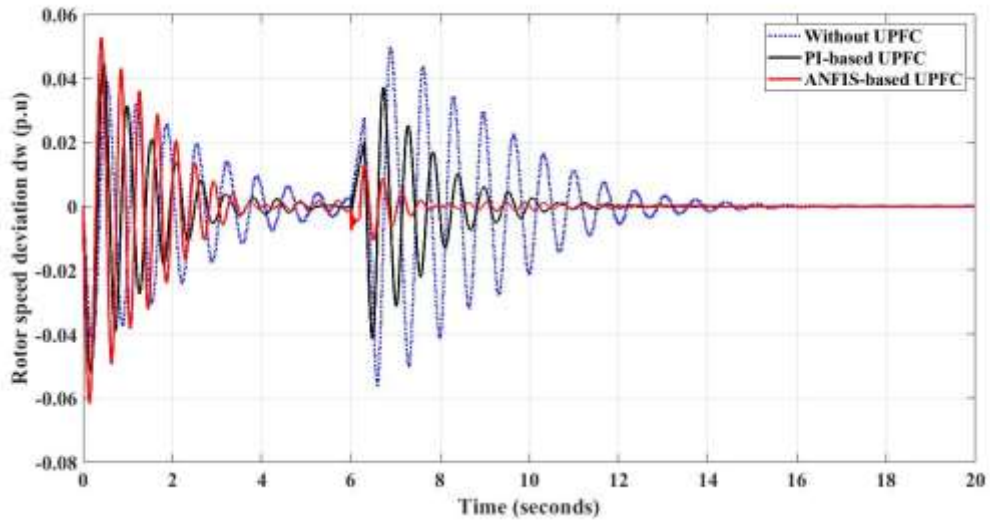


Figure 5. 9: Rotor speed deviation response for 3ph-G fault occurred at the midpoint of the Tana Beles to Bahir Dar transmission line with and without UPFC

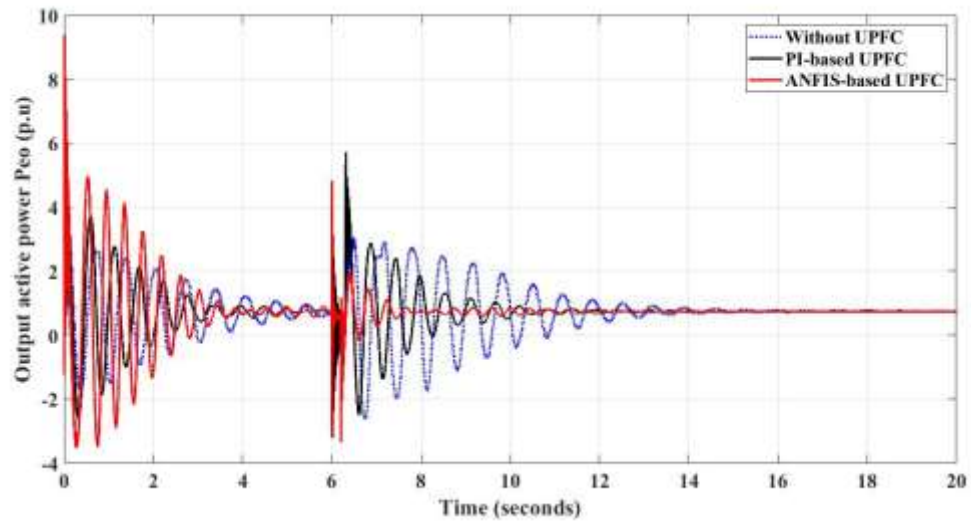


Figure 5. 10: Output active power response for 3ph-G fault occurred at the midpoint of the Tana Beles to Bahir Dar transmission line with and without UPFC

Table 5. 2: Comparison of the system response for different variables with and without UPFC when 3ph-G fault occurred at the midpoint of the Tana Beles to Bahir Dar transmission line

Variable type	Controller	Maximum peak value (Mp)	Percentage overshoot (%)	Settling time (sec)
Rotor angle deviation	Without UPFC	1.8	100	8.5
	PI-based UPFC	1.0	52.63	6.0
	ANFIS-based UPFC	0.3	12.5	2.5
Rotor speed	Without UPFC	0.05	5	9.8
	PI-based UPFC	0.039	3.9	6.3
	ANFIS-based UPFC	0.01	1	6.1
Rotor speed deviation	Without UPFC	0.05	5	9.8
	PI-based UPFC	0.039	3.9	6.3
	ANFIS-based UPFC	0.01	1	6.1
Output active power	Without UPFC	2.3	230	8.0
	PI-based UPFC	2.1	210	5.5
	ANFIS-based UPFC	0.1	10	4.5

The table above shows that an ANFIS-based UPFC and a PI-based UPFC improve the settling time of rotor angle deviation by 70.58 and 29.41 percent, respectively. ANFIS-based UPFC and a PI-based UPFC improve the settling time of rotor speed by 37.75 and 35.71 percent, respectively. ANFIS-based UPFC and a PI-based UPFC improve the settling time of rotor speed deviation by 37.75 and 35.71 percent, respectively. While an ANFIS-based UPFC and a PI-based UPFC improve the settling time of the output active power by 43.75 and 31.25 percent, respectively.

II. System response for a single-phase with ground fault

The responses of rotor angle deviation, rotor speed, output active power, and rotor speed deviation of North-West region generators when a single-phase ground fault occurred at the midpoint of the Tana Beles to Bahir Dar transmission line at 6 seconds and cleared at 6.25 seconds are shown in the figure below.

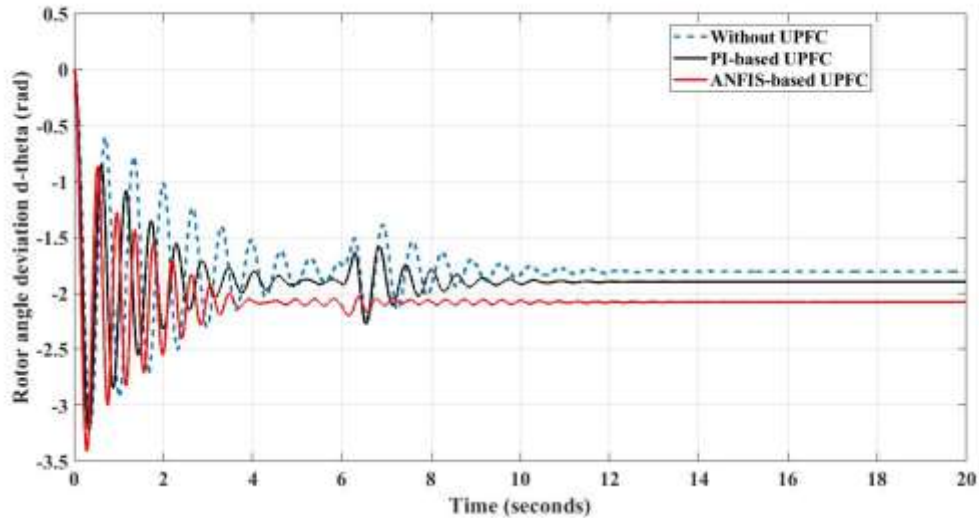


Figure 5. 11:Rotor angle deviation response for 1ph-G fault occurred at the midpoint of the Tana Beles to Bahir Dar transmission line with and without UPFC

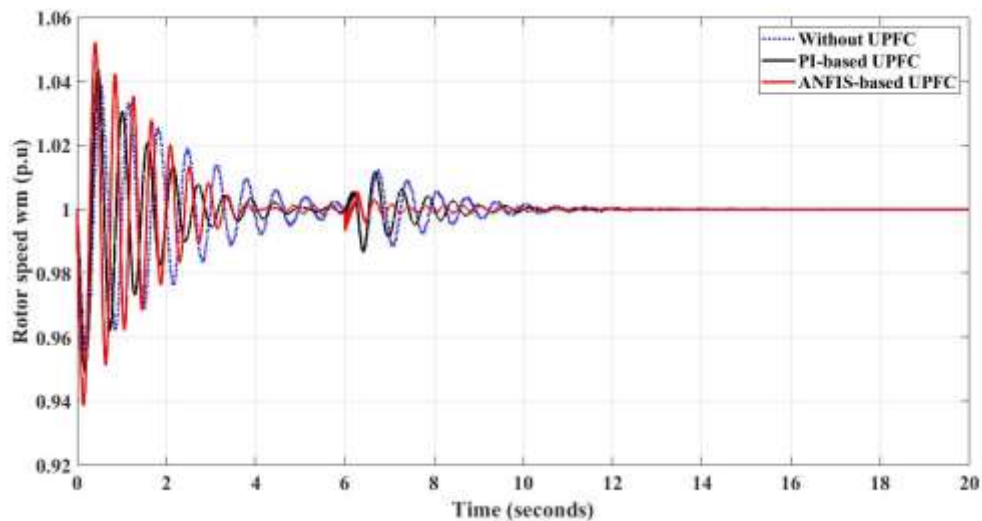


Figure 5. 12:Rotor speed response for 1ph-G fault occurred at the midpoint of the Tana Beles to Bahir Dar transmission line with and without UPFC

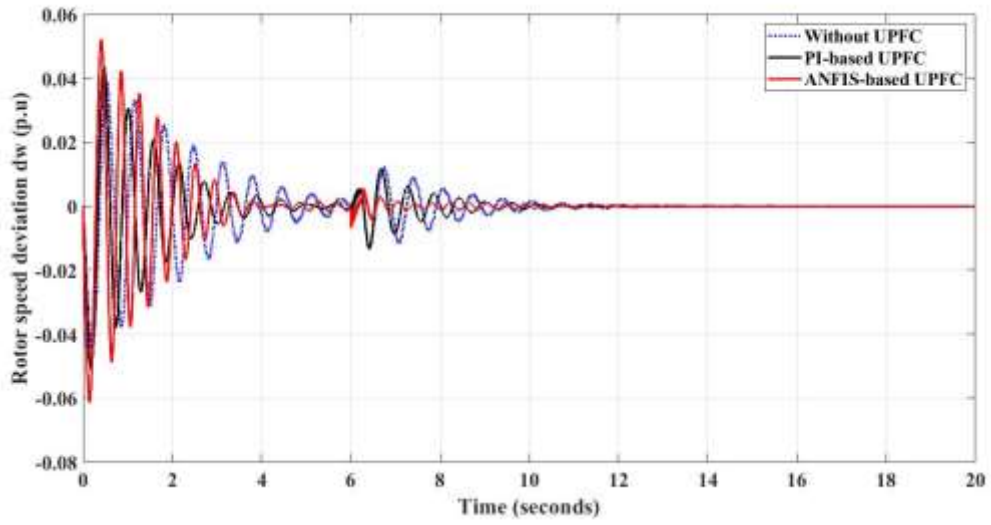


Figure 5. 13:Rotor speed deviation response for 1ph-G fault occurred at the midpoint of the Tana Beles to Bahir Dar transmission line with and without UPFC

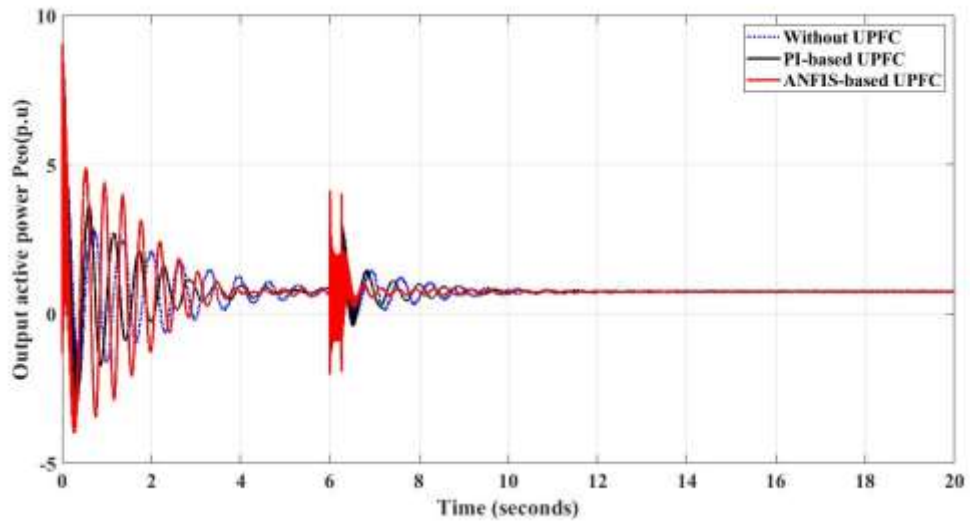


Figure 5. 14:Output active power response for 1ph-G fault occurred at the midpoint of the Tana Beles to Bahir Dar transmission line with and without UPFC

Table 5. 3: Comparison of the system response for different variables with and without UPFC when 1ph-G fault occurred at the midpoint of the Tana Beles to Bahir Dar transmission line

Variable type	Controller	Maximum peak value (Mp)	Percentage overshoot (%)	Settling time (sec)
Rotor angle deviation	Without UPFC	0.20	10.00	6.50
	PI-based UPFC	0.12	6.31	4.40
	ANFIS-based UPFC	0.10	4.76	2.00
Rotor speed	Without UPFC	0.010	10	3.700
	PI-based UPFC	0.010	10	2.500
	ANFIS-based UPFC	0.005	5	0.86
Rotor speed deviation	Without UPFC	0.010	10	3.700
	PI-based UPFC	0.010	10	2.500
	ANFIS-based UPFC	0.005	5	0.86
Output active power	Without UPFC	0.70	70	2.8
	PI-based UPFC	0.75	75	2.5
	ANFIS-based UPFC	0.11	11	2.0

The table above shows that an ANFIS-based UPFC and a PI-based UPFC improve the settling time of rotor angle deviation by 69.23 and 32.30 percent, respectively. ANFIS-based UPFC and a PI-based UPFC improve the settling time of rotor speed by 76.75 and 32.40 percent, respectively. ANFIS-based UPFC and a PI-based UPFC improve the settling time of rotor speed deviation by 76.75 and 32.40 percent, respectively. While an ANFIS-based UPFC and a PI-based UPFC improve the settling time of the output active power by 28.57 and 10.71 percent, respectively.

5.5.2 System Response when a Fault Occurred at the Midpoint of the Bahir Dar to D/Markos Transmission Line

In this section, the Simulink model is used to investigate the influence of incorporating UPFC on enhancing transient stability when a disturbance is applied at the Midpoint of the Bahir Dar to D/Markos 400 kV transmission line. When a three-phase ground fault and a single-phase ground fault are applied at the midpoint of the Bahir Dar to D/Markos 400 kV transmission line, the responses of active power, rotor angle deviation, rotor speed, and rotor speed deviation of North-West region generators are depicted, as shown below.

i. System response for a balanced three-phase with ground fault

The responses of rotor angle deviation, rotor speed, output active power, and rotor speed deviation of North-West region generators when a balanced three-phase ground fault occurred at the midpoint of the Bahir Dar to D/Markos transmission line at 6 seconds and cleared at 6.25 seconds are shown in the figure below.

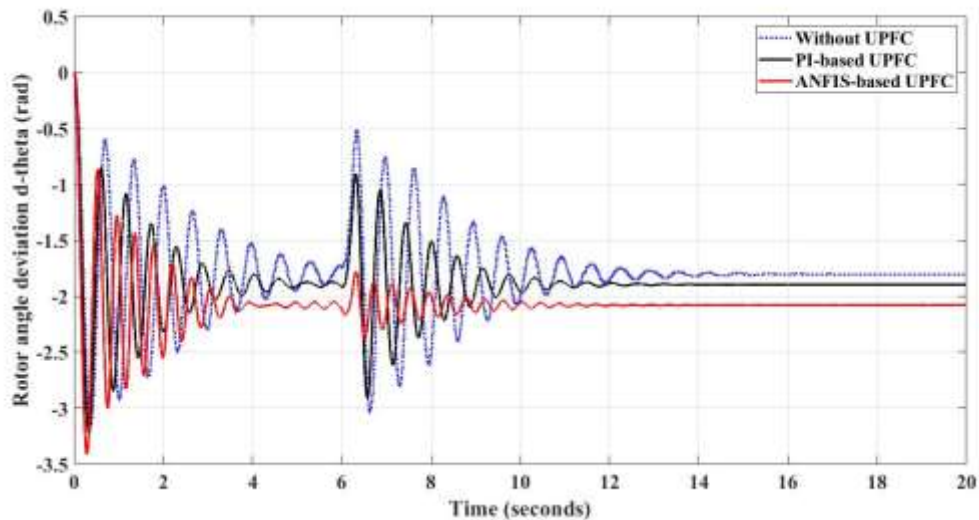


Figure 5. 15: Rotor angle deviation response for 3ph-G fault occurred at the midpoint of the Bahir Dar to D/Markos transmission line with and without UPFC

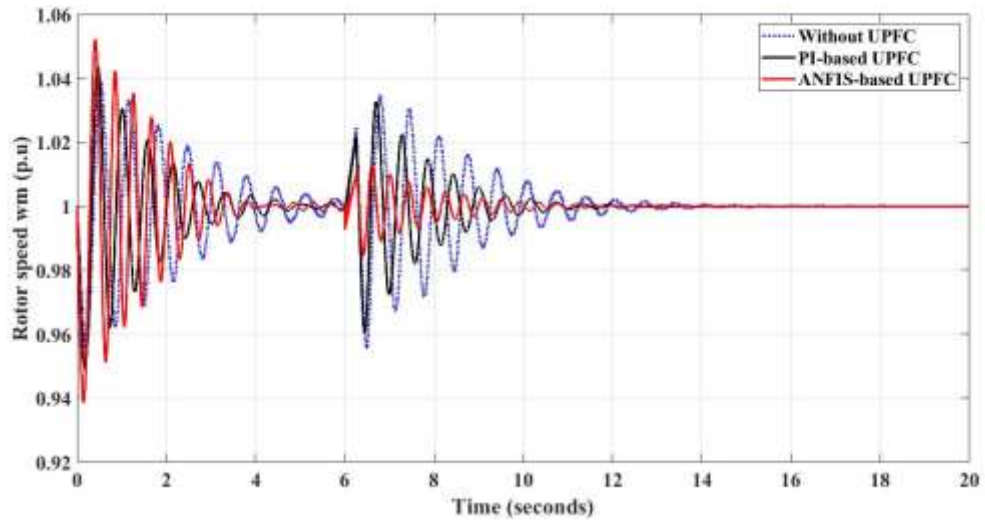


Figure 5. 16:Rotor speed response for 3ph-G fault occurred at the midpoint of the Bahir Dar to D/Markos transmission line with and without UPFC

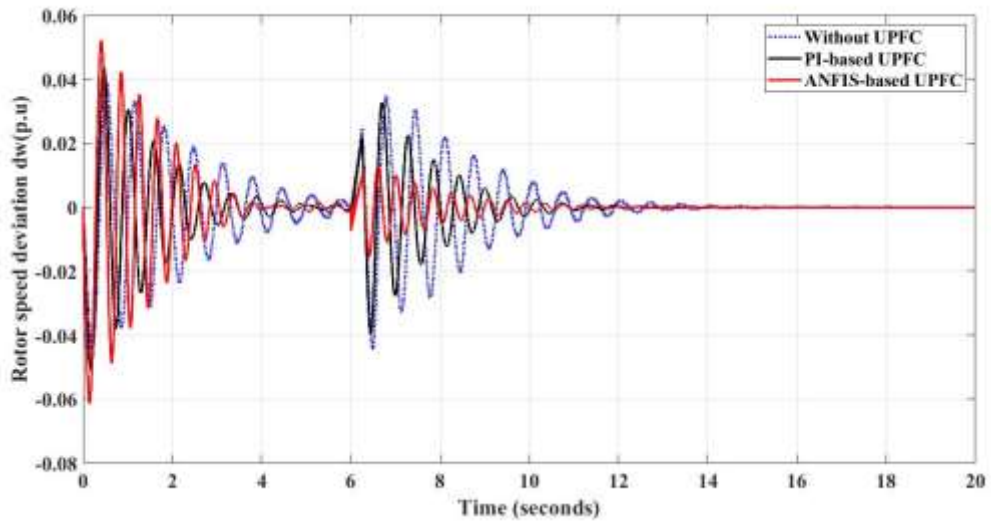


Figure 5. 17:Rotor speed deviation response for 3ph-G fault occurred at the midpoint of the Bahir Dar to D/Markos transmission line with and without UPFC

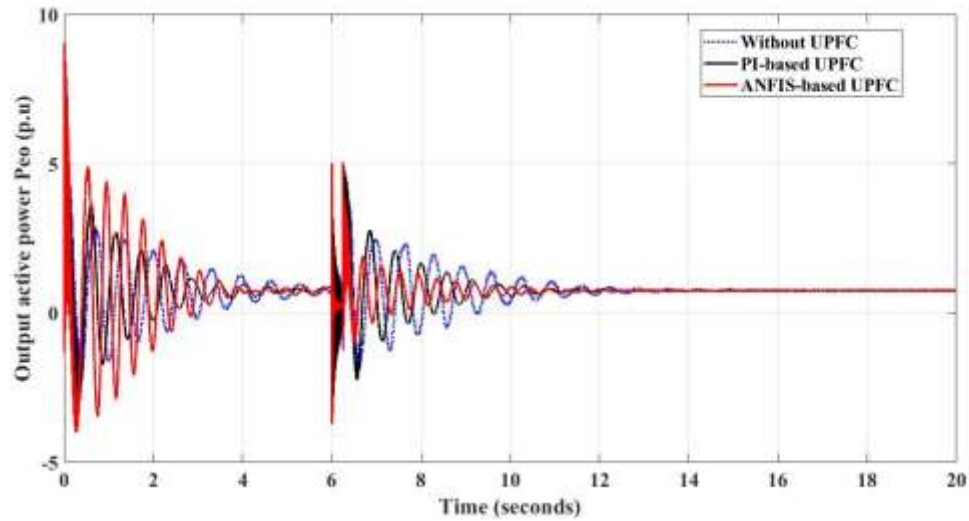


Figure 5. 18: Output active power response for 3ph-G fault occurred at the midpoint of the Bahir Dar to D/Markos transmission line with and without UPFC

Table 5. 4: Comparison of the system response for different variables with and without UPFC when 3ph-G fault occurred at the midpoint of the Bahir Dar to D/Markos line

Variable type	Controller	Maximum peak value (Mp)	Percentage overshoot (%)	Settling time (sec)
Rotor angle deviation	Without UPFC	1.3	72	7.8
	PI-based UPFC	1.0	52.63	4.9
	ANFIS-based UPFC	0.3	14.28	4.2
Rotor speed	Without UPFC	0.038	3.8	7.2
	PI-based UPFC	0.035	3.5	5.9
	ANFIS-based UPFC	0.01	1	4.8
Rotor speed deviation	Without UPFC	0.038	3.8	7.2
	PI-based UPFC	0.035	3.5	5.9
	ANFIS-based UPFC	0.01	1	4.8
Output active power	Without UPFC	1.5	150	6.5
	PI-based UPFC	3.9	390	4.5
	ANFIS-based UPFC	4	400	3.6

The table above shows that an ANFIS-based UPFC and a PI-based UPFC improves the settling time of rotor angle deviation by 46.15 and 37.17 percent, respectively. ANFIS-based UPFC and a PI-based UPFC improve the settling time of rotor speed by 33.33 and 18.05 percent, respectively. ANFIS-based UPFC and a PI-based UPFC improve the settling time of rotor speed deviation by 33.33 and 18.05 percent, respectively. While an ANFIS-based UPFC and a PI-based UPFC improves the settling time of the output active power by 44.61 and 30.76 percent, respectively.

ii. System response for a single-phase with ground fault

The responses of rotor angle deviation, rotor speed, output active power, and rotor speed deviation of North-West region generators when a single-phase ground fault occurred at the midpoint of the Bahir Dar to D/Markos transmission line at 6 seconds and cleared at 6.25 seconds are shown in the figure below.

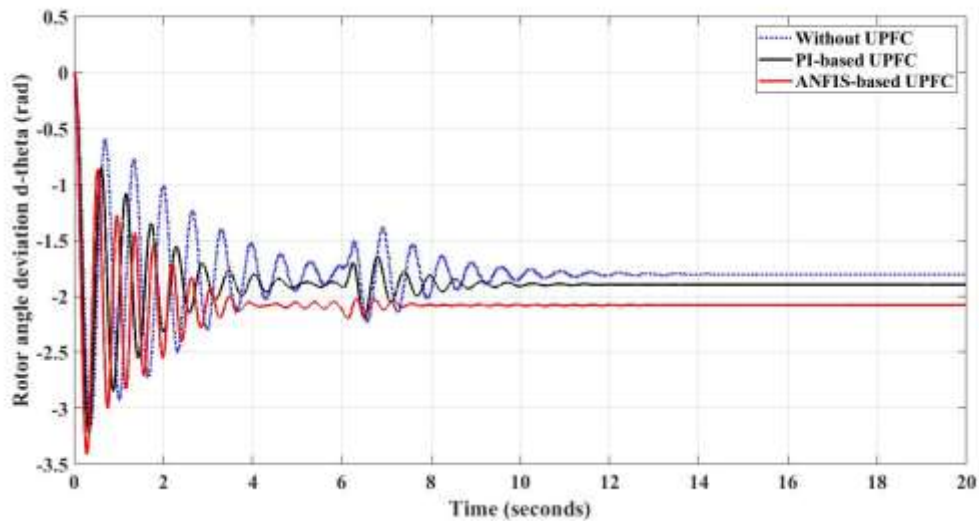


Figure 5. 19:Rotor angle deviation response for 1ph-G fault occurred at the midpoint of the Bahir Dar to D/Markos transmission line with and without UPFC

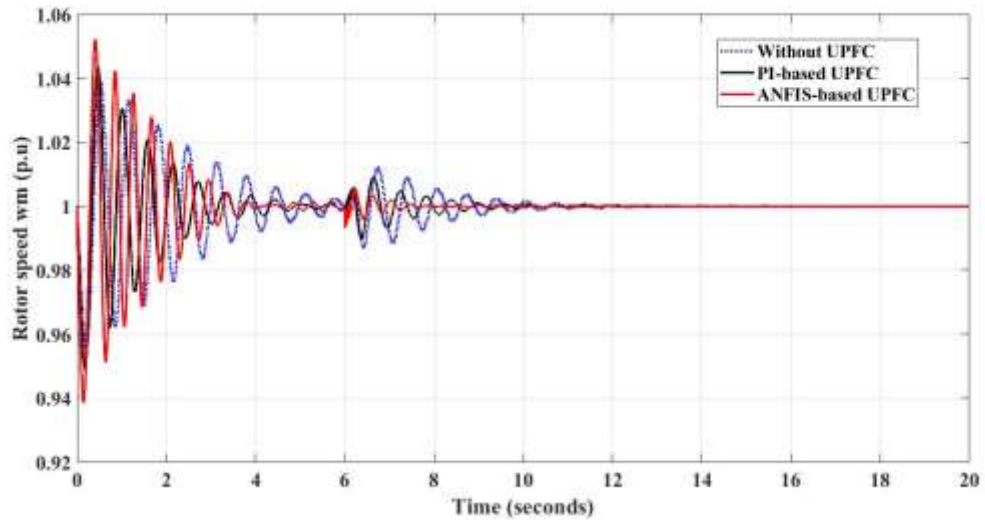


Figure 5. 20:Rotor speed response for 1ph-G fault occurred at the midpoint of the Bahir Dar to D/Markos transmission line with and without UPFC

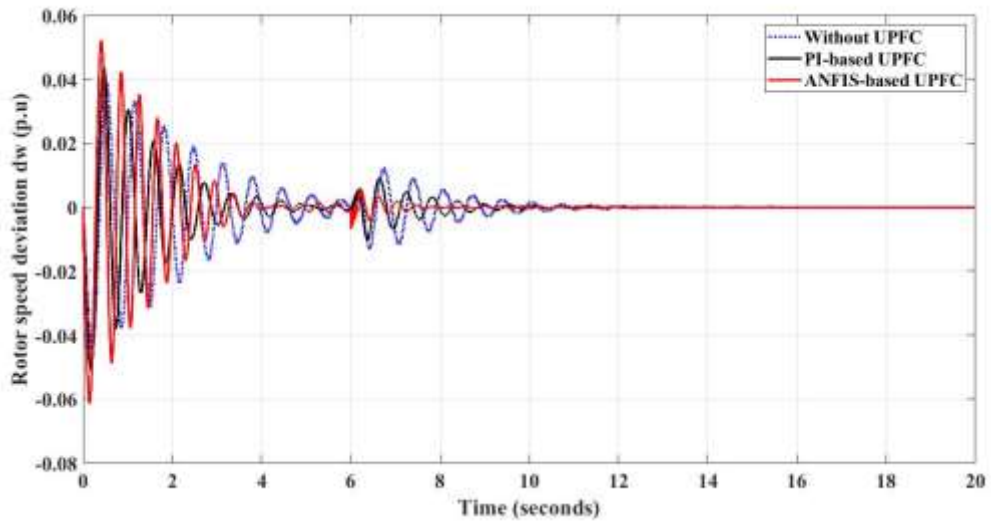


Figure 5. 21:Rotor speed deviation response for 1ph-G fault occurred at the midpoint of the Bahir Dar to D/Markos transmission line with and without UPFC

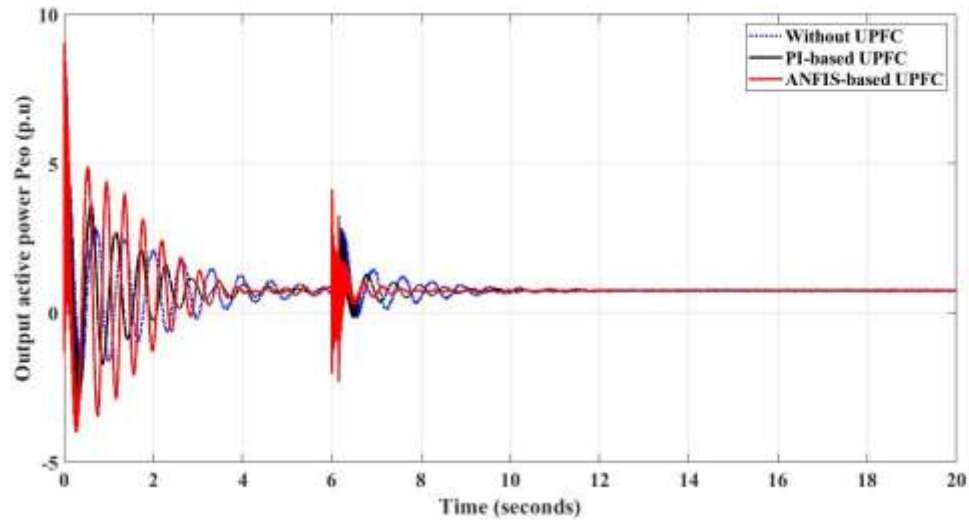


Figure 5. 22: Output active power response for 1ph-G fault occurred at the midpoint of the Bahir Dar to D/Markos transmission line with and without UPFC

Table 5. 5: Comparison of the system response for different variables with and without UPFC when 1ph-G fault occurred at the midpoint of the Bahir Dar to D/Markos line

Variable type	Controller	Maximum peak value (Mp)	Percentage overshoot (%)	Settling time (sec)
Rotor angle deviation	Without UPFC	0.30	17.6	4.6
	PI-based UPFC	0.20	10.5	3.9
	ANFIS-based UPFC	0.10	4.3	2.0
Rotor speed	Without UPFC	0.010	1	3.0
	PI-based UPFC	0.010	1	2.1
	ANFIS-based UPFC	0.015	1.5	1.8
Rotor speed deviation	Without UPFC	0.010	1	3.0
	PI-based UPFC	0.010	1	2.1
	ANFIS-based UPFC	0.015	1.5	1.8
Output active power	Without UPFC	1	100	2.8
	PI-based UPFC	2	200	2.2
	ANFIS-based UPFC	5.2	520	1.9

The table above shows that an ANFIS-based UPFC and a PI-based UPFC improve the settling time of rotor angle deviation by 56.52 and 15.21 percent, respectively. ANFIS-based UPFC and a PI-based UPFC improve the settling time of rotor speed by 40 and 30 percent, respectively. ANFIS-based UPFC and a PI-based UPFC improve the settling time of rotor speed deviation by 40 and 30 percent, respectively. While an ANFIS-based UPFC and a PI-based UPFC improve the settling time of the output active power by 32.14 and 21.4 percent, respectively.

5.5.3 Sending end and receiving end active power for the NWR transmission line at peak load

The maximum real power transfer over a given transmission line can be increased by injecting a series voltage. As a result, voltage levels are increasing to allow large generating stations to transmit larger chunks of power over longer distances. For long overhead transmission lines, the voltage level cannot be raised beyond the limits placed by present-day high-voltage technology. To increase the power transmitted in such cases, the only choice is to reduce the line reactance. This is accomplished by adding ANFIS-based UPFC. For NWR high-voltage transmission lines, this can be tested as shown in the figure below.

I. Sending and receiving active power at peak load from Beles to Bahir Dar line

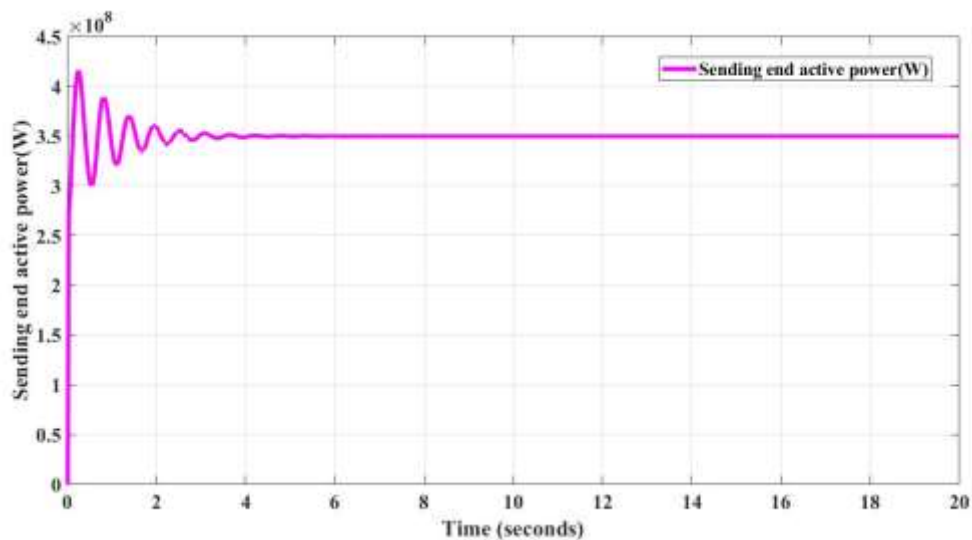


Figure 5. 23: Sending end active power from Tana beles to Bahir Dar transmission line

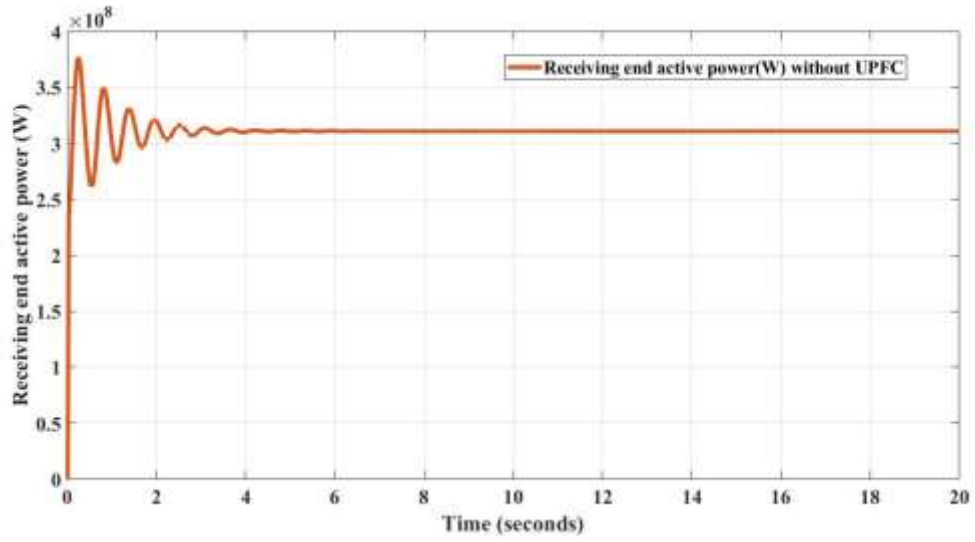


Figure 5. 24:Receiving end active power from Tana beles to Bahir Dar transmission line without UPFC

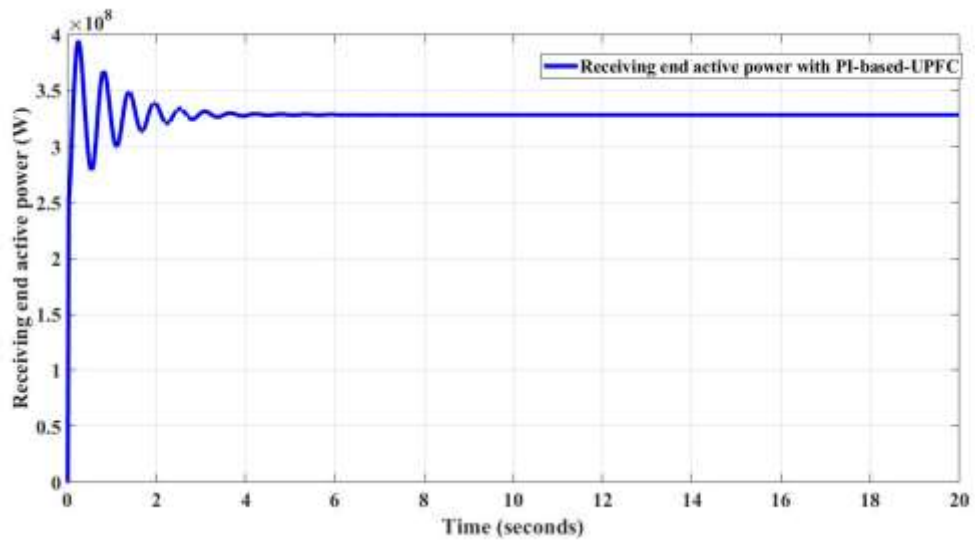


Figure 5. 25:Receiving end active power from Tana beles to Bahir Dar transmission line with PI-based UPFC

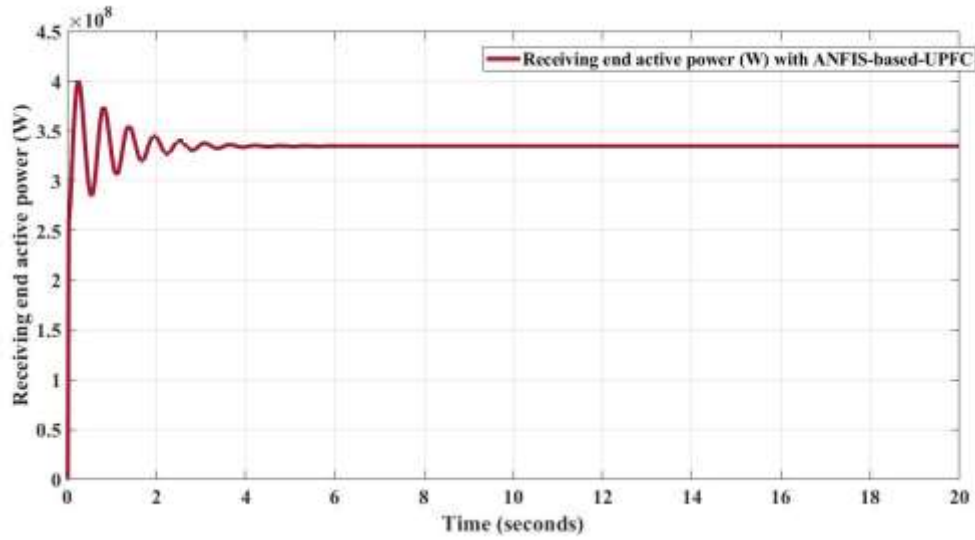


Figure 5. 26:Receiving end active power from Tana beles to Bahir Dar transmission line with ANFIS-based UPFC

The sending-end active power transferred at peak load from Tana Beles to Bahir Dar is 350 MW. while the receiving end's active power without UPFC, with PI-based UPFC, and with ANFIS-based UPFC is 310, 330.5, and 338.6 MW, respectively.

Table 5. 6:Loss minimized after incorporating UPFC to the transmission line

Controller	Receiving end power (MW)	Power loss (MW)	Loss mimized (%)
without	310	40	-----
With PI-based-UPFC	330.5	19.5	51.25
With ANFIS-based-UPFC	338.6	11.4	71.50

Table 5. 7: Comparison of the system response for peak load with and without UPFC from Beles to Bahir Dar transmission line

Controller	Maximum peak value (Mp)	Settling time (second)
Sending end power	0.60	3.00
Receiving end without UPFC	0.65	3.25
Receiving end with PI-based-UPFC	0.59	3.15
Receiving end with ANFIS-based-UPFC	0.45	3.00

II. Sending and receiving active power at peak load from Bahir Dar to D/Markos line

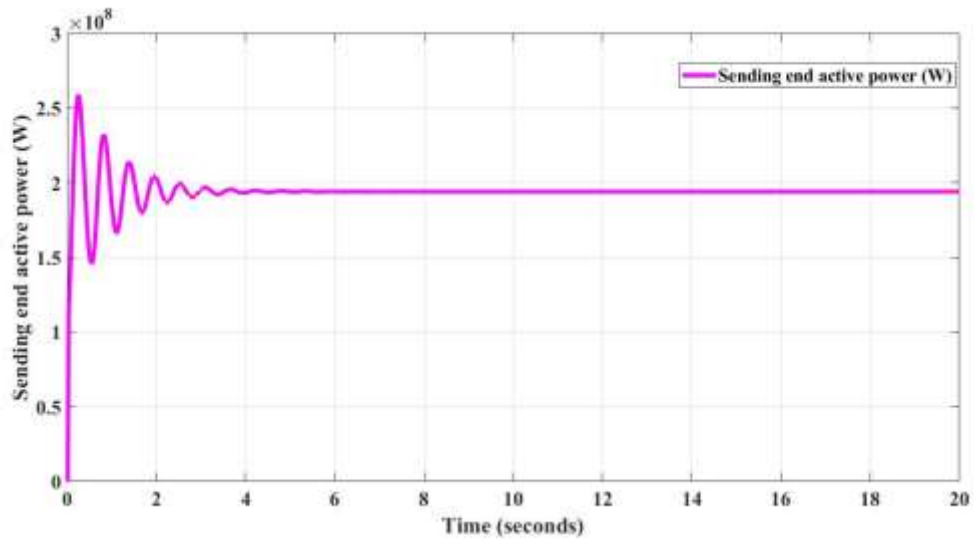


Figure 5. 27: Sending end active power from Bahir Dar to D/Markos transmission line

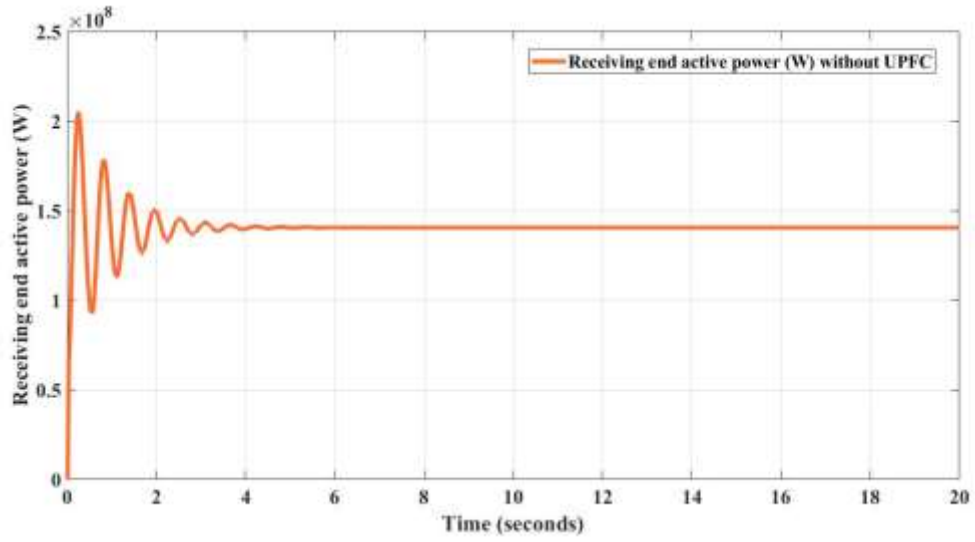


Figure 5. 28:Receiving end active power from Bahir Dar to D/Markos transmission line without UPFC

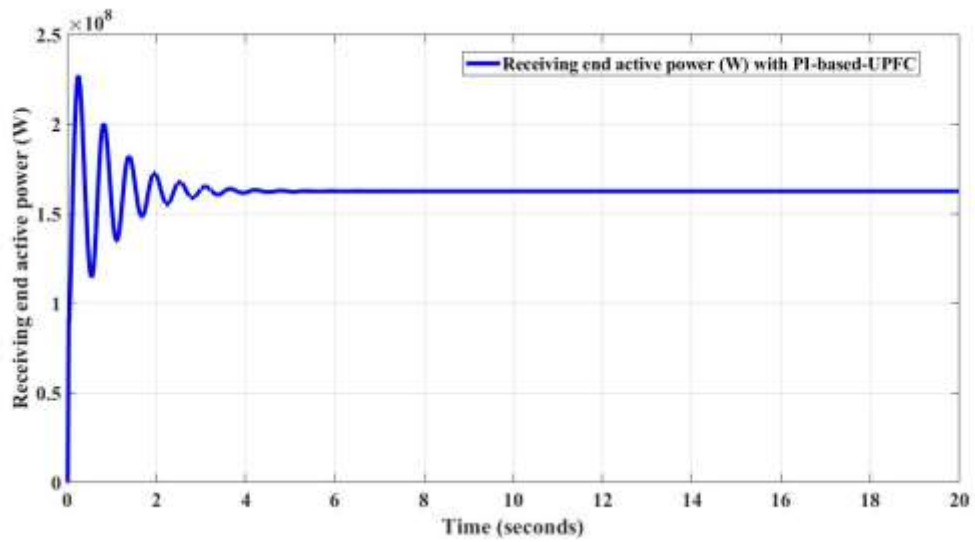


Figure 5. 29:Receiving end active power from Bahir Dar to D/Markos transmission line with PI-based UPFC

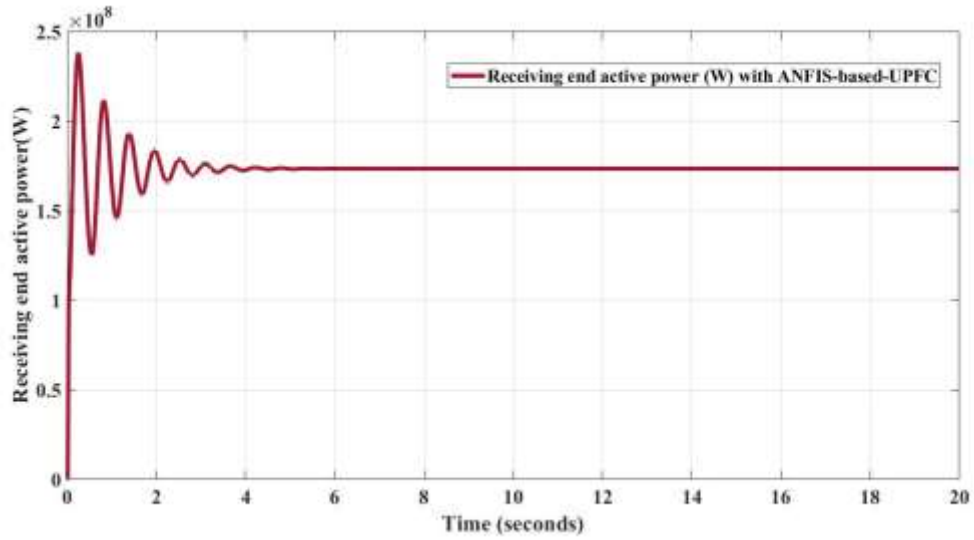


Figure 5. 30:Receiving end active power from Bahir Dar to D/Markos transmission line with ANFIS-based UPFC

The sending-end active power transferred at peak load from Bahir Dar to D/Markos is 196MW. while the receiving end's active power without UPFC, with PI-based UPFC, and with ANFIS-based UPFC is 148, 156, and 171 MW, respectively.

Table 5. 8:Loss minimized after incorporating UPFC to the transmission line

Controller	Receiving end power (MW)	Power loss (MW)	Loss mimized (%)
without	148	48	-----
With PI-based-UPFC	156	40	20
With ANFIS-based-UPFC	171	25	47.9

Table 5. 9: Comparison of the system response for peak load with and without UPFC from Bahir Dar to D/Markos transmission line

Controller	Maximum peak value (Mp)	Settling time (second)
Sending end power	0.64	3.00
Receiving end without UPFC	0.62	3.25
Receiving end with PI-based-UPFC	0.59	3.15
Receiving end with ANFIS-based-UPFC	0.64	3.00

5.5.4 Voltage magnitude at all buses after incorporating UPFC to the system

The table below shows the magnitude of the bus voltage in p.u. at peak load after and before incorporating UPFC into the system. As expected, incorporating ANFIS-based UPFC has maintained acceptable voltages at all buses in the system after being subjected to a disturbance and under normal operating conditions of the power system.

Table 5. 10: Voltage magnitude at all buses after incorporating UPFC to the system

Bus No	Bus location	Voltage magnitude (p.u) without UPFC	Voltage magnitude (p.u) with ANFIS-based UPFC
1	Tana Beles	1.0200	1.0200
2	Tis Abay II	1.0100	1.0100
3	Bahir Dar 400kV	0.9365	0.9826
4	Bahir Dar 230kV	0.9365	0.9651
5	Bahir Dar 132kV	0.9532	0.9720
6	D/markos 400kV	0.9532	1.0086
7	D/markos 230kV	0.9432	1.0023
8	Mota 230kV	0.9532	0.9845
9	Alamata 230kV	0.9432	1.0047
10	Gonder I 230kV	0.9570	0.9780
11	Gonder II 230kV	0.9548	0.9782

CHAPTER SIX

6. CONCLUSION AND RECOMMENDATION

6.1 Conclusion

This thesis discusses transient stability issues for Ethiopia's 400 kV interconnected power system in the North-West region. In this study, a neuro-fuzzy inference system is applied to the UPFC for adaptively controlling the power flow in high-voltage interconnected transmission power systems. To investigate the performance of the controller, three-phase faults and single-line ground faults are applied to the system. Also, to evaluate the performance of the power flow capability of transmission lines, peak load, average load, and minimum load have been applied to the system. This allows increased utilization of existing network closer to its thermal loading capacity, and thus avoiding the need to construct new transmission lines.

When a three-phase ground fault is applied at the midpoint of the Beles to Bahir Dar transmission line, the settling time of rotor angle deviation, rotor speed, rotor speed deviation, and output active power of synchronous generators using ANFIS-based UPFC is reduced by 70.58 %, 37.75 %, 37.75 %, and 43.75 %, respectively, compared to a system without UPFC. The active power loss reduced by PI-based UPFC and ANFIS-based UPFC on the Beles to Bahir Dar transmission line at peak load is 51.25 % and 71.50 %, respectively, compared to a system without UPFC. On the other hand, the active power loss reduced by PI-based UPFC and ANFIS-based UPFC on the Bahir Dar to D/Markos transmission line at peak load is 20 % and 47.9 % percent, respectively, compared to a system without UPFC. Also, the ANFIS-based UPFC has maintained acceptable voltages at all buses in the system after being subjected to a disturbance and under normal operating conditions of the power system.

From the result, the neuro-fuzzy controller shows a lower settling time during the fault than a conventional PI-based UPFC controller. From the obtained simulation results, it is seen that both the PI-based UPFC controller and the ANFIS-based UPFC significantly enhance

the power system's transient stability and power transmission capability of the line. However, the performances obtained by the proposed ANFIS are better compared to those obtained by the standard PI controller, especially under unfavourable operating conditions.

6.2 Recommendation and Suggestion for future work

The ANFIS-based UPFC developed in this thesis work is intended for transient stability enhancement in a high voltage transmission line. The existing power networks in North-West region are stressed with increased load demands, resulting in network operations being carried out at the system stability margins. From the simulation result, ANFIS-based UPFC shows it can clearly resolve this problem. It secures the power system and increases the efficiency of the power system components by reducing the power losses on the transmission line and enhancing transient stability.

UPFC device in general has a high cost compared to conventional power flow controller devices due to the great technology improvement involved on it. But its cost can be compromised by its unique properties which can controls all the transmission line parameters. This fact is taken in to account in this thesis. Therefore, the researcher recommends the EEP to install the UPFC at the specified place with its optimal rating.

Further studies can be done on the application of ANFIS-based UPFC for transient stability enhancement on the full Ethiopian high-voltage transmission power system network rather than the North-West region only.

REFERENCE

- [1] P. Kundur, J. Paserba and S. Vite, "Overview on Definition and Classification of Power System Stability," in *CIGRE/IEEE PES International Symposium Quality and Security of Electric Power Delivery Systems*, 2003.
- [2] B. Wang, B. Fang, Y. Wang, . H. Liu and Y. Liu, "Power System Transient Stability Assessment Based on Big Data and the Core Vector Machine," *JOURNAL OF LATEX CLASS FILES*, vol. 13, no. 9, SEPTEMBER 2014.
- [3] M. Eremia and M. Shahidehpour, Power System Stability and Protection, in Handbook of Electrical Power System Dynamics: Modeling, Stability, and Control , IEEE, 2013.
- [4] S. Yang, X. Fan, B. Zhang, Z. Hao and H. Masahide, "A Unified Scheme for Power System Transient Stability Simulation and Transient Stability Assessment," in *2019 IEEE 8th International Conference on Advanced Power System Automation and Protection (APAP)*, 2019.
- [5] R. J. Kumar and T. Rammohan, "Enhancement of Transient Stability in Power System with Multi-Machine Using Facts Device," in *IEEE International Conference on Advances and Developments in Electrical and Electronics Engineering (ICADEE)*, pp. 1-7, Coimbatore, 2020.
- [6] P. Kundur, Power System Stability and Control, New York: McGraw-Hill, 1994.
- [7] A. Hasanovic, "Modeling and Control of the Unified Power Flow Controller (UPFC)," College of Engineering and Mineral Resources at West Virginia, Morgantown, West Virginia, 2000.
- [8] R. Mihalic, P. Zunko and D. Povh, "Improvement of transient stability using unified power flow controller," in *IEEE Transactions on Power Delivery*, vol. 11, no. 1, pp. 485-492, Jan 1996.

- [9] F. G. Balakrishnan and S. K. Sreedharan, "Transient stability improvement in power system using unified power flow controller (UPFC)," in *2013 Fourth International Conference on Computing, Communications and Networking Technologies (ICCCNT)*, pp. 1-6, 2013.
- [10] Q. Wei, W. Guo, X. Han, T. Li and M. Yang, "Analysis on the effect of rotor angle control for transient stability enhancement," in *IEEE PES Innovative Smart Grid Technologies, Europe*, pp. 1-6, istanbul, 2014.
- [11] Y. Shao and Y. Tang, "Voltage stability analysis of multi-infeed HVDC systems using small-signal stability assessment," in *IEEE PES T&D*, pp. 1-6, 2010.
- [12] P. Singh, S. K. arida, B. Chauhan and N. Choudhary, "Online Voltage Stability Assessment Using Artificial Neural Network considering Voltage stability indices," in *2020 21st National Power Systems Conference (NPSC)*, pp. 1-5, 2020.
- [13] Z. A. Obaid, R. A. Mejeed and A. Al-Mashhadani, "Investigating the Impact of using Modern Power System Stabilizers on Frequency Stability in Large Dynamic Multi-Machine Power System," in *2020 55th International Universities Power Engineering Conference (UPEC)*, Baqouba, Diyala, Iraq, 2020.
- [14] Ashley-Edison, "Power quality in Ethiopia," Sinalda, Bedford, England, United Kingdom, 2020.
- [15] S. Akele, "Customer Service Quality in Ethiopian Electric," Uppsala University, Department of Business Studies, Spring Semester2012.
- [16] A. Kassie, "Transient stability improvement using unified power flow controller with fuzzy logic," Bahir Dar University, Bahir Dar, 2019.
- [17] L. Dires, "power transmission capacity and power system stability imrovement of existng HVAC lines with simultaneous AC-DC transmission," Bahird University, Bahir Dar, july 2021.

- [18] I. Muzaffer and M. ud din Mufti, "Modeling of a Multi-Machine System Aided with Power System Stabilizers and Shunt Compensator for Transient Stability Enhancement," *International Conference on Energy, Communication, Data Analytics and Soft Computing (ICECDS)*, pp. 1716-1721, 2017.
- [19] S. Siddula, T. V. Achyut, K. Vigneshwar and M. V. UdayTeja, "Improvement of power quality using fuzzy-based Unified Power Flow Controller," in *2020 International Conference on Smart Technologies in Computing, Electrical and Electronics (ICSTCEE)*, pp. 55-60, 2020.
- [20] R. Kumar and M. Kumar, "Improvement Power System Stability Using Unified Power Flow Controller Based On Hybrid Fuzzy Logic-PID Tuning In SMIB System," in *2015 International Conference on Green Computing and Internet of Things (ICGCIoT)*, pp. 815-819, Kota, 2015.
- [21] O. M. Benaissa, S. Hadjeri and S. A. Zidi, "Impact of PSS and SVC on the power system transient stability," in *8th International Conference on Modelling, Identification and Control (ICMIC)*, pp. 303-307, 2016.
- [22] B. V. Khurana and L. S. Titare, "Improvement of Power flow and voltage stability using UPFC with Artificial Neural Network in Matlab," in *2020 IEEE International Symposium on Sustainable Energy, Signal Processing and Cyber Security (iSSSC)*, pp. 1-4, 2020.
- [23] K. B. Mohanty and S. Pati, "Fuzzy logic controller based STATCOM for voltage profile improvement in a micro-grid," in *2016 Annual IEEE Systems Conference (SysCon)*, pp. 1-6, 2016.
- [24] M. Roy and A. K. Kori, "FUZZY LOGIC based Improvement of UPFC Performance in Power System," in *2021 6th International Conference on Inventive Computation Technologies (ICICT)*, pp. 245-250, 2021.

- [25] P. Das, S. M. Desmukh and L. Sahu, "Voltage Stability Improvement by using Fuzzy Logic Controller in Multi -Machine Power System," *International Journal of Scientific Engineering and Applied Science (IJSEAS)*, vol. 2, no. 6, June 2016.
- [26] H. Rahman, M. F. Rahman and H. O. rashid, "Stability Improvement of Power System By Using SVC With PID Controller," *International Journal of Emerging Technology and Advanced Engineering*, vol. 2, no. 7, July 2012.
- [27] V. K. Yadv, C. H. Bindu and M. N. , "Enhancement of Transient Stability in A Multi-Machine Power System Using Adaptive Neuro-Fuzzy Controller for Facts Devices," *international journal and magazine of Engineering, Technology, Management and Research*, vol. 2, 2015.
- [28] L. Vetoshkin, J. Votava, J. Kyncl and Z. Müller, "Improvement of transient stability using STATCOM combined with optimization," in *2019 20th International Scientific Conference on Electric Power Engineering (EPE)*, pp. 1-5, Prague, Czech Republic, 2019.
- [29] S. Khan and S. Bhowmick, "A Fuzzy TCSC Controller for transient stability improvement," in *2015 Annual IEEE India Conference (INDICON), New Delhi, India, 2015*, pp. 1-5, 2015.
- [30] Imdadullah, S. M. Amrr, M. S. Jamil Asghar and M. Meraj, "A Comprehensive Review of Power Flow Controllers in Interconnected Power System Networks," in *IEEE Access*, vol. 8, pp. 18036-18063, 2020.
- [31] F. Z. Peng, "Flexible AC Transmission Systems (FACTS) and Resilient AC Distribution Systems (RACDS) in Smart Grid," in *Proceedings of the IEEE*, vol. 105, no. 11, pp. 2099-2115, Nov. 2017.
- [32] B. Chen, W. Fei, C. Tian and J. Yuan, "Research on an Improved Hybrid Unified Power Flow Controller," in *IEEE Transactions on Industry Applications*, vol. 54, no. 6, pp. 5649-5660, Nov.-Dec. 2018.

- [33] B. Yuan, L. Xing, S. Zhang, Y. Hu, Z. Zhange and G. Li, "Several Key Issues of the Unified Power Flow Controller in its Actual Application," in *2020 7th International Forum on Electrical Engineering and Automation (IFEAA)*, 2020.
- [34] S. Wang, L. Jing, Y. Zhao, H. R. Wickramasinghe, X. Wu and G. Konstantinou, "Operation of Unified Power Flow Controller as Virtual Synchronous Generator," in *IEEE Access*, vol. 8, pp. 162569-162580, 2020.
- [35] C. D. Schauder et al., "Operation of the unified power flow controller (UPFC) under practical constraints," in *IEEE Transactions on Power Delivery*, vol. 13, no. 2, pp. 630-639, April 1998.
- [36] K. Sreenivasachar, "Unified power flow controller :modelling, stability analysis, control strategy and control system design," University of Waterloo, Ontario, Canada, 2001.
- [37] S. K. Samal and P. C. Panda, "Damping of Power System Oscillations by Using Unified Power Flow Controller with POD and PID Controllers," in *2014 International Conference on Circuit, Power and Computing Technologies [ICCPCT]*, 2014.
- [38] B. Abdelkrim, C. Abdelkader, A. Zoubida and A. Mohamed, "Neural adaptive control by state space system UPFC (SSNN) for compensation of active And reactive power," *International Journal of Scientific & Engineering Research*, vol. 3, no. 3, 2012.
- [39] Q. Li, "Analysis, design, and laboratory evaluation of a distributed unified power flow controller concept," College of Engineering at the University of Kentucky, 2006.
- [40] D. P. Kothari, *Modern Power System Analysis*, New Delhi: Tata McGraw Hill, New Delhi, 2011.

- [41] D. Das, *Electrical Power Systems*, West Bengal: New Age International (P) Ltd,publisher, 2006.
- [42] J. B. Abugri and M. Karam, "Particle Swarm Optimization for the Minimization of Power Losses in Distribution Networks," in *2015 12th International Conference on Information Technology - New Generations*, 2015.
- [43] Y. Shen, Y. Li, . H. Kang, Y. Zhang, X. Sun, Q. Chen, J. Peng and H. Wang, "Research on Swarm Size of Multi-swarm Particle Swarm Optimization Algorithm," in *2018 IEEE 4th International Conference on Computer and Communications (ICCC)*, 2018.
- [44] F. R. Cabezas Soldevilla and F. A. Cabezas Huerta, "Minimization of Losses in Power Systems by Reactive Power Dispatch using Particle Swarm Optimization," in *2019 54th International Universities Power Engineering Conference (UPEC)*, 2019.
- [45] J. B. Abugri and M. Karam, "Particle Swarm Optimization for the Minimization of Power Losses in Distribution Networks," in *2015 12th International Conference on Information Technology - New Generations*, 2015.
- [46] E. Baharozu, G. Soykan, O. Altay and O. Kalenderli, "An Improved Particle Swarm Optimization Method to Optimal Reactive Power Flow Problems," Bahcesehir University, Istanbul, Turkey, 2015.
- [47] S. Kandasamy and A. Rajapalan, "Dynamic control modeling and simulation of a UPFC–SMES compensator in power systems," *Ainf Shams Engineering Journal*, 2015.
- [48] A. Hasanovic, "Modeling and Control of the Unified Power Flow Controller (UPFC)," The College of Engineering and Mineral Resources, Morgantown, West Virginia, 2000.

- [49] S. Latha and C. K. Rani, "Transient Stability Improvement with Unified Power Flow Controller Using Fuzzy Logic and ANFIS Approach," *Advanced Materials Research*, vol. 768, no. 12, pp. 378-387, 2013.
- [50] F. G. Balakrishnan , S. K. Sreedharan and J. Michael, "Transient Stability Improvement in Power System Using Unified Power Flow Controller (UPFC)," in *2013 Fourth International Conference on Computing, Communications and Networking Technologies (ICCCNT)*, 2013.
- [51] R. Chourasia, V. Saxena, N. Yadala and F. C. Rhee, "Visualization of Two-dimensional Interval Type-2 Fuzzy Membership Functions using General Type-2 Fuzzy Membership Functions," in *2017 Joint 17th World Congress of International Fuzzy Systems Association and 9th International Conference on Soft Computing and Intelligent Systems (IFSA-SCIS)*, 2017.
- [52] F. Liu, H. Wang, Q. Shi, H. Wang, M. Zhang and H. Zhao, "Comparison of an ANFIS and Fuzzy PID Control Model for Performance in a Two-axis Inertial Stabilized Platform," *IEEE Access*, vol. 14, no. 8, 2017.
- [53] N. K. Sharma and P. P. Jagtap, "Modelling and application of Unified Power Flow Controller (UPFC)," in *IEEE Third International Conference on Emerging Trends in Engineering and Technology*, Goa (2010.11.19-2010.11.21), 2010.
- [54] A. Tsehay, "Investigation and minimization of power loss and voltage profile enhancement using a unified power flow controller," Bahir Dar University, Bahir Dar, 2019.
- [55] F. Taki, S. Abazari and G. R. Arab Markadeh, "Transient Stability Improvement Using ANFIS Controlled UPFC Based on Energy Function," *Proceedings of ICEE*, 2010.
- [56] H. Fujita, Y. Watanabe and H. Akagi, "Control and Analysis of a Unified Power Flow Controller," in *IEEE Transactions on Power Electronics*, vol. 14, no. 6, pp. 1021-1027, 1999.

- [57] K. R. Sudha and K. H. Reddy, "A fuzzy controller for enhancement of power system stability with FACTS device," *Journal of Theoretical and Applied Information Technology*, 2009.
- [58] G. Srinivasa and V. Reddy, "Improvement of Transient stability in Power Systems with NeuroFuzzy UPFC," *American Journal of Engineering Research (AJER)*, vol. 02, 2013.
- [59] M. S. Kumar, P. Renuga and K. Saravanan, "Adaptive Neuro-Fuzzy Based Transient Stability Improvement Using UPFC," *International Journal of Recent Trends in Engineering*, 2009.
- [60] Q. Li, "Analysis, design, and laboratory evaluation of a distributed unified power flow controller concept," University of Kentucky, 2006.
- [61] R. Singh and M. Kirar, "Transient stability analysis and improvement in microgrid," in *2016 International Conference on Electrical Power and Energy Systems (ICEPES), Bhopal, India, 2016*, pp. 239-245, 2016.

APPENDICES

Appendix A: Transmission Line Data

From Bus	To Bus	Voltage (kV)	Rating (MVA)	Length (km)	R (Ω /km)	X (Ω /km)	C (nF/km)
T.beles	Bahir Dar	400	1341	62.84	0.00209	0.03096	12
Tis Abay 2	Bahir Dar	132	80	28.9	0.00124	0.00244	9.5
Bahir Dar	D/Markos	400	1341	193.7	0.00209	0.03096	12.2
Bahir Dar	Mota	230	280	81	0.00725	0.04089	8.8
Bahir Dar	Alamata	230	318	341	0.00918	0.03195	11.4
Bahir Dar	Gonder	230	318	137	0.00918	0.03205	11.4
Bahir Dar	Dangila	66	24	68.6	0.000127	0.00063	1.27

Appendix B: Generator Data

G.station	Voltage (kV)	MVA	H(s)	T'do	T''do =T''qo	Xd	Xq	X'd	X''d =X''q
Tis-Abay II	10.5	40	2.5	7.1	0.12	1.00	0.6	0.29	0.365
Tana Beles	15	133	3.14	9.2	0.10	1.03	0.7	0.31	0.250

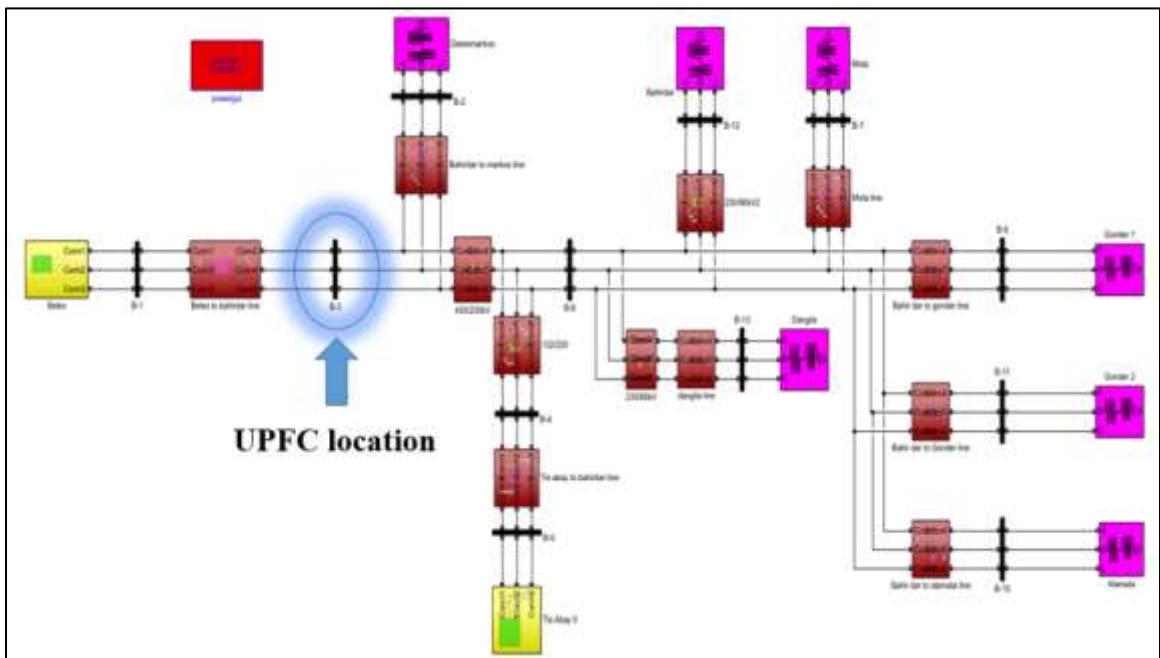
Appendix C: Transformer Data

Voltage(kv)	Rating (MVA)	R (%)	X (%)	X/R (%)
400/230	133	0.176	12.045	68.44
400/15	133	0.215	13.5	62.79
230/132	133	0.233	13.36	57.33
230/66	133	0.43	12.368	28.76
230/33	6.3	0.302	8.4	27.78
132/10.5	24	0.257	7.8	30.35
132/6	6.3	0.322	6.387	28.85

Appendix D: Load Data

No	Bus name	Average active power (MW)	Reactive power (Mvar)	Voltage level (KV)
1	Mota	25.77	1.7	230
2	Alamata	96.095	57.08	230
3	Gonder I	38.725	18	230
4	Gonder II	35.489	18	230
5	Dangila	20.004	2.1	66
6	Bahirdar II	15.187	30.57	66
7	D/markos	18.4	8.22	400

Appendix E: Simulink model of the system



Appendix F: MATLAB code for UPFC placement using PSO integrated with Newton Raphson

I. PSO.m

```

clc
clc;
clear all;
close all;
%% Problem Definition;
%error.....power balance error
%Pgs.....slack power
%Toldev.....tolerance deviation of load flow
%angdev....angle deviation
%Vdev.....voltage deviation
%Llim.....line capacity limit
%Pgsdev.....slack power deviation
CostFunction = @(x,Pgs,error,Plos,Toldev, Vdev, angdev, Llim,Pgsdev)
Fitness (x,error,Plos,Pgs, Toldev, Vdev, angdev, Llim,Pgsdev);% Cost
Function
nVar = 2; % Number of Decision Variables
VarSize = [1 nVar]; % Size of Decision Variables Matrix

VarMin = [20 20]; % Lower Bound of Variables
VarMax = [80 50]; % Upper Bound of Variables

%% PSO Parameters

MaxIt =100; % Maximum Number of Iterations

nPop = 100; % Population Size (Swarm Size)

% PSO Parameters
wmax=0.9; % Inertia Weight
wmin=0.4;
c1max = 2.5; % Personal Learning Coefficient
c1min = 1.5;
c2max = 2.5; % Global Learning Coefficient
c2min=1.5;
% Velocity Limits
VelMax = 0.1*(VarMax-VarMin);
VelMin = -VelMax;
%% Initialization

empty_particle.Position = [];
empty_particle.Cost = [];
empty_particle.Velocity = [];
empty_particle.Best.Position = [];
empty_particle.Best.Cost = [];
particle = repmat(empty_particle, nPop, 1);

GlobalBest.Cost = inf;

```

```

for i = 1:nPop

    % Initialize Position
    particle(i).Position = unifrnd(VarMin, VarMax, VarSize);
    % Initialize Velocity
    particle(i).Velocity = zeros(VarSize);
    [Pgs,Pl,Plos,Toldev,Vdev,angdev,
Llim,Pgsdev]=newton_raphson(particle(i).Position);
    error=PowerBalance(particle(i).Position,Plos,Pl,Pgs);
    particle(i).Cost = CostFunction(particle(i).Position,Plos,Pgs,error
,Toldev, Vdev, angdev, Llim,Pgsdev);

    % Update Personal Best
    particle(i).Best.Position = particle(i).Position;
    particle(i).Best.Cost = particle(i).Cost;

    % Update Global Best
    if particle(i).Best.Cost<GlobalBest.Cost

        GlobalBest = particle(i).Best;
    end
end

BestCost = zeros(MaxIt, 1);
%% PSO Main Loop

for it = 1:MaxIt
    for i = 1:nPop
        w(it)=wmax-(wmax-wmin)*it/MaxIt;
        c1(it)=c1max-(c1max-c1min)*it/MaxIt;
        c2(it)=c2min + (c2max-c2min)*it/MaxIt;
        % Update Velocity
        particle(i).Velocity = w(it)*particle(i).Velocity ...
            +c1(it)*rand(VarSize).*(particle(i).Best.Position-
particle(i).Position) ...
            +c2(it)*rand(VarSize).*(GlobalBest.Position-
particle(i).Position);

        % Apply Velocity Limits
        particle(i).Velocity = max(particle(i).Velocity, VelMin);
        particle(i).Velocity = min(particle(i).Velocity, VelMax);

        % Update Position
        particle(i).Position = particle(i).Position +
particle(i).Velocity;

        % Velocity Mirror Effect
        IsOutside = (particle(i).Position<VarMin |
particle(i).Position>VarMax);
        particle(i).Velocity(IsOutside) = -
particle(i).Velocity(IsOutside);

        % Apply Position Limits
        particle(i).Position = max(particle(i).Position, VarMin);
        particle(i).Position = min(particle(i).Position, VarMax);
    end
end
    
```

```

        [Pgs,Pl,Plos,Toldev, Vdev, angdev,
Llim,Pgsdev]=newton_raphson(particle(i).Position);
        error=PowerBalance(particle(i).Position,Plos,Pl,Pgs);
        %           particle(i).Cost =
CostFunction(particle(i).Position);
        particle(i).Cost = CostFunction(particle(i).Position,Pgs,error
,Plos,Toldev, Vdev, angdev, Llim,Pgsdev);
        % Update Personal Best
        if particle(i).Cost<particle(i).Best.Cost

            particle(i).Best.Position = particle(i).Position;
            particle(i).Best.Cost = particle(i).Cost;

            % Update Global Best
            if particle(i).Best.Cost<GlobalBest.Cost

                GlobalBest = particle(i).Best;

            end

        end

    end

    BestCost(it) = GlobalBest.Cost;
    disp(['Iteration ' num2str(it) ':Slack power=' num2str(Pgs(1)) ':
Best Fitness = ' num2str(BestCost(it))]);
end
BestSol = GlobalBest;
%% Results

figure;
semilogy(BestCost, 'b','LineWidth', 3);
xlabel('Iteration');
ylabel('Best Fitness');
grid on;

```

II. Newton_Raphson.m

```

function[Pgs,Pl,Plos,Toldev, Vdev, angdev,
Llim,Pgsdev]=newton_raphson(X)
MVA_base=133.0;
[linedata,busdata,acceleration_factor,tolerance,nPV,nLB] =
Data11();%Calling the function containing the input data(Stevenson-337)

fb=linedata(:,1); % Storing the from-bus numbers
tb=linedata(:,2); % Storing the to-bus numbers
r=linedata(:,3); % Storing the resistance(s)
x=linedata(:,4); % Storing the reactance(s)
b=linedata(:,5); % Storing the half-line charging(shunt-admittance)

```

```

a=linedata(:,6); % Storing the off-nominal trans-ratio
bus_type=(busdata(:,2)); % Storing the bus-type(s)
v_bus_initial=(busdata(:,3)); % Storing the initial bus-voltage(s) in
(p.u.)
P_gen=((busdata(:,5))*(MVA_base)); % Storing the active power generated
at bus(s)
Q_gen=((busdata(:,6))*(MVA_base)); % Storing the reactive power
generated at bus(s)
S_gen=((P_gen)+(1i)*(Q_gen)); % Storing the complex power generated at
bus(s)
Pl=((busdata(:,7))*(MVA_base)); % Storing the active power at load(s)
at bus(s)
P_gen(2)=X(1,1);
P_gen(3)=X(1,2);
Q_load=((busdata(:,8))*(MVA_base)); % Storing the reactive power at
load(s) at bus(s)
S_load=((Pl)+(1i)*(Q_load)); % Storing the complex power at load(s) at
bus(s)
Q_min=((busdata(:,9))*(MVA_base)); % Storing the minimum Q-range of the
PV-bus(s)
Q_max=((busdata(:,10))*(MVA_base)); % Storing the maximum Q-range of
the PV-bus(s)
B_shunt=((busdata(:,11))); % Storing the data corresponding to the
static shunt capacitance
z_elementary=((r)+(1i)*(x));
Z=z_elementary;
b_elementary=((1i)*(b)); % Calculating the 'b'
nbus = max(max(fb),max(tb)); % no. of buses
nbranch = length(fb); % no. of branches

z=zeros(nbus,nbus); % Initialising the elementary [z]
b=zeros(nbus,nbus); % Initialising the elementary [b]
Ybus=zeros(nbus,nbus); % Initialising the elementary [Y] (Bus-
admittance matrix)
tolerance_checker=1; % Initialising the 'tolerance_checker' as '1'
iteration=0; % Initialising the 'iteration' as '0'
V_new=v_bus_initial; % Initialising the 'V_new[]' as 'V_initial[]'
v_scheduled=v_bus_initial; % Initialising the 'v_scheduled[]' as
'V_initial[]' (to get the scheduled voltages at the PV-bus(s))
V_new_accelerated=zeros(1,nbus); % Initialising the
'V_new_accelerated[]'
V_new_del=zeros(1,nbus); % Initialising the 'v_new_del[]' (to get the
difference(s) of bus-voltage(s) of two(02) consecutive iteration(s))
difference=zeros(1,nbus); % Initialising the 'difference[]'
real_diff=zeros(1,nbus); % Initialising the 'real_diff[]' (to store the
real part of the difference)
imag_diff=zeros(1,nbus); % Initialising the 'imag_diff[]' (to store the
imaginary part of the difference)
delta=zeros(1,nbus); % Initialising the 'delta[]' (for getting the
angle at PV-bus(s))
E_new=zeros(1,nbus); % Initialising the 'E_new[]' (to store the real
part of the voltage at PV-bus)
F_new=zeros(1,nbus); % Initialising the 'F_new[]' (to store the
imaginary part of the voltage at PV-bus)
Q_intermediate=zeros(1,nbus); % Initialising the 'Q_intermediate'
Q_final=zeros(1,nbus); % Initialising 'Q_final[]'
    
```

```

complex_flow_line=zeros(1,nbranch); % Initialising
'complex_flow_line[]'
line_flows=zeros(nbus,nbus); % Initialising 'line_flows[]'
active_flow_line=zeros(1,nbranch); % Initialising 'active_flow_line[]'
reactive_flow_line=zeros(1,nbranch); % Initialising
'reactive_flow_line[]'
bus_power_injection=zeros(1,nbus); % Initialising
'bus_power_injection[]'
bus_power_mismatch=zeros(1,nbus); % Initialising 'bus_power_mismatch[]'
line_loss=zeros(nbus,nbus); % Initialising 'line_loss[]'
flow_count=1; % Initialising the 'flow_count' as (1) //(for tracking
the total no. of lines)
sum_line_loss=((0.0)+(1i)*(0.0)); % Initialising 'sum_line_loss' as '0'
sum=zeros(1,nbus); % Initialising the 'sum' (used in calculating the
digaonal [Ybus] elements)
shunt_fb_onr=zeros(1,nbranch); % storing the ((a^2)/(1-a)) as seen from
the FB(From Bus)
shunt_tb_onr=zeros(1,nbranch); % storing the ((a)/(a-1)) as seen from
the TB(To Bus)
P_injected_sum=zeros(nbus,1); % Initialising 'P_injected_sum[]' for
intermediate calculation(s) of injected (P)
Q_injected_sum=zeros(nbus,1); % Initialising 'Q_injected_sum[]' for
intermediate calculation(s) of injected (Q)
P_injected_bus=zeros(nbus,1); % for storing the intermediate 'active
power injection(s)' at different bus(s)
Q_injected_bus=zeros(nbus,1); % for storing the intermediate 'reactive
power injection(s)' at different bus(s)
partial_P_delta=zeros(nbus-1,nbus-1); % Initialising
'partial_P_delta[]'corresponding to the [J11]
partial_Q_delta=zeros(nbus-nPV-1,nbus-1); % Initialising
'partial_Q_delta[]'corresponding to the [J21]
partial_P_vol_mag=zeros(nbus-1,nbus-nPV-1); % Initialising
'partial_P_vol_mag[]'corresponding to the [J12]
partial_Q_vol_mag=zeros(nbus-nPV-1,nbus-nPV-1); % Initialising
'partial_Q_vol_mag[]'corresponding to the [J12]
J=zeros(((2*(nbus-1))-nPV),((2*(nbus-1))-nPV)); % Initialising 'J[]'
i.e. THE COMPLETE JACOBIAN MATRIX
inj_active_pow_mismatch_vector=zeros(nbus-1,1); % Initialising the
'inj_active_pow_mismatch_vector[]'
inj_reactive_pow_mismatch_vector=zeros(nbus-nPV-1,1); % Initialising
the 'inj_reactive_pow_mismatch_vector[]'
inj_pow_mismatch_vector=zeros(((2*(nbus-1))-nPV),1); % Initialising the
'inj_pow_mismatch_vector[]'
correction_vector=zeros(((2*(nbus-1))-nPV),1); % Initialising the
'correction_vector[]'
correction_voltage_angle=zeros((nbus-1),1); % Initialising the
'correction_voltage_angle[]'
correction_voltage_magnitude=zeros((nbus-1-nPV),1); % Initialising the
'correction_voltage_magnitude[]'
mismatch_active_vector_element_count=1; % Initialising the
'mismatch_active_vector_element_count' as (1)
mismatch_reactive_vector_element_count=1; % Initialising the
'mismatch_reactive_vector_element_count' as (1)
mismatch_vector_element_count=0;% Initialising the
'mismatch_active_vector_element_count' as (0)
real_mismatch=zeros(nbus-1,1);
imag_mismatch=zeros(nbus-1-nPV,1);
    
```

```

for u=1:((2*(nbus-1))-nPv)
    correction_vector(u)=1.0; % Initialising the correction vector
    element(s) as (1.0); so that loop can be started
end

% Forming the elementary z-matrix & b-matrix

for u=1:nbranch
    z(fb(u),tb(u))=z_elementary(u); % Storing the mutual element(s)
    (Z(i,j))
    z(tb(u),fb(u))=z(fb(u),tb(u)); % Storing the similar element(s) in
    (Z(j,i))
    b(fb(u),tb(u))=b_elementary(u); % Storing the mutual element(s)
    (B(i,j))
    b(tb(u),fb(u))=b(fb(u),tb(u)); % Storing the similar element(s) in
    (B(j,i))
end

% Modification(s) in the element(s) of 'z' & 'b' due to OFF-NOMINAL
TRANS RATIO

for u=1:nbranch
    if((a(u,1))~=1.0)
        shunt_fb_onr(1,u)=(((a(u,1))^(2))/(1-(a(u,1)))); % Calculating
the (a^2/(1-a))

b(fb(u),tb(u))=(1/((shunt_fb_onr(1,u))*(z(fb(u),tb(u))))+(b(fb(u),tb(u)
))); % Modifying the element 'b' matrix w.r.t. 'fb'
        shunt_tb_onr(1,u)=(a(u,1)/(a(u,1)-1)); % Calculating the
(a/(a-1))
        b(tb(u),fb(u))=(1/((shunt_tb_onr(1,u))*(z(fb(u),tb(u))))); %
Modifying the element 'b' matrix w.r.t. 'tb'
        z(fb(u),tb(u))=z(fb(u),tb(u))*(a(u,1)); % Modifying the 'z'
matrix
        z(tb(u),fb(u))=z(fb(u),tb(u)); % Storing the similar element(s)
in (Z(j,i))
    end
end

% Including the effect(s) of static shunt-capacitance

for u=1:nbus
    if(B_shunt(u)~=0.0)
        sum(1,u)=B_shunt(u); % Updating the 'sum(1,u)' with the data
for static shunt capacitance
    end
end

% STEP-1 - CALCULATION OF BUS-ADMITTANCE MATRIX
%-----
for u=1:nbus
    for j=1:nbus
        if(z(u,j)==0.0)
            Ybus(u,j)=0.0; % No connection between (u) & (j)
        end
    end
end
    
```



```

        else
            Ybus(u,j)=- (1/z(u,j)); % Calculating the mutual-admittances
        end
    end
end
for u=1:nbus
    for j=1:nbus
        sum(1,u)=sum(1,u)+b(u,j)-Ybus(u,j);
        if(j==nbus)
            Ybus(u,u)=sum(1,u); % Calculating the self-admittances
        end
    end
end
Gbus=real(Ybus); % Generating the conductance matrix[G] by taking the
real part of the [Ybus] element(s); (y=g+jb)
Bbus=imag((+1)*(Ybus)); % Generating the susceptance matrix[B] by
taking the imaginary part of the [Ybus] element(s); (y=g+jb)

%-----END OF STEP-1-----
-----

while((tolerance_checker>0)&&(iteration<71))
    mismatch_vector_element_count=0;% Resetting the
    'mismatch_active_vector_element_count' as (0)
    mismatch_active_vector_element_count=1; % Resetting the
    'mismatch_active_vector_element_count' as (1)
    mismatch_reactive_vector_element_count=1; % Resetting the
    'mismatch_reactive_vector_element_count' as (1)
    P_injected_sum=zeros(nbus,1); % Resetting 'P_injected_sum[]' for
    intermediate calculation(s) of injected (P)
    Q_injected_sum=zeros(nbus,1); % Resetting 'Q_injected_sum[]' for
    intermediate calculation(s) of injected (Q)
    tolerance_checker=0; % resetting the 'tolerance_checker' to (0)
%-----STARTING OF STEP-2-----
-----

P_injected_scheduled=((P_gen-P1)/(MVA_base)); % calculating the
scheduled injected active power at each bus
Q_injected_scheduled=((Q_gen-Q_load)/(MVA_base)); % calculating the
scheduled injected reactive power at each bus
for u=1:nbus
    for j=1:nbus
        if((u~=j) && (abs(Ybus(u,j)))~=0.0)

P_injected_sum(u,1)=((P_injected_sum(u,1))+(((abs((V_new(u,1))*(V_new(j
,1))*(Ybus(u,j))))*(cos((angle(Ybus(u,j)))+(angle(V_new(j,1)))-
(angle(V_new(u,1))))))); % calculating the mutual summation part
        end
        if((u~=j) && ((abs(Ybus(u,j)))~=0.0) && (bus_type(u)~=2))

Q_injected_sum(u,1)=((Q_injected_sum(u,1))+(((abs((V_new(u,1))*(V_new(j
,1))*(Ybus(u,j))))*(sin((angle(Ybus(u,j)))+(angle(V_new(j,1)))-
(angle(V_new(u,1))))))); % calculating the mutual summation part
        end
        if(j==nbus)

```

```

P_injected_bus(u,1)=((((abs(V_new(u,1)))^(2))*Gbus(u,u)))+(P_injected_
sum(u,1)); % calculating the injectedd 'P' at bus-(u)
    end
    if((j==nbus)&&(bus_type(u)~=2))
        Q_injected_bus(u,1)=(-
        (((abs(V_new(u,1)))^(2))*Bbus(u,u)))+(Q_injected_sum(u,1)); %
        calculating the injectedd 'Q' at bus-(u)
    end
end
end
for u=1:nbus
    if(bus_type(u)~=1)

inj_active_pow_mismatch_vector(mismatch_active_vector_element_count,1)=
((P_injected_scheduled(u,1))-(P_injected_bus(u,1))); % calculating the
mismatch vector for active power injection

mismatch_active_vector_element_count=mismatch_active_vector_element_cou
nt+1; % updating the value of 'mismatch_vector_element_count'
    end
    if((bus_type(u)~=1)&&(bus_type(u)~=2))

inj_reactive_pow_mismatch_vector(mismatch_reactive_vector_element_count
,1)=((Q_injected_scheduled(u,1))-(Q_injected_bus(u,1))); % calculating
the mismatch vector for reactive power injection

mismatch_reactive_vector_element_count=mismatch_reactive_vector_element
_count+1; % updating the value of 'mismatch_vector_element_count'
    end
end
for u=2:nbus

if(mismatch_vector_element_count<=((mismatch_active_vector_element_coun
t-1)+(mismatch_reactive_vector_element_count-1)))
    inj_pow_mismatch_vector((u-
1),1)=inj_active_pow_mismatch_vector(u-1,1); % storing the mismatch in
the active power
    mismatch_vector_element_count=mismatch_vector_element_count+1;
% updating the 'mismatch_vector_element_count'
    end

if((mismatch_vector_element_count<((mismatch_active_vector_element_coun
t-1)+(mismatch_reactive_vector_element_count-1))&&((u-1)<=(nbus-1-
nPV)))
    inj_pow_mismatch_vector((u+nbus-
2),1)=inj_reactive_pow_mismatch_vector(u-1,1); % storing the mismatch
in the reactive power
    mismatch_vector_element_count=mismatch_vector_element_count+1;
% updating the 'mismatch_vector_element_count'
    end
end

for u=1:nbus-1
    real_mismatch(u,1)=inj_pow_mismatch_vector(u,1); % storing the
real-power mismatch(s)

```

```

        if ((u+nbus-1) <= ((2*(nbus-1))-nPV))
            imag_mismatch(u,1)=inj_pow_mismatch_vector(u+nbus-1,1); %
            storing the imaginary-power mismatch(s)
        end
    end
    for u=1:((2*(nbus-1))-nPV)
        if ((abs(inj_pow_mismatch_vector(u,1))) > (tolerance))
            tolerance_checker=tolerance_checker+1;
        end
    end
end

%-----END OF STEP-2-----
%-----STARTING OF STEP-3-----

% STEP-3: CALCULATES THE [J] OR THE JACOBIAN MATRIX ([J]=[J11] [J12] :
% [J21] [J22]])
% UNDER THIS STEP SUB-STEP HAS BEEN PRFORMED FOR CALCULATING THE [J11],
% [J12], [J21], [J22] IN INDIVIDUAL
%-----
% STEP-(3.a): CALCULATING THE [J11]
%-----

sum_pv=0; % initialising 'sum_pv' for getting the [J] elements
dependent on PV-bus (Q)
for u=1:nbus-1
    for j=1:nbus-1
        if ((u+1)~= (j+1))
            partial_P_delta(u,j)=(-
            ((abs((V_new(u+1,1))*(V_new(j+1,1))*(Ybus(u+1,j+1))))*(sin((angle(Ybus(
            u+1,j+1))+angle(V_new(j+1,1))-angle(V_new(u+1,1)))))); %
            calculating the off-diagonal element(s)
        else
            if ((bus_type(u+1))~=2)
                partial_P_delta(u,j)=(-
                (((abs(V_new(u+1,1)))^2)*(Bbus(u+1,u+1)))+(Q_injected_bus(u+1,1)));
                % calculating the diagonal element(s)
            else
                for k=1:nbus
                    if ((u+1)~= (k)) && (abs(Ybus(u+1,k))~=0.0))
                        %sum_pv=sum_pv-partial_P_delta(u-1,k-1);

                    sum_pv=sum_pv+((abs((V_new(u+1,1))*(V_new(k,1))*(Ybus(u+1,k))))*(sin((an
                    gle(Ybus(u+1,k))+angle(V_new(k,1))-angle(V_new(u+1,1))))));
                    end
                end
                partial_P_delta(u,j)=sum_pv; % calculating the
                (partial_P_delta(3,3)) for the PV-bus
                sum_pv=0; % resetting the 'sum_pv' to (0)
            end
        end
    end
end
end
end
end

```

```

%-----
% STEP-(3.b): CALCULATING THE [J21]
%-----

m=1;n=1;element_count=0;
for u=2:nbus
    for j=2:nbus
        if (m~=n) && ((bus_type(u)~=2) && (u~=j))
            partial_Q_delta(m,n)=(-
            ((abs((V_new(u,1))* (V_new(j,1))* (Ybus(u,j))))*(cos((angle(Ybus(u,j)))+(
            angle(V_new(j,1))-(angle(V_new(u,1)))))); % calculating the off-
            diagonal element(s)
            n=n+1;
            element_count=element_count+1;
        elseif (m~=n) && ((bus_type(u)~=2) && (u==j))
            partial_Q_delta(m,n)=((P_injected_bus(u,1))-
            (((abs(V_new(u,1)))^(2))* (Gbus(u,u))));
            n=n+1;
            element_count=element_count+1;
        elseif (m==n) && ((bus_type(u)~=2) && (u~=j))
            partial_Q_delta(m,n)=(-
            ((abs((V_new(u,1))* (V_new(j,1))* (Ybus(u,j))))*(cos((angle(Ybus(u,j)))+(
            angle(V_new(j,1))-(angle(V_new(u,1)))))); % calculating the off-
            diagonal element(s)
            n=n+1;
            element_count=element_count+1;
        elseif (m==n) && ((bus_type(u)~=2) && (u==j))
            partial_Q_delta(m,n)=((P_injected_bus(u,1))-
            (((abs(V_new(u,1)))^(2))* (Gbus(u,u))));
            n=n+1;
            element_count=element_count+1;
        end
    end
    if ((j==nbus) && (element_count>0))
        m=m+1;n=1;element_count=0;
    end
end

%-----
% STEP-(3.c): CALCULATING THE [J12]
%-----

m=1;n=1;element_count=0;
for u=2:nbus
    for j=2:nbus
        if (m==n) && (bus_type(j)~=2) && (u~=j) && (bus_type(u)~=2))
            %partial_P_vol_mag(m,n)=(-(partial_Q_delta(u-nPV-1,j-1)));
            % calculating the off-diagonal element(s)

            partial_P_vol_mag(m,n)=((abs((V_new(u,1))* (V_new(j,1))* (Ybus(u,j))))*(c
            os((angle(Ybus(u,j)))+(angle(V_new(j,1))-(angle(V_new(u,1))))));
            n=n+1;
            element_count=element_count+1;
        elseif (m==n) && (bus_type(j)~=2) && (u==j) && (bus_type(u)~=2))

```

```

partial_P_vol_mag(m,n)=((P_injected_bus(u,1))+(((abs(V_new(u,1)))^(2))*
(Gbus(u,u))));
    n=n+1;
    element_count=element_count+1;
    elseif((m==n)&&(bus_type(j)~=2)&&(u~=j)&&(bus_type(u)==2))

partial_P_vol_mag(m,n)=((abs((V_new(u,1))*(V_new(j,1))*(Ybus(u,j))))*(c
os((angle(Ybus(u,j)))+(angle(V_new(j,1)))-(angle(V_new(u,1))))));
    n=n+1;
    element_count=element_count+1;
    elseif((m~=n)&&(bus_type(j)~=2)&&(u~=j)&&(bus_type(u)~=2))

partial_P_vol_mag(m,n)=((abs((V_new(u,1))*(V_new(j,1))*(Ybus(u,j))))*(c
os((angle(Ybus(u,j)))+(angle(V_new(j,1)))-(angle(V_new(u,1))))));
    n=n+1;
    element_count=element_count+1;
    elseif((m~=n)&&(bus_type(j)~=2)&&(u==j)&&(bus_type(u)~=2))

partial_P_vol_mag(m,n)=((P_injected_bus(u,1))+(((abs(V_new(u,1)))^(2))*
(Gbus(u,u))));
    n=n+1;
    element_count=element_count+1;
    elseif((m~=n)&&(bus_type(j)~=2)&&(u~=j)&&(bus_type(u)==2))

partial_P_vol_mag(m,n)=((abs((V_new(u,1))*(V_new(j,1))*(Ybus(u,j))))*(c
os((angle(Ybus(u,j)))+(angle(V_new(j,1)))-(angle(V_new(u,1))))));
    n=n+1;
    element_count=element_count+1;
end
end
if((j==nbus)&&(element_count>0))
    m=m+1;n=1;element_count=0;
end
end

%-----
% STEP-(3.d): CALCULATING THE [J22]
%-----

m=1;n=1;element_count=0;
for u=2:nbus
    for j=2:nbus
        if((m~=n)&&(u~=j)&&((bus_type(u)~=2)&&(bus_type(j)~=2))
            partial_Q_vol_mag(m,n)=(-
            ((abs((V_new(u,1))*(V_new(j,1))*(Ybus(u,j))))*(sin((angle(Ybus(u,j)))+(
            angle(V_new(j,1)))-(angle(V_new(u,1))))));
            n=n+1;
            element_count=element_count+1;
        elseif((m~=n)&&(u==j)&&((bus_type(u)~=2)&&(bus_type(j)~=2))
            partial_Q_vol_mag(m,n)=((Q_injected_bus(u,1))-
            (((abs(V_new(u,1)))^(2))*(Bbus(u,u))));
            n=n+1;
            element_count=element_count+1;
        elseif((m==n)&&(u~=j)&&((bus_type(u)~=2)&&(bus_type(j)~=2))
    
```

```

        %partial_Q_vol_mag(m,n)=partial_P_delta(u-nPV-1,j-nPV-1);
        partial_Q_vol_mag(m,n)=(-
        ((abs((V_new(u,1))*(V_new(j,1))*(Ybus(u,j))))*(sin((angle(Ybus(u,j)))+(
        angle(V_new(j,1))-(angle(V_new(u,1))))));
        n=n+1;
        element_count=element_count+1;
        elseif((m==n)&&(u==j)&&((bus_type(u))~=2)&&((bus_type(j))~=2))
        partial_Q_vol_mag(m,n)=((Q_injected_bus(u,1))-
        (((abs(V_new(u,1)))^(2))*(Bbus(u,u))));
        n=n+1;
        element_count=element_count+1;
    end
end
if((j==nbus)&&(element_count>0))
    m=m+1;n=1;element_count=0;
end
end
end

%-----
% STEP-(3.e): CALCULATING THE COMPLETE [J]
%-----

J=[partial_P_delta partial_P_vol_mag ; partial_Q_delta
partial_Q_vol_mag];

%-----END OF STEP-3-----

%-----STARTING OF STEP-4-----

% STEP-4: CALCULATING THE CORRECTION VECTOR BY ((inv(J))*(MISMATCH-
VECTOR)) & THE UPDATED VALUES OF THE
% STATE VARIABLES i.e. (|v_i|,DELTA_i)
%-----

for u=1:(2*(nbus-1))
    correction_vector(u,1)=0.0; % Initialising the 'correction_vector'
as (0.0)
end
correction_vector=(inv(J))*(inj_pow_mismatch_vector); % calculating the
'correction_vector[]'
for u=1:(nbus-1)
    correction_voltage_angle(u,1)=correction_vector(u,1); % storing the
correction(s) in the voltage angle(s)
    if(u<=(nbus-1-nPV))
        correction_voltage_magnitude(u,1)=correction_vector((u+nbus-
1),1); % storing the correction(s) in the voltage angle(s)
    end
end
end
correction_voltage_magnitude_count=1; % initialising the
'correction_voltage_magnitude_count' as (1)
for u=1:(nbus-1)

voltage_angle_updated=angle((V_new(u+1,1)))+(correction_voltage_angle(u
,1)); % calculating the updated voltage-angle
    
```

```

        if(bus_type(u+1)~=2)

voltage_magnitude_updated=abs((V_new(u+1,1)))+(correction_voltage_magn
itude(correction_voltage_magnitude_count,1))*(abs((V_new(u+1,1))))); %
calculating the updated voltage-magnitude

correction_voltage_magnitude_count=correction_voltage_magnitude_count+1
; % updating 'correction_voltage_magnitude_count' by (1)
        end
        if(bus_type(u+1)~=2)

V_new(u+1,1)=voltage_magnitude_updated*((cos(voltage_angle_updated))+(s
in(voltage_angle_updated)*(1i))); % calculating the updated voltage
        end
        if(bus_type(u+1)==2)

V_new(u+1,1)=abs(V_new(u+1,1))*((cos(voltage_angle_updated))+(sin(volta
ge_angle_updated)*(1i))); % calculating the updated voltage
        end
    end
%-----
%-----
end

% STEP-4 - CALCULATING THE LINE-FLOW(s) & THE BUS-INJECTION(s) & THE
BUS-POWER MISMATCH(s) & THE LINE-LOSS(s)
%-----
%-----

for u=1:nbus
    for j=1:nbus
        if((u~=j)&&(Ybus(u,j))~=0.0)

complex_flow_line(1,flow_count)=((conj(V_new(u,1))*(V_new(u,1))-
(V_new(j,1)))*(-Ybus(u,j)))+(conj(V_new(u,1))*(V_new(u,1))*(b(u,j)));
% Calculating the line-flows
        line_flows(u,j)=conj(complex_flow_line(1,flow_count)); %
Storing the power flow in the line-flow matrix

active_flow_line(1,flow_count)=real(complex_flow_line(1,flow_count)); %
P.U. active power flow from (u->j)
        reactive_flow_line(1,flow_count)=(-
(imag(complex_flow_line(1,flow_count)))); % P.U. reactive power flow
from (u->j)

bus_power_injection(1,u)=bus_power_injection(1,u)+conj(complex_flow_lin
e(1,flow_count)); % Calculating the bus-power-injection(s)
        bus_power_mismatch(1,u)=((S_gen(u,1)-S_load(u,1))/MVA_base)-
(bus_power_injection(1,u)); % Calculating the bus-power-mismatch
        flow_count=flow_count+1; % Updating the flow_count by (1)
        end
    end
end
Tol1=max(real(bus_power_mismatch));
Tol2=max(imag(bus_power_mismatch));
    
```

```

Tol=max(Tol1,Tol2);

for u=1:nbus
    for j=1:nbus
        if (u<j) && (abs(line_flows(u,j))~=0.0)
            line_loss(u,j)=line_flows(u,j)+line_flows(j,u); %
Calculating the individual line-loss
            real_line_loss=abs(real(line_loss(u,j))); % Absolute value
of the active-line-loss
            imag_line_loss=abs(imag(line_loss(u,j))); % Absolute value
of the reactive-line-loss
            line_loss(u,j)=(real_line_loss)+(imag_line_loss)*(1i);
            sum_line_loss=sum_line_loss+line_loss(u,j); % Calculating
the total line-loss
        end
    end
end
%caclulating branch current
Vs=V_new(fb);
Vr=V_new(tb);
for i=1:11
Iline(i)=(Vs(i)-(Vr(i)))*a(i)/Z(i);
end
VS=abs(Vs)
VR=abs(V_new(tb));
ILINE=abs(Iline)';

V=abs(V_new);
del=angle(V_new);
Plos=real(sum_line_loss);
P=real(bus_power_injection);
Pgs=P(1)*100;
if Pgs>=160
    Pglim=160;
elseif Pgs<=10
    Pglim=10;
else
    Pglim=Pgs;
end
Pgsdev=Pgs-Pglim;
% convergency cheker
if Tol>=tolerence
    penalty=10000;
else
    penalty=0;
end
Toldev=penalty*(Tol-tolerance);
%angle ang voltage limit

for i=1:11
    if V(i)>=1.05
        vlim(i)=1.05;
    elseif V(i)<=0.95
        vlim(i)=0.95;
    else
        vlim(i)=V(i);
    end
end
    
```



```

end

end
vdev=V-vlim';
Vdev=max(vdev);
for i=1:11
    if del(i)>=0.785
        anglim(i)=0.785;
    elseif del(i)<=-0.785
        anglim(i)=-0.785;
    else
        anglim(i)=del(i);
    end
end
Angdev=del-anglim';
angdev=max(Angdev);%take maximum deviation
linecap=linedata(:,7);
linecapacity=[linecap;-linecap];
for i=1:22
    llim(i)=(abs(complex_flow_line(i))-abs(linecapacity(i)));
end
Llim=max(llim); %take maximem deviation
end

```